Applications of Smoothed Particle Hydrodynamics on 3D Nonlinear Free Surface Flows

By

Liang Shen

A thesis submitted in accordance with the regulation of

University of Strathclyde in part fulfillment of the requirements

For the degree of Doctor of Philosophy

Department of Naval Architecture & Marine Engineering

University of Strathclyde

July 2011

Acknowledgement

The research of this thesis has been carried out at the Ship Stability Research Centre (SSRC), Department of Naval Architecture & Marine Engineering, University of Strathclyde., during the years 2006 and 2011. The research was funded by SSRC. I gratefully acknowledge this support.

I would like to thank Professor Dracos Vassalos for the supervising of this thesis. I want to express sincere gratitude to Professor Dracos Vassalos for his guidance throughout the period of my work.

Special thanks also go to Mr. Qiuxin Gao and Mr. Dag Skaar for their support on my work.

I would also like to thank my colleagues at SSRC and the department of Naval Architecture & Marine Engineering for providing great work environment.

Lastly, thanks to my family for their constant support.

Abstract

As a branch of CFD, Meshless method called ‘Smoothed Particle Hydrodynamics’ (SPH) has the advantage to deal with complicated free surface flows and some other attractive features. In this thesis, a robust, accurate and efficient SPH code was developed to simulate the 3D nonlinear free surface flows. MPI (message passing interface) was adopted for parallelization. Approximate solid ghost particles were proposed to simulate general 3D geometry on solid boundaries. Local pressure evaluation method was used to calculate response loads on structure and to simulate fully coupling motion between solid and liquid. Some other techniques were developed and adopted in our code in order to construct a more accurate and stable simulation.

For verification and validation of SPH method, one-phase and two-phase dam break and wedge entry were tested with discussion of solid boundary, pressure evaluation method and variable smoothed length. Subsequently, the method was used to study 2D and 3D sloshing and flooding problems. Comparisons were carried out between experimental and other numerical results. The features of the phenomenon for instance in terms of wave height, structural loads and large deformation of free surface were analyzed and discussed.

Key words: SPH (Smoothed Particle Hydrodynamics), three dimension, nonlinear, free surface, sloshing, flooding

CONTENT

List of figures

List of tables

Nomenclature

Abbreviations

ALE	Arbitrary Lagrange Euler
CFD	Computational Fluid Dynamics
CFL	Courant Friedrichs Levy
CSPH	Corrected Smoothed Particle Hydrodynamics
DOF	Degree of Freedom
EOS	Equation of state
LES	Large eddy simulations
LNG	Liquefied natural gas
MPI	Message Passing Interface
ISPH	Incompressible Smoothed Particle Hydrodynamics
PDE	Partial differential equations
PPE	Pressure Poisson Equation
SPH	Smoothed Particle Hydrodynamics
VOF	Volume of Fluid
WCSPH	Weakly Compressible Smoothed Particle Hydrodynamics
W	Kernel function
h	Length scale of kernel function
V	Volume
∇W	Derivative of the kernel

S	Surface
m	Mass
ρ	Density
r	Distance between two particles
u	Velocity
t	Time
E	Energy
p	Pressure
ν	Viscosity
g	Gravitational acceleration
γ	Ratio of the heat capacity of the gas at constant pressure to that at constant volume
α	Artificial viscosity coefficient
$M\vec{G}$	External force of the tank
ω	Frequency
ξ	Amplitude
ω_n	Natural frequency

1 Introduction

The problems of nonlinear free surface flows are critical issues that have to be addressed by the research community within the field of naval shipbuilding. For example, slamming is one of the leading hydro-elastic problems which persistently defy the designers understanding of ship behavior at sea. The problem of sloshing is of particular interest when designing ships with large liquid tanks as well as investigating the behavior of a breached hull with flooding water, which is increasingly considered now as part of the new approach to safety at sea.

However, the theoretical analysis is limited to the cases with small deformations of the interface. The non-linearity, viscous effects and strong coupling of fluid-solid interaction are the main problems when performing calculations. Therefore the development of feasible calculation methods to accurately predict nonlinear hydrodynamics should be based on CFD methods. When focusing on CFD methods, the standard approach to solving the equations of fluid dynamics with interface numerically is to define fluid quantities on a regular spatial grid coupled with techniques to capture interface evolution, such as *Level Set* (LS) or *Volume Of Fluid* (VOF), which are computing derivatives using finite difference or finite volume schemes. This is an extremely well studied approach and although most 'state of the art' methods for fluid dynamics have been developed in this manner, there is still much work required to improve them for more general validity. An alternative to all of these methods is to remove the spatial grid entirely in which fluid quantities are carried by a set of moving interpolation points, which follow the fluid motion. They are called the 'meshless method'. *Smoothed Particle Hydrodynamics* (SPH) is one of the meshless methods. As it is set in a fully Lagrangian frame, SPH has a great advantage to capture interface of the fluid naturally without the need of mesh refinement. Since SPH was firstly proposed in 1977 (Lucy and Monaghan), it has been applied in free surface flows (dam break, Monaghan 1994; slamming, Oger

2005). However, SPH still has to overcome the problems of how to handle complex boundaries, the stability of calculations and three dimension case calculation efficiency. This thesis aims to delve deeply into the SPH method and establish it as a creditable method for non-linear hydrodynamics as well as further extend its applications to actual 3D nonlinear free surface flows of contemporary significance and focus, such as sloshing, slamming and flooding.

1.1 Background and motivation

Sloshing is one of the nonlinear free-surface flows, which can be defined as dynamic load acting over a tank structure as a result of the motion of a fluid with free surface confined in the tank. It is a highly nonlinear resonant phenomenon appearing in all marine structures containing liquids. This can lead to large local structural loads in the tank and has an important effect on the global ship motion.

Fig 1.1 Fluid sloshing dynamics

The effects of sloshing loads are of great importance when designing LNG carriers. It

is necessary to develop numerical methods which can describe the fluid loading and coupling between ship motions and sloshing.

Fig 1.2 LNG carrier

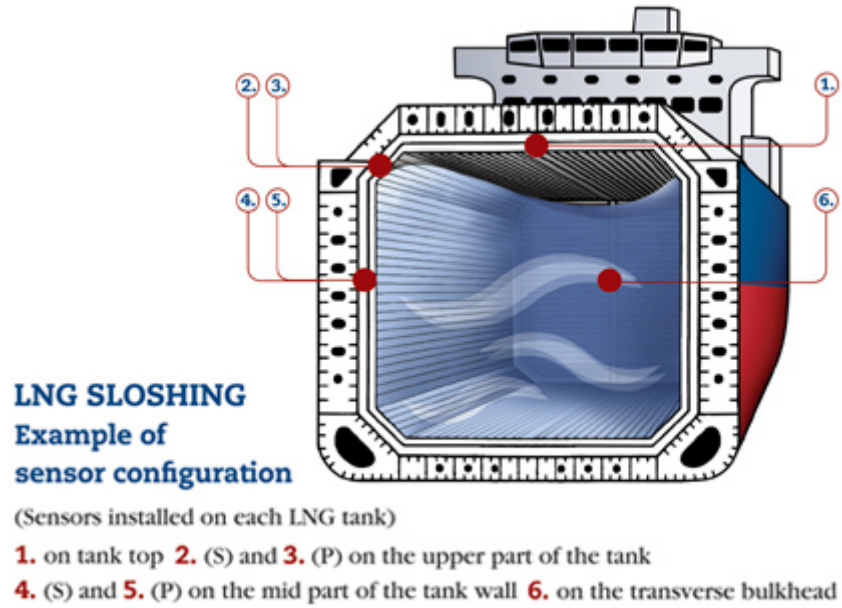

Fig 1.3 liquid sloshing in LNG carrier

Several studies based on different numerical approaches to sloshing have been conducted by Su Tsung-Chow (1992), Buechmann (1996), Tanizawa (1996), Chen et al. (1997), Pawell (1997) and Faltinsen (1999). The majority of them used the potential flow model where an incompressible fluid in irrotational motion can be used

in many cases to model sloshing, in particular for smooth tanks with limited depths. However, dissipation and damping occurs within intermediate and shallow depths due to the run-up and overturning of the fluid near the wall and wave breaking in the middle of the free surface. Therefore CFD approaches have been employed in recent years to resolve free surface flow problems such as VOF (Hirt and Nichols, 1981) and the SPH method (Monaghan, 1994).

Concerning water flooding in damaged vessels, a high nonlinear hydrodynamic phenomenon was found to be present in this process. Vessel motion can affect water flooding and water sloshing in the compartment and conversely, liquid loads due to water sloshing in the compartment influence the vessel motion.

Fig 1.4 Estonia

The size of passenger ships has been growing for decades, and nowadays many ships can accommodate several thousands of people. Therefore, the safety of these ships is of the uttermost importance, both in the design phase and onboard in the event of accident. When a ship is damaged, for example due to a collision or grounding, water

starts to flood in. The internal openings and non-watertight subdivision in the watertight (WT) compartment can have a significant effect on the motions of the ship during the flooding process. Between the intact position and the final damaged condition, if equilibrium can be found, the flooding ship can pass through the intermediate stages that can be more hazardous than the final condition. Therefore, it is important to be able to evaluate these intermediate stages. Practically, the only feasible and accurate way to do this is to use the time-domain simulation of the flooding process and recreate the motions of the damaged ship. Moreover, the simulation will give an estimation of the available time for an orderly evacuation and abandonment, where there is a risk that the ship will capsize or sink.

Fig 1.5 Estonia (sailing)

Fig 1.6 Estonia (capsized and sank)

The time-domain simulation methods for damage stability and progressive flooding have been established for about two decades. The capsizing of the car passenger ferry "Herald of Free Enterprise" in 1987 and the sinking of the ferry "Estonia" in 1994 have had a major influence on this work. Therefore, it is easy to understand why so much effort has been put into finding solutions to the problem of water on the vehicle deck. However, recently also the performance based damage stability of large passenger ships has been studied using simulations. This has become feasible since the calculation capacity of the computers has significantly improved. The most significant approaches on the flooding simulation are briefly reviewed in the following paragraph.

The classical hydraulic model has widely been used in previous studies to calculate the floodwater dynamics studies (Santos et al., 2002; Palazzi and De Kat, 2004; Ruponen, 2007). The inflow and outflow of water through the damaged opening is determined by the modified empirical Bernoulli Equation. The motion of floodwater inside the compartment is ignored and its free surface is assumed to be horizontal. An improved model for the internal water motion was proposed by Papanikolaou et al. (2000), in which the internal water is considered as a lump mass moving freely over a

specific path surface. However, the surface of water is assumed to remain flat. A more sophisticated model for calculating the internal water dynamics involves using the shallow water equation (Santos and Guedes Soares, 2002; Valanto, 2006; Santos and Guedes Soares, 2006). Although all the approaches mentioned above are practical and efficient in predicting the flood water motion and its impact on the vessel, there are some limitations. Firstly, a simple hydraulic model drives the water ingress/egress through the opening, and hence the transient dynamics of the flow are ignored. Secondly, the surface of floodwater in the compartment is assumed to be either horizontal or flat. In the case when the vessel undergoes large amplitudes of motion, these approaches lack the ability to model the violent flows with the non-linear free surface, even when employing the shallow water theory. Thirdly, the above models cannot fully consider the influences of the geometry of the damaged opening and the internal layout of complex compartments on the motion of the flood water. Therefore, more effective and accurate methods to predict the flood water dynamics are required.

Some methods have been presented in the past few years. The Volume of Fluid (VOF) method, proposed by Hirt and Nichols (1981), has become the most popular method for calculating free surface flows. Many studies have shown that the VOF method is capable to capture sharp interfaces even with large scale overturning and deforming (Van't Veer and De Kat, 2000; Gao, 2001; Woodburn et al., 2002; Gao et al., 2004; Cho et al., 2005).

As a 'meshless method', SPH was originally developed to deal with astro-dynamical problems and has successfully extended to a variety of fluid-dynamic systems. In SPH, the formulation is Lagrangian and the fluid is divided into a set of particles. This is the main advantage of the method when dealing with free-surface problems, compared to Eulerian schemes. The particles in SPH carry the basic characters of fluid such as velocity, position and density. The characters come from the use of an integral interpolation technique.

In the present thesis, the SPH method has been the focus for further development leading to an accurate simulation of 3D nonlinear free surface flows. The major contributions of this thesis are summarized in the next section.

1.2 Aims and Objectives

The main objective of this thesis is to develop fast and accurate CFD tools based on Smoothed Particle Hydrodynamics to simulate 3D Nonlinear Free Surface Flows.

Specific objectives include the following:

1. To critically review SPH theory and relevant applications on Hydrodynamics

2. To construct a more accurate and robust simulation by applying new solid boundary condition called 'approximate ghost particles' for simulating three dimensional cases with general geometries. To search other suitable modifications on SPH algorithm to improve the stability of SPH method.

3. To construct fast and efficient CFD tool by increasing the calculation capability: Parallelization of the SPH code using Message Passing Interface (MPI) technique and reducing the calculation cost: Variable smoothed length technique.

4. To extract correct local properties of fluid (such as local pressure) to construct correctly the relation between solid response motion and fluid dynamics.

5. To verify and validate the developed algorithm for stability, consistency and accuracy using available analytical, numerical and experimental results.

6. To extend the applications of SPH to 3D free surface flows: three dimensional

sloshing and flooding with highly nonlinear phenomenon.

7. To discuss the results deriving from this work and make recommendations for further research in this area.

1.3 Structure of the thesis

This thesis can be divided into two main parts consisting of seven chapters. The first one is dedicated to the description of the mathematical model and corresponding numerical method. The second part describes the verification and validation of the SPH code which has been developed for free surface and interface flow. Then applications of SPH are extended to 3D nonlinear free surface flows.

A review of the SPH method is presented in chapter 2 and a description of the theory of SPH is discussed in chapter 3. Specification of solid boundary conditions is detailed present in Chapter 4. Chapter 5 is dedicated to the description of Parallel and time evolution strategies. Chapter 6 verifies the SPH method and validates the obtained SPH solver with analytical and experimental results. In order to implement the SPH method in 3D nonlinear cases, sloshing (Chapter 7) and flooding (Chapter 8) cases are simulated using SPH and discussed in detail. Finally, to conclude chapter 9 presents developments, findings and discusses the main contributions of this thesis.

2 Background to SPH

As a CFD method, the Smoothed Particle Hydrodynamics (SPH) has some features which make it highly attractive for simulating dynamic responses of materials involving fractures and fragmentation. In this chapter the theory and application of Smoothed Particle Hydrodynamics since its inception in 1977 are critically reviewed.

2.1 Overview

Recently, a new class of numerical solvers - based on the use of scattered sets of nodes or particles - has started to be successfully applied to partial differential equations (PDE). The name of this class of methods could be characterized as *meshless, gridless, mesh-free or particle* because their main feature is that they do not require any mesh.

Smoothed Particle Hydrodynamics (SPH) is one particle method used for obtaining approximate numerical solutions of the equations of fluid dynamics by replacing the fluid with a set of particles. For mathematicians, the particles are approximate interpolation points which carry properties of the fluid. For the physicist, SPH particles are discrete material particles of fluid. Either way, this method has a number of attractive features. The first of these is that there are no additional advection terms in fluid equations because it is in the Lagrangian frame. Secondly, whatever the free surface problems, whether they are with one-phase or interface problems with multi-phase, SPH can capture the free surface and interface naturally, in contrast to finite difference schemes which may find it more difficult. Thirdly, SPH is a mesh free method which means there would never be a dynamic mesh problem where fitted numerical techniques are required for finite difference methods to deal with fluid-solid interaction problems. Finally, SPH has the advantage in the areas of

developing codes and computational optimization because the standard SPH method uses an explicit algorithm to calculate velocity and pressure. Additionally, there is close similarity between SPH and molecular dynamics which means it is possible to easily include complex physics.

Over the recent past, much research has been devoted to the case of convection problems with the presence of deformable interfaces. When using the common numerical methods such as finite-difference and finite element it is difficult to find efficient solutions to these complex cases. Such problems could be effectively solved by employing particle methods. However, it is difficult to determine which interactions between the particles will accurately reproduce the equations of fluid dynamics or continuum mechanics. Lucy (1977) and Gingold & Monaghan (1977) derived the equations of motion using a 'kernel estimation technique' for the density term. This gave birth to the 'Smoothed Particle Hydrodynamics' (SPH) method. The basic idea of this solver is to consider the fluid as a set of (smooth) particles. Each one is associated with a kernel function that represents the particle mass as distributed along a finite area. The particle moves according to the forces induced by the whole particle system and carries information about the dynamic and thermodynamic properties of the fluid and their gradients. These quantities evolve according to specific mechanical laws. Monaghan and Gingold used this new solver and proposed numerical schemes which produced positive results for modeling the fluid dynamics of astrophysical phenomena without boundaries.

As SPH is a numerical method to solve the continuum equations which are essentially a technique for approximating the real physics, it can be used for a wide range of fluid dynamical problems. Although the first application of SPH was to solve astrophysical problems, it has also been applied to incompressible flow problems by treating the fluid as slightly compressible with an appropriate equation of state between density and pressure of fluid (Monaghan 1994). Using this idea, waves breaking on arbitrary structures (Monaghan *et al* 2004, Colagrossi and Landrini 2003) as well as the more

classical problems of re-creating waves on beaches (Monaghan and Kos 1999) could be simulated. Colagrossi (2004) has made a detailed study based on the application of using SPH to simulate breaking waves. In his thesis it is also showed that the SPH simulation of sloshing tanks and the bow waves produced by certain ship hulls are consistent with results from the experiments. Oger (2005) aimed to create an accurate numerical simulation of solid-fluid coupling in free surface flow and tested wedge water entries. The evaluation of fluid pressure on solid boundaries proposes that SPH could produce results which highlight simple solutions for solving complex hydrodynamic problems such as floating bodies coupled with free surface dynamic responses, sinking vessels trapped in waves, rogue waves impacting upon structures.

The achievement of solving fluid dynamic problems with interface using the SPH method are due to the development of comprehensive techniques which are available in the SPH solver. The next section is dedicated to discussion of this state of the art specific kind of solver.

2.2 SPH: state-of-the-art

More than thirty years ago, the first paper describing the SPH technique appeared (Lucy 1977) but it was dismissed as a ‘quick and dirty’ scheme. In recent years, the SPH solver has been substantially improved and has become a competitive and established CFD method. Its main advantage is that the SPH can evaluate fluid properties and spatial derivatives without using a computational grid. This avoids the complicated numerical problems due to mesh tangling and distortion. Initially this technique has been applied to problems in the astrophysical field, as stated in the review of the literature Benz (1988). Therefore relevant improvements of the solver were achieved within that research area. In recent years, with the advancements in computer technology, SPH has become ever more popular in the hydrodynamic field because its Lagrangian character makes it simple to be implemented in fluid flows

with existing interfaces and free surface even for 3D cases. The main steps leading to the most up to date SPH method are summarized and analyzed below

Accuracy and Stability of SPH

In past research (Gingold and Monaghan 1977, Lucy 1977) the proposed numerical schemes did not conserve linear and angular momentum. The basic SPH algorithm was improved using a similar method with molecular dynamics in order to conserve the exact linear and angular momentum which was applied for compressible non-dissipative fluid (Gingold and Monaghan 1983). Moussa and Vila (2000) investigated the convergence of SPH by studying the solution of Euler compressible equations. Libersky et al. (1993) developed a new meshless formulation to solve the solid mechanics. Dilts (1999) showed that the Lagrangian SPH discrete equations can be obtained by applying a Galerkin weighted residual scheme to the Eulerian conservation laws.

Much of the research into SPH has been done to derive the new SPH form and improve its ability to perform accurate interpolations when the particles are not uniformly distributed (randomly distributed, close to surface or have particles that are not the same size) (Belytschko et al. 1998). In the development of meshless solvers, it is apparent that moving least square (MLS) approximations is a generalization of the SPH using an interpolate leading to accurate derivatives regardless of the particle distribution. A comprehensive description of the MLS is given by Lancaster & Salkauskas (1981). The first order form of MLS is named ‘Shepard Function’ (Shepard 1968) which can be applied to the data-fitting field. Nayroles et al. (1992) proposed using the ‘Diffuse Element Method’ (DEM) when applying the MLS approximation within a Galerkin method. Belytschko et al. (1994) improved upon this idea and further modified the solver. He renamed it the ‘Element-free Galerkin Method’. These new methods are consistent and stable but much more expensive than the original SPH form.

SPH suffers the crucial problem of a lack of stability. Swegle et al. (1995) demonstrated the occurrence of such instability through a dispersion analysis of the linear equations. It is caused by the interaction between the spatial derivatives of the kernel function and the tensile stresses in the momentum conservation equations. When the SPH is applied to the problems where the negative stresses appear, the particles don't repel but attract each other and tend to clump together forming stable configurations. Although similar to the fractures and fragmentation of the material, these clumping processes are unphysical. Several solutions have been proposed to avoid the tensile instability. Morris (1996) investigated the type of instability occurring in the case of negative stress and concluded that spline interpolate kernels with compact support resulted in instabilities for the standard implementation of 2D SPH. Morris (1996) resolved this problem by rearranging the kernel to achieve the desired stability properties. If there are a sufficient large number of particle neighbors in the interactions, then the Gaussian kernel has good stability properties. However, this will lead to an expensive calculation. Monaghan (2000) introduced a small repulsive force between the particles with negative pressure to avoid particles clumping. The idea is inspired from a similar phenomenon observed with what happens in a real stretched solid. This correction ensures the stability of SPH and results in small errors in the cases of pressure wave propagation providing the proper parameters are used for this artificial repulsive force. In the literature of Gray, Monaghan, & Swift (2001), the correction was improved to handle problems with elastic solids.

Quinlan et al.(2006) analyzed the truncation error of the gradient estimate using Tayler series expansion in 1D. The study showed the main factors responsible for second-order convergence of interpolation accuracy. Moreover, Quinlan et al.(2006) also showed the interpolation sensitivity could be reduced by renormalization of the kernel. Springel (2010) provided a characterization of the overall accuracy of the standard SPH scheme with testing the SPH model on several simple cases. The convergence of the simulation is achieved by keeping the number of neighbors

constant.

Viscosity of SPH

Monaghan (1992) introduced an artificial viscosity term and added it into the momentum equation. This idea is inspired from Von Neumann and Richtmyer (1950) who used it to model hydrodynamic shocks. This term solves the problems that the SPH scheme suffers from in terms of its instability due to its explicit time integration. However, it could bring additional dissipation into the calculation especially in long time simulations of low-dynamics flows where strict conservation properties are required.

Morris et al. (1997) introduced a way to express the realistic viscous term with the SPH formulation in the low Reynolds number flows. This method gives the SPH scheme exact conservations of the linear momentum and an approximate conversation of angular momentum. Consistency is shown in the cases of Couette and Poiseuille flows. Potapov et al. (2001) applies the same formula to the more complex problem of a shear flow of large neutrally buoyant particles in a viscous fluid current.

In the first application of SPH towards viscous turbulence flows, the form of a Monte-Carlo probability density function particle method is applied to study a variety of 2D flows. This shows consistency with the referenced solutions (Welton 1998). Wagner & Liu (2000) show that advanced Kernel Particle Methods can be used as a basis for a sub grid scale model within Large Eddy Simulations (LES). Reza ISSA (2005) applies a SPH mixing length model to a 2D free surface channel and attempts to adapt Large Eddy simulation concepts to SPH which is applied to a 3D turbulent free surface channel. Recently, Colagrossi et al.(2010) studied the behavior of the viscous term for incompressible flows and proved its consistency with the Navier-Stokes' viscous term.

Boundary conditions

SPH has a major advantage when dealing with free surface flows because it is not necessary to explicitly enforce the free surface boundary conditions: The kinematic condition is intrinsically incorporated in the Lagrangian flow description and the dynamic condition is also automatically satisfied. When simulating violent free-surface flows, for instance during sloshing processes with highly nonlinear resonant phenomenon appearing; or during slamming processes when breaking waves makes the free surface extremely complex, the SPH method shows great superiority over other mesh-based CFD tools which have to solve the algorithm to capture the free surface shape and to configure mesh, even dynamic mesh carefully in the free surface. Within the SPH strategy it is also possible to model the surface tension (Morris 2000, Nugent & Posch 2000). In the latter case, the surface tension is introduced by modifying the equation of state. This approach is much easier than the technique developed by Morris (2000) and this approach also provides a simple mechanism to control the numerical fragmentation of the interface.

With respect to the free-surface conditions, the SPH has difficulties in handling the presence of solid boundaries. In the initial use of the SPH method in attempting to solve astrophysics problems, the solid boundary condition is not included since practical solid boundaries are not of interest in this context. Research into this field has been used to apply SPH within fluid dynamics. The first attempt to deal with the problem of solid walls employed the method of exerting forces upon the fluid particles. The form for the force was guided by the known forces between molecules. In real cases, the exerting force has the Lennard-Jones form and the value is based on the distance between a fluid particle and a boundary particle. The main drawbacks of this repulsive force are: 1) it causes pressure-wave disturbances at the beginning of the numerical simulation; 2) It is not suitable to accurately calculate the local hydrodynamic loads induced on the structures. Monaghan (1995) uses boundary particle forces to simulate boundary forces. This force is based on the SPH kernel and it seems appropriate because the pressure forces involve the gradient of the kernel. An alternative to this approach is to model the body presence by introducing a layer of

“ghost particles” along the body and outside of the physical domain. The density, pressure and velocity of such particles are deduced from those of the real particles adjacent to the solid boundary. With this technique the local loads on the body can be calculated accurately. Colagrossi A and Landrini M (2004) proposed mirroring ghost particles to mimic the solid boundary. This approach results in the smooth behavior of the particles close to the modeled boundary. However, close attention is necessary when dealing with the complex geometries of the structures.

Recently many other techniques have been proposed to simulate solid boundaries. Kulasegaram et al.(2004) introduced a contact force in the momentum equation based on boundary integrals. Similarly, Feldman and Bonet (2007) and Di Monaco et al.(2009) used an analytic method to compute the intersection between the kernel support and solid boundary. This approach could give more accurate results on solid boundaries but it leads to a more expensive calculation. Yildiz et al.(2009) proposed the multi-tangent algorithm as an extension of ghost technique. The ghost particles are obtained using different local boundary normals for non-flat geometry.

Variable smoothed length

Monaghan (1992) introduced the notion of spatially varying resolution. In the simulations performed within astrophysics studies the smoothing lengths are allowed to vary their position according to the local density of particles. However, meshless methods do not conserve energy when using variable smoothed lengths. Various studies (Benz, M.B. Liu & al, Nelson and Papaloizou, Oger G) have been carried with the aim of improving the formulation and the efficiency of the variable smoothing length technique in SPH.

The variable smoothing length technique is an important tool for general use in the field of fluid dynamics. In many cases we only need high accuracy somewhere in the fluid domain to avoid expensive calculations. For example, we only distribute a high density of particles in the impacting zone of slamming cases which is similar to the

idea employed within local refinement. This technique is commonly used in mesh-based methods.

Applications of SPH to Hydrodynamics

Monaghan (1994) presents the first applications of SPH towards free-surface flows. The use of a stiff equation of state is proposed to link the density and pressure field of fluid particles in this approach which has now become quite popular. The density field shows fluctuations where amplitude is proportional to the square of Mach number of the problem. In particular, the Mach number of fluids is extremely small which means the fluid could be treated as perfectly incompressible. In the numerical simulation, the fluid is modeled more compressible than in reality in order to avoid expensive calculations. However, the speed of sound is still ten times larger than the maximum flow velocity. This implies the maximum fluctuations of density are of the order of 1%. Following the simulations of the 2D dam break (Monaghan 1994) and propagation of waves on an inclined beach (Monaghan & Kos 1999), more applications on free surface flows have been studied in recent years. Monaghan (1999) shows the SPH capability to treat weakly compressible multi-phase flows with small density differences between the phases. SPH methods dealing with multi-phase fluid-solid flows are available in the literature (Monaghan & Kocharyan 1995 and Ritchie & Thomas 2002). González et al., (2003) and Skaar et al., (2006) used the Smoothed Particle Hydrodynamics (SPH) method to model the water flooding process. Souto Iglesias. A (2006) simulates the highly nonlinear 2D sloshing phenomenon produced in a rectangular tank. Oger (2005) gives two dimensional SPH simulations of wedge water entries. In this literature, the variable smooth length technique is used to reduce calculation time and evaluate the local pressure. Large scale calculation of SPH is used for 3D ship slamming cases which produces positive results compared with experimental data (Oger 2007).

Recently, Marsh et al. (2010) investigated a shallow-depth sloshing absorber for

structural control. Ferrari et al. (2010) simulated a 3D dambreak case with impacting problem. Marrone et al.(2011) proposed ‘δ-SPH’ model for the simulation of violent impact flows. Moreover, gravity wave propagation problems in different regimes were studied by Antuono et al.(2011) Dalrymple and Rogers (2006); Landrini et al, (2007)

In these cases mentioned above, the trend of the applications of SPH can be clearly concluded: complex case with large-scale calculation. The SPH shows the great foreground of the actual application in the ship industry.

3 Numerical Solution

In this chapter, the theory of SPH is firstly introduced that includes integral interpolation techniques, kernel function and neighbor particle search algorithm. The second part of this chapter is to describe the SPH strategy developed to simulate Euler equations. Finally, viscosity and tensile instability in SPH are discussed and some techniques are developed to increase the calculation efficiency.

3.1 SPH mathematical model

SPH (Smoothed Particle Hydrodynamics) is a grid-less Lagrangin technique, which is considered as an alternative numerical technique to analyze high deformation on interface. Although Arbitrary Lagrange-Euler (ALE) method and VOF method based on pure Eulerian techniques can easily handle gross motions with large deformation involved, there will be constraints within accuracy and efficiency of calculations if there is severe distortion and material fragment on the interface. In addition, when dealing with solid-fluid interaction problem, dynamic mesh will become another difficulty in Eulerian method especially for multi-phase cases.

SPH offers a possible solution to these difficulties. The technique is Lagrangian so it provides complete fluid information in history by particles without any grid and makes interface tracking simple and natural. The lack of a grid also means that 3D calculations are as easy as 1D case. Many researchers have chosen SPH as a natural technique for large deformation calculations and produced numerous results that proved its robust capabilities.

Kernel approximation

For better understanding of SPH, we start with standard Lagrangian finite-difference techniques with spatial grid. The grid purposed here is to create a possible way to construct approximations of spatial derivatives.

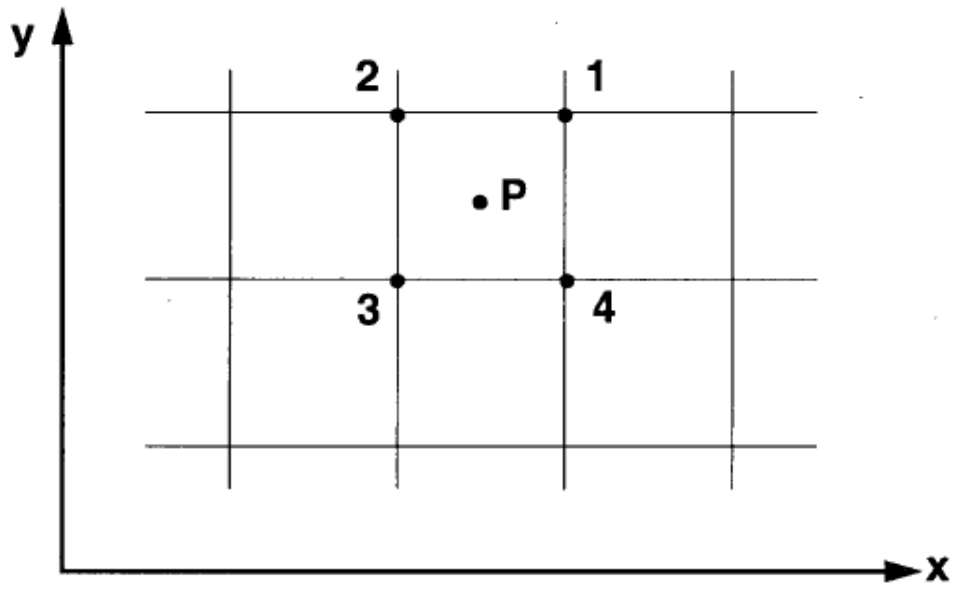

Fig 3.1 finite difference grids

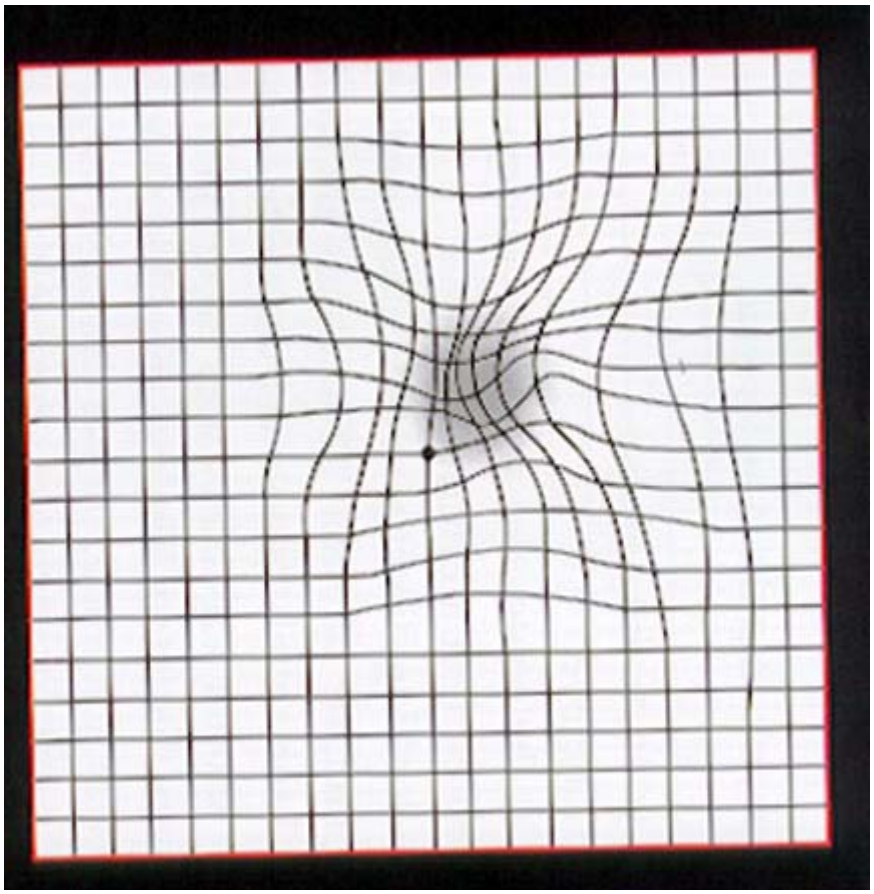

Fig 3.2 finite difference grid distortion

This technique is based on the assumption that the same four nodes will always surround point P. When the grid distorts, the finite difference approximation will lose accuracy. This is different from standard grid-based Lagrangian method. The Smoothed Particle Hydrodynamics use an arbitrary collection of interpolation points instead of grid based approximations. Using this idea, SPH could avoid grid distortion and accuracy problem. The basis of this method is to model fluid domain as a finite number of particles, each one carry its local mass and other physical properties. The evolution of these particles still obeys to relevant PDE equation but the approximation of their properties and spatial derivative doesn't base on the gird but the kernel estimate.

More in detail,

$$f(x_P) = \int f(x')\delta(x_P - x')dV' \qquad (3.1)$$

Where $\delta(x_p - x')$ is the Dirac delta function. If $\delta(x_p - x')$ is replaced by a kernel function $W(x_p - x', h)$ where h is known as the smoothing length, the result is

$$f(x_P) = \int f(x')W(x_P - x', h)dV' \tag{3.2}$$

Here x_P is the location of point P where $f(x_P)$ is evaluated by interpolating known value $f(x')$ in position x' over the domain Ω. In equation (3.2), $W(x_P - x', h)$ is the kernel function and h is the length scale of the support of W where the value of kernel differs from zero. Physically, h represents the domain of influence Ω_{x_P} of x_P. dV' is a differential volume element. This interpolation reproduces $f(x_P)$ if the kernel is delta function. In practice, the kernels are functions which tend to the delta function as the length scale h tends to zero. They should also be normalized to 1 so that the constants are interpolated exactly (Equation 3.3-1).

$$\int_\Omega W(x_P - x', h)dV' = 1 \tag{3.3-1}$$

The kernel function should have other properties:

$W(x_P - x', h) \geq 0$, if $x' \in \Omega_{x_P}$, and zero otherwise. (3.3-2)

$W(x_P - x', h)$ decreases monotonously as $\|x_P - x'\|$ increases. (3.3-3)

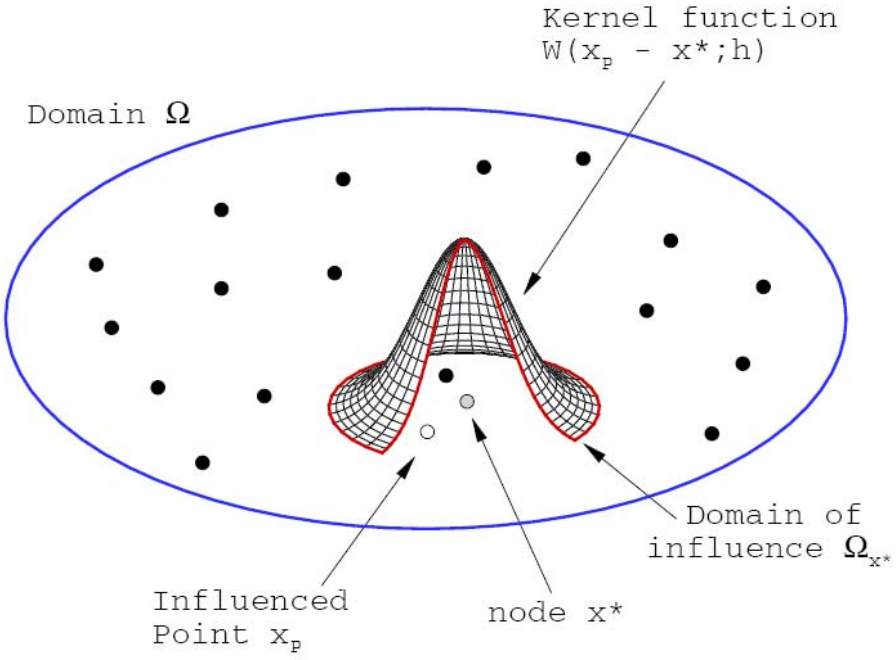

Fig 3.3 Sketch of the kernel function

The approximation for spatial derivatives is obtained by substituting $\nabla f(x_P)$ for $f(x_P)$ in Equation (3.2)

$$\nabla f(x_P) = \int \nabla f(x') W(x_P - x', h) dV' \tag{3.4}$$

The divergence in the integral is taken with respect to the primed coordinate system. Now

$$\nabla f(x') W(x_P - x', h) = \nabla (f(x') W(x_P - x', h)) - f(x') \nabla W(x_P - x', h) \tag{3.5}$$

So that

$$\nabla f(x_P) = \int \nabla (f(x') W(x_P - x', h)) dV' - \int f(x') \nabla W(x_P - x', h) dV' \tag{3.6}$$

The first term on the right side the equation can be converted by means of the divergence theorem into an integral over the surface of the domain of integration

$$\int \nabla (f(x') W(x_P - x', h)) dV' = \int_S f(x') W(x_P - x', h) \cdot \hat{n} dS = 0 \tag{3.7}$$

Because of Equation (3.3-2) the surface integral is zero. Thus,

$$\nabla f(x_P) = -\int f(x') \nabla W(x_P - x', h) dV' \tag{3.8}$$

Now, the kernel approximation allows spatial gradients to be determined from the values of the function and the derivative of the kernel, rather than the derivatives of the function itself. Finally, convert from continuous volume integrals to sums over discrete interpolation points.

$$f(x_i) = \sum_{j=1}^{N} \frac{m_j}{\rho_j} f(x_j) W(x_i - x_j, h) \tag{3.9}$$

And

$$\nabla f(x_i) = -\sum_{j=1}^{N} \frac{m_j}{\rho_j} f(x_j) \nabla W(x_i - x_j, h) \tag{3.10}$$

Where ρ is the density of particle and N in the number of interpolation particles in the domain Ω_i.

The above equations provide continuous approximations to a function and its spatial gradient based on an arbitrary set of discrete interpolation points. No connectivity or spatial relation of the points is required. Theoretically, the choice of kernel is arbitrary as long as it satisfies Equation (3.3). However, in practical computations, choices of the smoothing function affect both the CPU requirements and the stability properties of the algorithm.

Kernel function

The most commonly used kernel functions, $W(r,h)$ where $r = \left\| x_i - x_j \right\|$, belong to a family of B-Spline kernels of both third and fifth order. In addition, the Gaussian kernel is also used in the paper (Morris 1996) detailed in Equation (3.11)

$$W(r,h) = \frac{1}{h^d \pi^{d/2}} e^{-(r/h)^2} \tag{3.11}$$

Where d is the dimension of the problem (1, 2, or 3). Equation (3.11) does not have a compact support. Therefore, a cut-off limit δ is introduced. For the Gaussian type kernel, $3h$ is the typical value, which means $W(r,h) = 0$, if $r > 3h$.

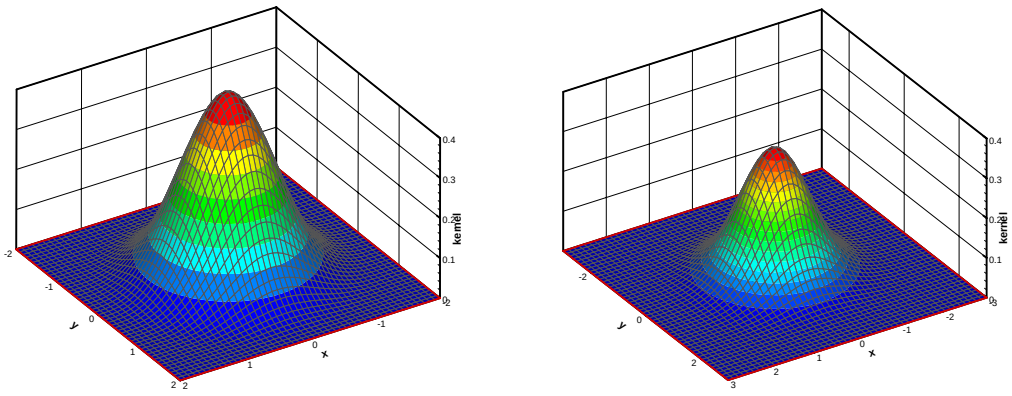

Fig 3.4 Kernel function (Left: Cubic Spline kernel 2D, Right: Gaussian kernel 2D)

Cubic spline and quintic spline kernel functions are also presented here, *i.e.* Equation

(3.12) is a cubic spline with $2h$ as cut-off limit is mostly used for its simplicity. Equation (3.13) is quintic function which has $3h$ as cut-off limit.

$$W(r,h)=\frac{\alpha_1}{h^d}\begin{cases}\frac{2}{3}-(\frac{r}{h})^2+\frac{3}{2}(\frac{r}{h})^3 & 0\le r<1\\ \frac{1}{6}(2-\frac{r}{h})^3 & 1\le r<2\\ 0 & r\ge 2\end{cases} \tag{3.12}$$

$$W(r,h)=\frac{\alpha_2}{h^d}\begin{cases}(3-\frac{r}{h})^5-6(2-\frac{r}{h})^5+15(1-\frac{r}{h})^5 & 0\le r<1\\ (3-\frac{r}{h})^5-6(2-\frac{r}{h})^5 & 1\le r<2\\ (3-\frac{r}{h})^5 & 2\le r<3\\ 0 & r\ge 3\end{cases} \tag{3.13}$$

where α_1 and α_2 are constant determined by the dimension of the problem and the shape of the kernel function. See Table 1

	1D	2D	3D
α_1	1	$\frac{15}{7\pi}$	$\frac{3}{2\pi}$
α_2	$\frac{1}{120}$	$\frac{7}{478\pi}$	$\frac{1}{120\pi}$

Table 1: kernel function

A higher order kernel function is superior to low order kernel functions in that the second derivative is smooth. The stability of the SPH method depends highly upon the second derivative (Morris, 1997). The cubic kernel function has a piece-wise second order derivative, which occasionally makes the stability problematic. The three kernel functions of 2D is shown below *Fig 3.5*

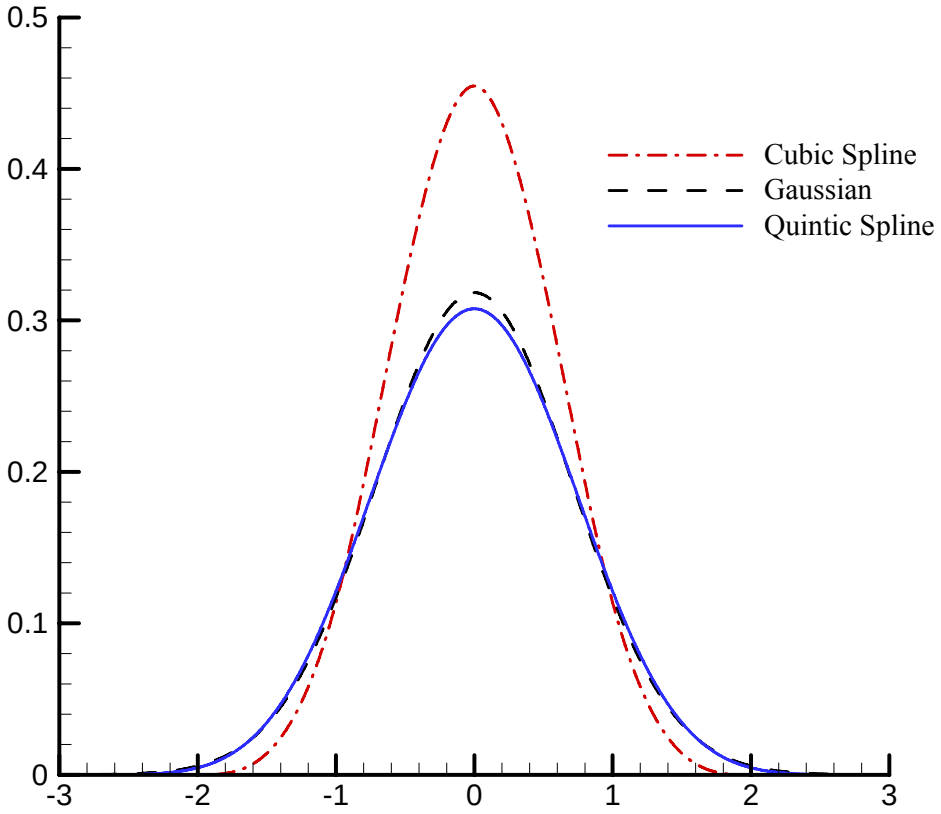

Fig 3.5 Kernel functions in 2D (Cubic spline, Gaussian and Quintic spline).

The derivative of the kernel function $W(r,h)$ is

$$\frac{\partial W(r,h)}{\partial x} = \frac{\partial W(r,h)}{\partial r}\frac{x_i - x_j}{r} \tag{3.14}$$

Derived from Equation (3.11-3.13), $\frac{\partial W(r,h)}{\partial r}$ would be Equation (3.15-3.17) respectively.

$$\frac{\partial W(r,h)}{\partial x} = \frac{-2r}{h^{d+2}\pi^{d/2}} e^{-(r/h)^2} \tag{3.15}$$

$$\frac{\partial W(r,h)}{\partial x}=\frac{\alpha_1}{h^d}\begin{cases}\dfrac{-2r}{h^2}+\dfrac{3r^2}{2h^3} & 0\le r<1\\ \dfrac{(2-\frac{r}{h})^2}{2h} & 1\le r<2\\ 0 & r\ge 2\end{cases} \tag{3.16}$$

$$\frac{\partial W(r,h)}{\partial x}=\frac{\alpha_2}{h^d}\begin{cases}5\dfrac{(3-\frac{r}{h})^4-6(2-\frac{r}{h})^4+15(1-\frac{r}{h})^4}{-h} & 0\le r<1\\ 5\dfrac{(3-\frac{r}{h})^4-6(2-\frac{r}{h})^4}{-h} & 1\le r<2\\ 5\dfrac{(3-\frac{r}{h})^4}{-h} & 2\le r<3\\ 0 & r\ge 3\end{cases} \tag{3.17}$$

See α_1 and α_2 in Table 1.

The comparison between different kernel functions shows cubic spline kernel's simplicity, the Gaussian kernel's stability and code efficiency (Morris 1996). Therefore, the cubic spline kernel with $2h$ as cut-off limit and the Gaussian kernel both with $3h$ as cut-off limit have been used for cases study in the latter chapter.

Kernel Correction

Due to the arbitrarily scattered particles, the kernel interpolation does not give perfect results which does not satisfy the following equations

$$\sum_j W_j(x_i)dV_j=1 \tag{3.18}$$

$$\sum_j x_j W_j(x_i)dV_j=x_i \tag{3.19}$$

$$\sum_j \nabla W_j(x_i)dV_j=0 \tag{3.20}$$

$$\sum_j x_j \otimes \nabla W_j(x_i) dV_j = I \tag{3.21}$$

Therefore, a constant field will not be reproduced correctly which lead to spurious gradient and other numerical errors.

Some alternative techniques can be used for kernel correction. The first order correction is Shepard interpolation technique, consists in using

$$f(x_i) = \sum_j f(x_j) W_j^S(x_i) dV_j \tag{3.22}$$

$$W_j^S(x_i) = \frac{W_j(x_i)}{\sum_k W_k(x_i) dV_k} \tag{3.23}$$

Equations (3.22-3.23) allow the reproduction of exact uniform function (3.18, 3.20). Furthermore, the computational cost of Shepard correction is quite small. Higher order approximations are also possible. Introducing a linear operator $\beta(x_i)$

$$W_j^{MLS}(x_i) = [\beta_0(x_i) + \beta_1(x_i)(x_j - x_i) + \beta_2(x_i)(y_j - y_i)] W_j(x_i) \tag{3.24}$$

This moving least square kernel W_j^{MLS} can reproduce correct linear functions and equations (3.18-3.21) are satisfied. $\beta(x_i)$ is computed through

$$\beta(x_i) = \begin{pmatrix} \beta_0 \\ \beta_1 \\ \beta_2 \end{pmatrix} = A^{-1}(x_i) \begin{bmatrix} 1 \\ 0 \\ 0 \end{bmatrix} \tag{3.25}$$

$$A(x_i) = \sum_j W_j(x_i) \tilde{A}_{ij} \tag{3.26}$$

$$\tilde{A}_{ij} = \begin{bmatrix} 1 & (x_i - x_j) & (y_i - y_j) \\ (x_i - x_j) & (x_i - x_j)^2 & (x_i - x_j)(y_i - y_j) \\ (y_i - y_j) & (x_i - x_j)(y_i - y_j) & (y_i - y_j)^2 \end{bmatrix} \tag{3.27}$$

Using this improved kernel the approximation of a given field and of its spatial derivatives are given by

$$f(x_i) = \sum_j f(x_j) W_j^{MLS}(x_i) dV_j \tag{3.28}$$

$$\nabla f(x_i) = \sum_j f(x_j) \nabla W_j^{MLS}(x_i) dV_j \tag{3.29}$$

Where ∇W_j^{MLS} can be evaluated with the formula

$$\frac{\partial W_j^{MLS}}{\partial x}(x_i) = [\beta_3(x_i) + \beta_4(x_i)(x_j - x_i) + \beta_5(x_i)(y_j - y_i)]W_j(x_i) \tag{3.30}$$

$$\frac{\partial W_j^{MLS}}{\partial y}(x_i) = [\beta_6(x_i) + \beta_7(x_i)(x_j - x_i) + \beta_8(x_i)(y_j - y_i)]W_j(x_i) \tag{3.31}$$

And the term $\beta_k(x_i)$ is estimated by solving a linear algebraic problem as below

$$\beta(x_i) = \begin{pmatrix} \beta_3 \\ \beta_4 \\ \beta_5 \end{pmatrix} = A^{-1}(x_i) \begin{bmatrix} 0 \\ 1 \\ 0 \end{bmatrix} \tag{3.32}$$

$$\beta(x_i) = \begin{pmatrix} \beta_6 \\ \beta_7 \\ \beta_8 \end{pmatrix} = A^{-1}(x_i) \begin{bmatrix} 0 \\ 0 \\ 1 \end{bmatrix} \tag{3.33}$$

This procedure will result in a slight increase in the computing time because of the inversion of the 3×3 matrix A for each fluid particle.

3.2 Neighbor Search Strategy

In practice, the use of a kernel $W(r,h)$ with cut-off limit implies that each particle has finite number of 'neighboring' particles which create non-zero contributions to it. As a result an efficient and accurate algorithm has to be developed to discover these interacting particles.

Following the work done by Hernquist & Katz (1989), consider the $W(r,h)$ contribution of a pair of particles depends on the distance between them, the following strategy is applied. A background Cartesian squared grid is introduced, covering the fluid domain and with mesh size equal to $2h(3h)$. Particles are stored in this grid and each particle will only interact with the particles inside the same grid cell or the particles belonging to the surrounding 8 cells (26 cells in 3D), as shown in

Figure 3.6. Therefore only particles that are likely to make contribution will be tested and any chance of missing an interaction will be avoided. Due to particle motions, this procedure needs to be periodically updated at each time step. This operation is rather computationally cheap and efficient. $O(N \log N)$ is expected in the neighboring search cost instead of straight search algorithm $O(N^2)$.

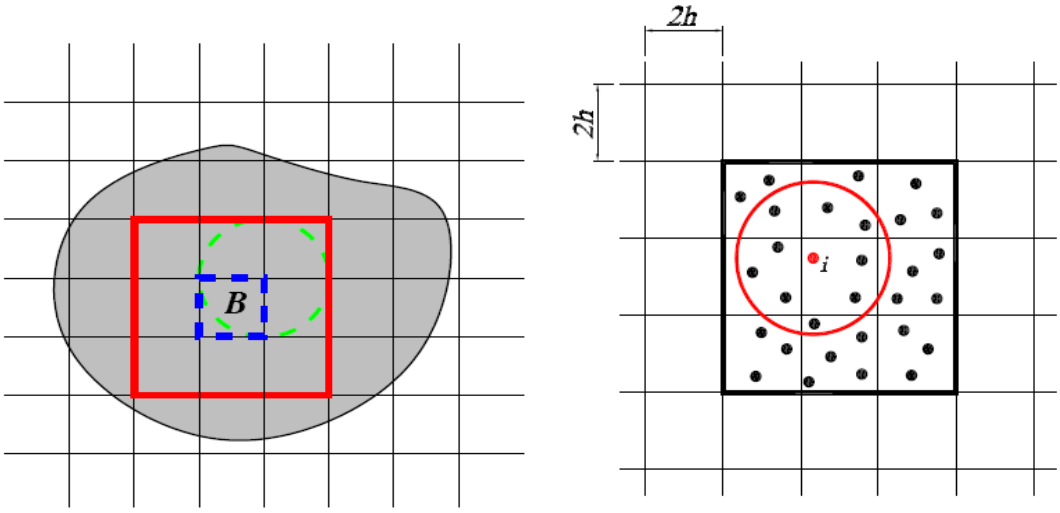

Fig 3.6 Neighbor Search Strategy (2D)

In the case of variable smooth length (h is allowed to vary), the interaction radius for each particle is different. In order to keep the exact conservation of momentum, symmetric combination is considered for each pair. The interaction length is $h_{ij} = \frac{h_i + h_j}{2}$.

If h does not vary much, $h = \max(h_{ij})$ is used as background grid size (Fig 3.6) and the efficiency of neighboring search will not decrease immensely. However, as the variation of h is increased, there will be regions where large numbers of particles (with small h) are clustered into single cells. Calculating the interactions between these particles in 'crowded' cell will be very expensive (Fig 3.7).

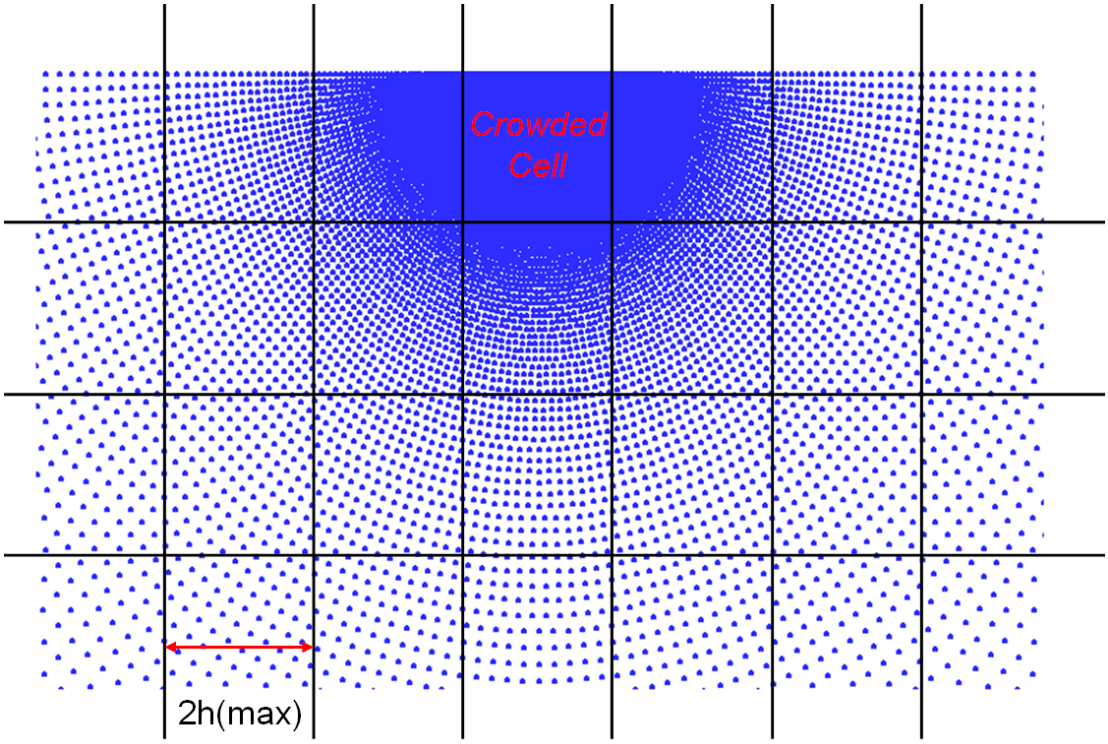

Fig 3.7 Expensive Neighbor search in crowed cell

The variable smoothed length technique is only used in slamming and flooding cases in present thesis, therefore the density of number of the particles is mostly predictable during time evolution. Following the idea of TreeSPH (Hernquist 1989), the calculation domain is discretized into several pieces in advance for processing individually in our parallel code. The maximum kernel length in each piece of domain will vary to adapt to the local density of particle number. This procedure can improve the efficiency of particles that links significantly (Fig 3.8).

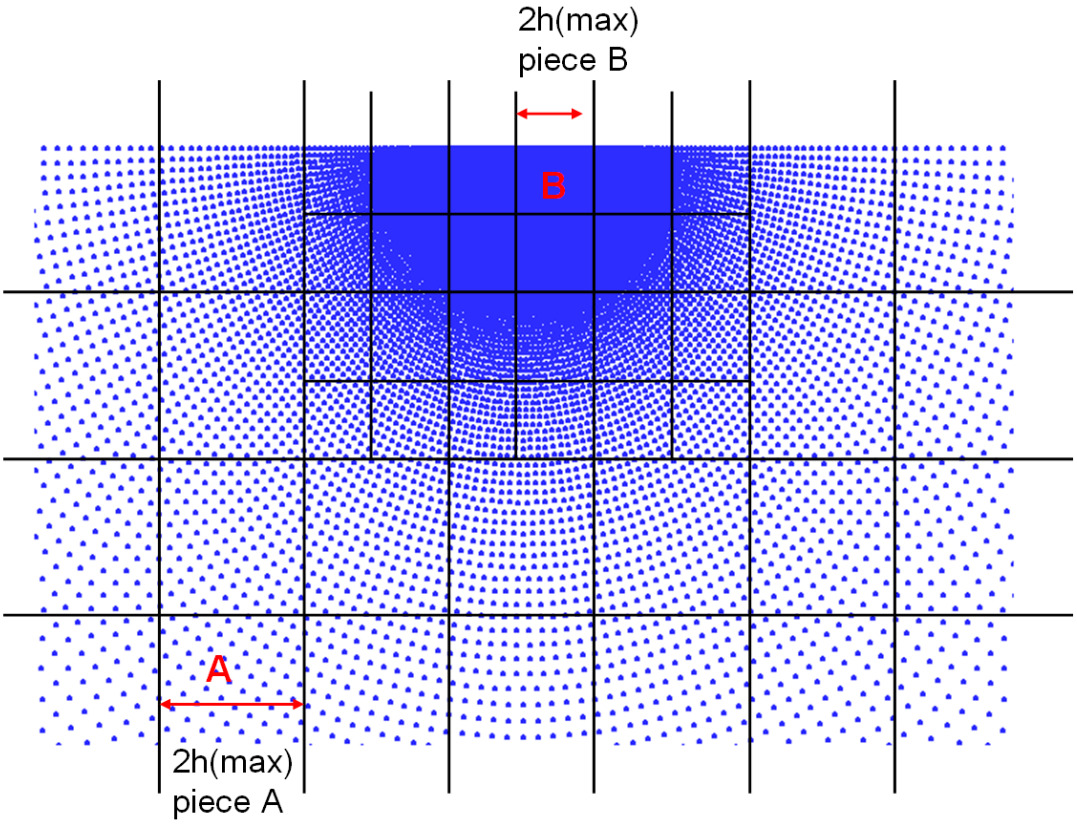

Fig 3.8 Neighbor search strategy with variable smoothed length

The developed code is actually organized in simple independent subroutines, without requiring any temporary storing within a time step.

3.3 SPH Euler Equations

In modeling free surface flows with high fragmentation, the Smoothed Particle Hydrodynamics (SPH) method has provided good results when used to simulate sloshing and flooding problems.

The advantages of SPH can be summarized as follow: SPH is conceptually both simple and easy for coding. The Lagrangian nature of SPH means that changes in density and flow morphology are automatically accounted for without the need for mesh refinement or other complicated procedures.

Here is the description of SPH strategy developed to simulate Euler equations.

Governing equations

The governing equations for fluid flow are the mass and momentum conservation. In Lagrangian form, these governing equations can be written as

$$\frac{1}{\rho}\frac{D\rho}{Dt} + \nabla \cdot u = 0 \tag{3.34}$$

$$\frac{Du}{Dt} = -\frac{1}{\rho}\nabla p + g + \nu\nabla^2 u \tag{3.35}$$

where ρ is the fluid particle density; t is time; u is the particle velocity; p is pressure at the particles; g is gravitational acceleration; and ν is the kinematic viscosity.

Without viscosity ν, Equation (3.35) will become Euler form

$$\frac{Du}{Dt} = -\frac{1}{\rho}\nabla p + g \tag{3.36}$$

Although Equation 3.36 could be converted straight into SPH form the equation will be asymmetric in particles i and j which means the momentum will not be accurately conserved. Instead, we use

$$\frac{\nabla p}{\rho} = \nabla(\frac{p}{\rho}) + \frac{p}{\rho^2}\nabla\rho \tag{3.37}$$

Then, the momentum equation in SPH form will be

$$\frac{Du_i}{Dt} = \sum m_j \cdot (\frac{p_j}{\rho_j^2} + \frac{p_i}{\rho_i^2}) \cdot \nabla W_j(x_i) \tag{3.38}$$

The linear and angular momentum is conserved exactly.

For compressible flows in SPH, density can be determined by simple summation

$$\rho_i = \sum m_j W_{ij} \tag{3.39}$$

When calculating the density on the surface, the result will become incorrect because the density falls discontinuously to zero.

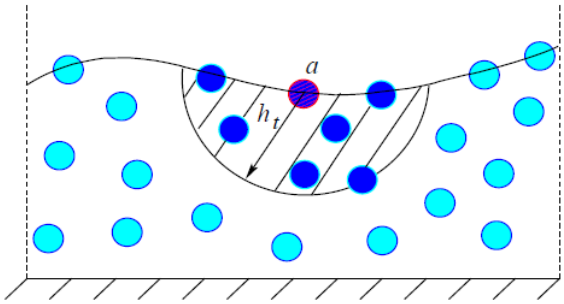

Fig 3.9 Lack of neighbor particles on the free surface

Instead, density is determined with the continuity equation (3.34). In SPH form, it is

$$\frac{D\rho_i}{Dt} = \sum m_j \cdot (u_j - u_i) \cdot \nabla W_j(x_i) \tag{3.40}$$

Having a differential equation for ρ means that it can be updated at the same time as other particle quantities and only one pass over the particles is required to obtain all the required information. Also, it can be helpful to improve the pressure field if using Equation (3.40) for several time steps and then correct the density by Equation (3.39).

If we move the particles with the velocity of the fluid, then

$$\frac{Dx_i}{Dt} = u_i \tag{3.41}$$

Monaghan (1989) suggested moving the particles with an average velocity of neighboring particles to keep an orderly arrangement of particles which is called XSPH.

Particles are moved according to

$$\frac{Dx_i}{Dt} = u_i + \varepsilon \sum \frac{2m_j}{(\rho_i + \rho_j)} (u_j - u_i) W_{ij} \tag{3.42}$$

Where, typically, $\varepsilon = 0.5$ for multi-phase flows, if particle i is near the interface, XSPH correction will lead to wrong results because the mean density is wrongly evaluated in Equation 3.42. In our simulations, XSPH correction is only computed

without considering the influence of other phase.

Equation of state

In order to close the Euler equations, equation of state (EOS) is introduced to determine the pressure from density which is given as $p = p(\rho) + C$. This involves the assumption of a *weakly-compressible* fluid which is not always true in most of hydrodynamic problems. However, if the deviations of local density from the reference fluid density are sufficiently small, this type of error is negligible. Moreover, the use of EOS avoids solving pressure from the Poisson equation. As a result, the interaction of the code is explicit which only requires small memory occupation proportional to the number of particles and it could be extended to parallel program easily.

The first equation of state used in the present SPH code is derived from internal potential energy. We use J to denote the volume ratio between the initial and current state of the material. J is defined as

$$J = \frac{V}{V^0} = \frac{\rho^0}{\rho} \tag{3.43}$$

The pressure is evaluated from

$$p = -\frac{dU}{dJ}, \tag{3.44}$$

Where $U = \frac{1}{2}\kappa(J-1)^2$ is for elastic solids and κ denotes the bulk modulus. Hence, the pressure can be derived from the change of density directly

$$p = -\kappa(\frac{\rho_0}{\rho} - 1) \tag{3.45}$$

The pressure is thus proportional to the change of the density and the bulk modulus of the fluid. Water is almost incompressible and the actual bulk modulus for water is

2.2GPa. The sound wave is approximately 1500m/sec and this yield a very small time step as the Courant stability requirement has to be met.

In the present problem, the velocities of particles are much smaller than the sound speed of the water. Batchelor (1973) gives an equation of state for water, which describes sound waves accurately, *i.e.* Equation (3.46),

$$p = \kappa[(\frac{\rho}{\rho_0})^{\gamma} - 1] \tag{3.46}$$

with $\gamma = 7$. The density variation in fluid flow is proportional to the square of Mach number, M. An estimation of the upper bound of the velocity of the particles is

$$v = \sqrt{2gH} \ . \tag{3.47}$$

Monaghan 1992 shows 0.1 is a good estimation of Mach number for this problem and using Equation (3.47) as estimation for sound speed. The bulk modulus, κ , is re-evaluated as

$$\kappa = \frac{200gH\rho}{\gamma} \tag{3.48}$$

This artificial bulk modulus is much lower than the actual value of 2.2Gpa, but it works much more efficient because the time step is inversely proportional to the bulk modulus. Moreover, the deformation result is also realistic.

This algorithm is rather robust particularly for large free-surface deformation and relatively easy for coding.

Alternatively, implicit algorithms depending on solver of the Poisson Equation are shown by some author to present exactly incompressible fluids (Koshizuka & Oka 1996, Cummins & Rudman 1999). Although enhanced stability are shown in these paper and their incompressible implicit method allow larger time step for interaction, they lost the native advantages to deal with free surface flow, especially high deformation free surface in slamming, sloshing and flooding because they have to

check the particles whether they are close to free surface or not. Two-phase implicit model could solve this problem but the calculation cost is not acceptable for our large scale computation because the very small density ratio of water and air will lead to much lesser time step to keep the stability between fluid particles and air particles on free surface.

3.4 Viscosity

Basic SPH formulism suffers the absence of dissipation of energy. In order to increase the stability of SPH, an additional term Π_{ij} is introduced in the momentum equation to model the dissipation due to viscous forces. Many forms of artificial viscosity (Balsara 1995, Morris 1997) have been proposed, but as the present study are built to capture the violent fluid dynamic, the most commonly used artificial viscosity is obtained by writing the momentum equation as

$$\frac{dv_i}{dt} = -\sum_j m_j \left(\frac{P_j}{\rho_j^2} + \frac{P_i}{\rho_i^2} + \Pi_{ij}\right)\nabla_i W_{ij} \tag{3.49}$$

Where Π_{ij} is given by

$$\Pi_{ij} = \begin{cases} \dfrac{-\alpha\mu_{ij}(c_i + c_j)}{(\rho_i + \rho_j)} & v_{ij} \cdot r_{ij} < 0; \\ 0 & v_{ij} \cdot r_{ij} > 0; \end{cases} \tag{3.50}$$

$$\mu_{ij} = \frac{h v_{ij} \cdot r_{ij}}{r_{ij}^2 + \eta^2 h^2} \tag{3.51}$$

Where $v_{ij} = (v_i - v_j)$ and $r_{ij} = (x_i - x_j)$. The expression for Π_{ij} contains a term that is linear in the velocity differences, which produces a shear and bulk viscosity. Typical value used for η is 0.1. The coefficient α denotes kinematic viscosity whose influence has been checked in the range 0.005-0.03. The best choice of α should keep stability of the results with acceptable energy dissipation. For instance for verification case of dam break, $\alpha = 0.03$ was chosen.

3.5 Tensile Stability

The tensile stability in SPH results in a clustering of particles. The clustering can be found in the cases if the particles carry negative pressure. Monaghan (2000) suggested using a small repulsive corrective term applied in the momentum equation. The pressure gradient term is modified accordingly to

$$\frac{P_i}{\rho_i^2}+\frac{P_j}{\rho_j^2}\rightarrow\frac{P_i}{\rho_i^2}+\frac{P_j}{\rho_j^2}+Rf_{ij}^n \tag{3.52}$$

The factor R can be determined by relating it to the pressure

$$R=R_i+R_j \tag{3.53}$$

And

$$R_i=\frac{\varepsilon|P_i|}{\rho_i^2}\ \text{ if }\ P_i<0 \tag{3.54}$$

otherwise $R_i=0$. A typical value of ε is 0.2 though the appropriate value depends on smooth length, n and the number of spatial dimensions.

Monaghan also suggested a slight force if $P_i>0$ and $P_j>0$ as the particles have the tendency to form local linear structures.

$$R=0.01(\frac{P_i}{\rho_i^2}+\frac{P_j}{\rho_j^2})\ \text{ if }\ P_i>0\ \text{ and }\ P_j>0 \tag{3.55}$$

Function f_{ij} is defined with respect to the kernel

$$f_{ij}=\frac{W_h(r_{ij})}{W_h(\delta r)} \tag{3.56}$$

In this corrective term, n must be positive with typically value 4 and δr is determined from initial distance between particles. Monaghan established that the repulsive force between two particles is about 20 times larger if the distance r_{ij} decreases from δr to 0 and decreases rapidly if the distance is larger than smooth length. Only nearest neighbors particles are influenced by the artificial pressure. This makes the calculation simple and accurate.

4 Boundary conditions

4.1 Introduction

If one wants to describe physical behavior of a material using strong form, the partial differential equations of continuum mechanics have to be completed by initial and by boundary conditions. SPH has the advantage in the case of free boundary condition, while the implementation of solid boundary conditions is a drawback for SPH. The treatment of solid boundary is one of the critical problems in the research of nonlinear free surface flows. In this chapter, different strategies of boundary conditions are introduced and discussed in detail.

4.2 Free boundary: kinematic and dynamic condition

As a basic idea of SPH, the particles are actual material element. The particles along the free surface at any given time instant will remain there. In conclusion, using Lagrangian tracking of particles will fulfill implicitly the kinematic free surface boundary condition.

Moreover, concerning about dynamic condition on free surface, the pressure field will fall to zero when approaching the free surface which also means the dynamic free surface boundary condition is implicitly fulfilled. However, high frequency pressure oscillation is observed because of weak compressibility (sound waves) of fluid. As an alternative, the pressure condition can be enforced to be zero along the free surface and using incompressible SPH with solving Pressure Poisson Equation. This method will become more complex and require the explicit capturing of the particles on the free surface that is still problematic especially in the case of high deformation and fragmentation of free surface. In another words, the greatest advantage of SPH will be

lost.

4.3 Solid boundary

In SPH method, in order to apply the correct solid boundary conditions for the equations in the SPH formulation, the detection of boundary particles is needed to impose correct boundary conditions on these particles. Concerning bounded domain problems, there are several strategies and mathematical artifacts that allow for modeling the presence of boundaries with different degrees of accuracy.

- Lennard-Jones Forces

The Lennard-Jones form for a boundary particle force is based on known forces between molecules (Monaghan 1994). The non-penetration boundary condition is enforced by these repulsive forces acting on the particles close to solid boundary. For a boundary and fluid particle separated by a distance r, the force per unit mass $f(r)$ has the Lennard-Jones form

$$f(r) = D((\frac{r_0}{r})^{p1} - (\frac{r_0}{r})^{p2})\frac{r}{r^2} \tag{4.1}$$

The Lennard-Jones force is purely repulsive and is set to zero if $r > r_0$, where r_0 is the initial particle spacing. The p constants must satisfy $p1 > p2$, and coefficient D was chosen by considering the physical configuration. For example, $p1 = 4$, $p2 = 2$ and $D = gH$ could be taken where H is initial water depth.

- Boundary Particle Forces

Another way to simulate boundary force is boundary particle forces. This force is based on the SPH kernel and it seems appropriate because the pressure forces involve

the gradient of the kernel (Monaghan 1995). A suitable form is,

$$f(r_\perp) = vc^2 \begin{cases} \frac{2}{3h} & if \quad 0 < \frac{r_\perp}{h} < \frac{2}{3} \\ \frac{r_\perp}{h^2}(2 - \frac{3r_\perp}{2h}) & if \quad \frac{2}{3} < \frac{r_\perp}{h} < 1 \\ \frac{1}{2h}(2 - \frac{r_\perp}{h})^2 & if \quad 1 < \frac{r_\perp}{h} < 2 \\ 0 & if \quad 2 < \frac{r_\perp}{h} < \infty \end{cases} \tag{4.2}$$

Where $r_\perp$ is the perpendicular distance between the fluid particle and the boundary particle and v is a free parameter which determines the strength of the boundary force, typically $v = 0.01$.

In order to apply smooth force from discretized boundary particles, Monaghan (1995) introduced a new method consisting of assigning each boundary particle a normal direction n and then calculating the perpendicular $r_\perp$ and tangential $r_=$ distances to fluid particles. The boundary force F proposed by Monaghan is

$$F = f(r_\perp)P(r_=)n \tag{4.3}$$

$$P(r_=) = \begin{cases} \frac{1}{2}(1 + \cos(\frac{\pi r_=}{\Delta p})) & if \quad |r_=| < \Delta p \\ 0 & if \quad |r_=| \geq \Delta p \end{cases} \tag{4.4}$$

- Dummy particles and Ghost particles boundary conditions

Both Lennard-Jones force and boundary particles force suffer the problems of disorder near the boundary. The boundary force is only dependent on the distance from the fluid particle to solid boundary without considering the gradient of velocity or pressure of the particles. In another words, a stationary fluid particle with high pressure is given the same boundary force as a fluid particle with low pressure.

Ghost particle boundary conditions are then proposed to take pressure and velocity into account. The basic idea is to simulate the boundary with several layer of ‘ghost

particle' which also carries pressure and velocity as fluid domain. These ghost particles are included in the calculation of neighbor search, momentum and continuum equations. There are two major ideas of ghost particles boundary condition, one of them is dummy particles boundary conditions.

Dummy particles are defined to satisfy the wall boundary no penetration condition. Several layers of ghost particles are lying within some specified distance (smoothing length) from the boundary. They carry the attributes with time history like fluid particles but the position is fixed and velocity is zero at every time step. The effects of the fictitious 'ghost' particles are explicitly included in the summation for the fields and for their gradients.

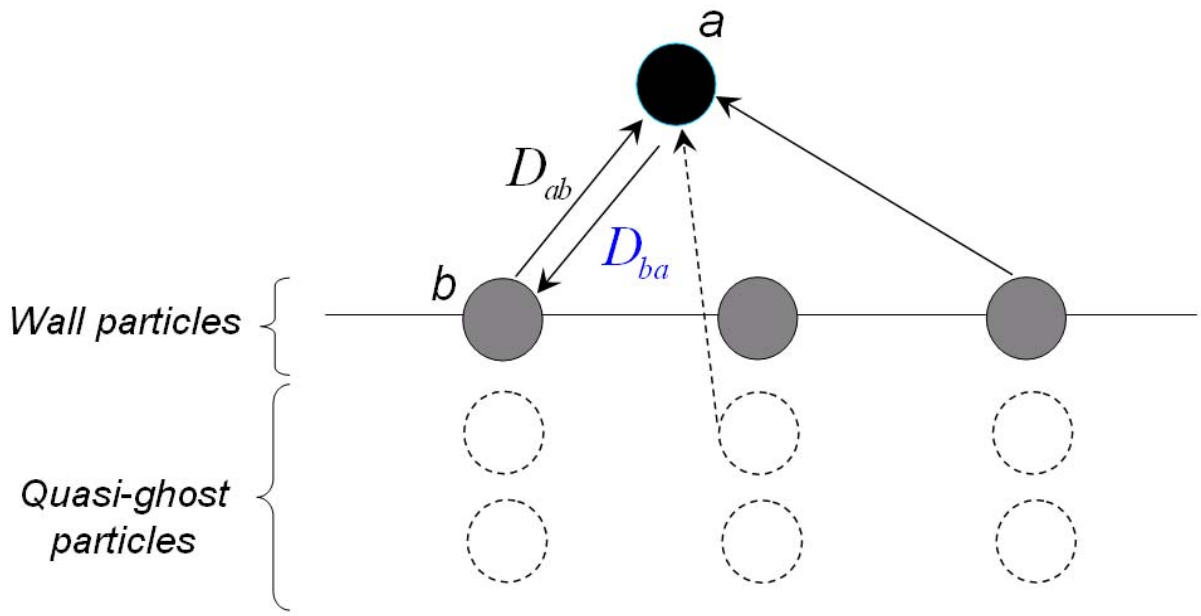

Fig 4.1 dummy particles

D_{ab} means the internal force on particles are due to ghost particles which depend on the pressure gradient.

Dummy particles can provide some accurate results in our tests but they disturb the fluid domain excessively. Alternatively dynamic ghost particles boundary conditions are available for the tests which offer some additional accurate results particular in the pressure evaluation on the boundary. Different from dummy particles, dynamic ghost

particles are mirroring particles from fluid domain near the wall boundary and they carry the same attributes as the fluid particles but the opposite velocity in normal direction of wall boundary.

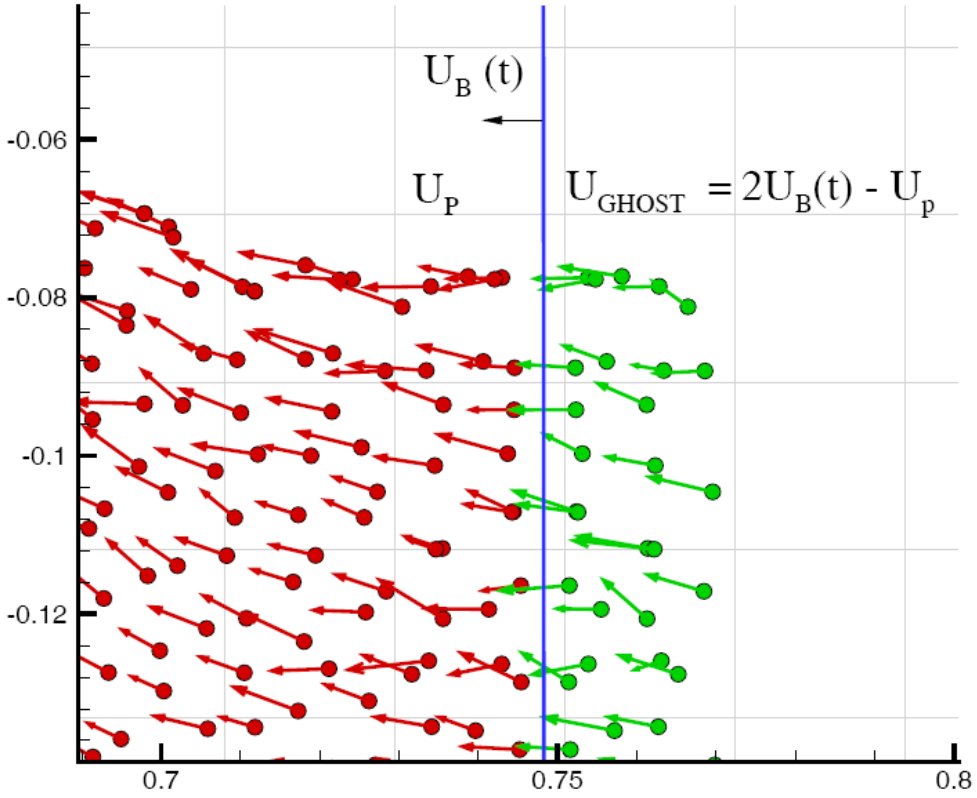

Fig 4.2 dynamic ghost particles

Consider a plane wall, as in figure 3. At each time step, all the particles within a layer with thickness $3h$ from the wall are mirrored inside the body. The characteristics given to the ghost particles are

$$x_{iG} = 2x_w - x_i$$

$$u_{niG} = 2U_{nw} - u_{ni}$$

$$p_{iG} = p_i$$

$$u_{tiG} = u_{ti} \qquad (4.5)$$

Where u_n and u_t are, respectively, the tangential and normal velocity components

to the solid boundary, and U_{nw} is the local displacement velocity of the solid boundary with instantaneous position x_w.

Unlike the free surface, the solid boundaries require special care and the no-penetration condition must be imposed. Ghost particles method still suffers the problem of penetration problem somewhere because of the tensile instability, so we constrain the fluid particles' motion when it is too close to the boundary. The typical distance $h(i)$ from fluid particle i to its mirror ghost particle g is the smooth length.

$$\left|\vec{r}_{ig}\right| = h(i) \quad \text{if} \quad r_{ig} < h(i), \tag{4.6}$$

and

$$\vec{v}_{ig} \cdot \vec{r}_{ig} = 0 \quad \text{if} \quad \vec{v}_{ig} \cdot \vec{r}_{ig} < 0 \tag{4.7}$$

Where $\vec{r}_{ig}$ and $\vec{v}_{ig}$ denote the relation between fluid particle i its mirror particle g

Ghost particle boundary condition is adopted in most of our test cases because it could offer more accurate results particularly for evaluation of local pressure. However, it will be difficult to handle the complex geometry particularly when containing convex and concave sharp corner. Corrections have to be enforced to avoid an excess or loss of ghost mass. Actually, in the application of SPH in ship hull case, the geometry could be believed to be sufficiently smooth. In the latter chapter, approximate solid boundary based on dynamic ghost technique will be introduced to simulate arbitrary complex geometry.

4.4 Comparison of Results

As previously outlined, four different methods that are used to deal with solid

boundary condition are dedicated to SPH simulation.

1. L-J force
2. Boundary force
3. dummy boundary particles
4. dynamic ghost particles

The present chapter is dedicated to show the comparisons between these methods in the simulations of free surface flow.

The first case analyzed concerns the accuracy and stability of particles pressure in a static tank under gravity effects. Since the particles mostly remain immobile, the pressure of single particle could represent the local pressure of the fluid. Two single particles are firstly monitored in the calculation with single point I, which is the particle on the left corner of the bottom and single point II is on the middle of the bottom.

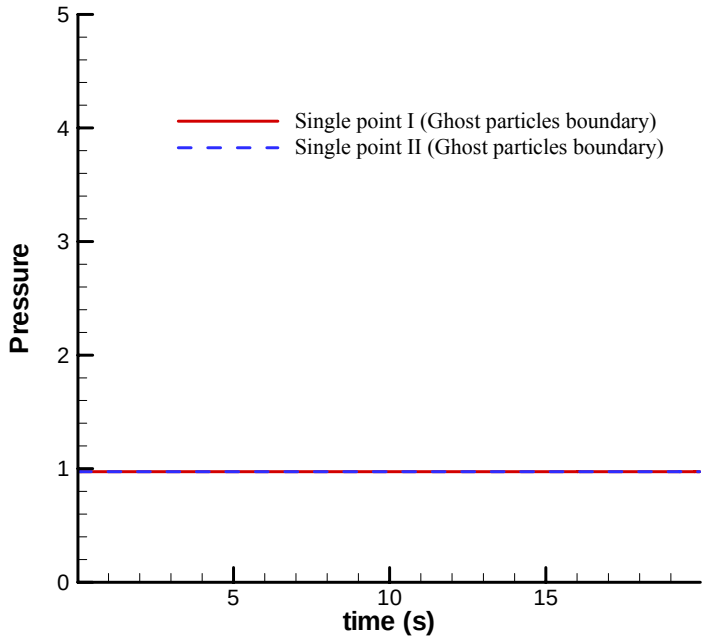

Fig 4.3 Pressure of particles with Ghost particle boundary

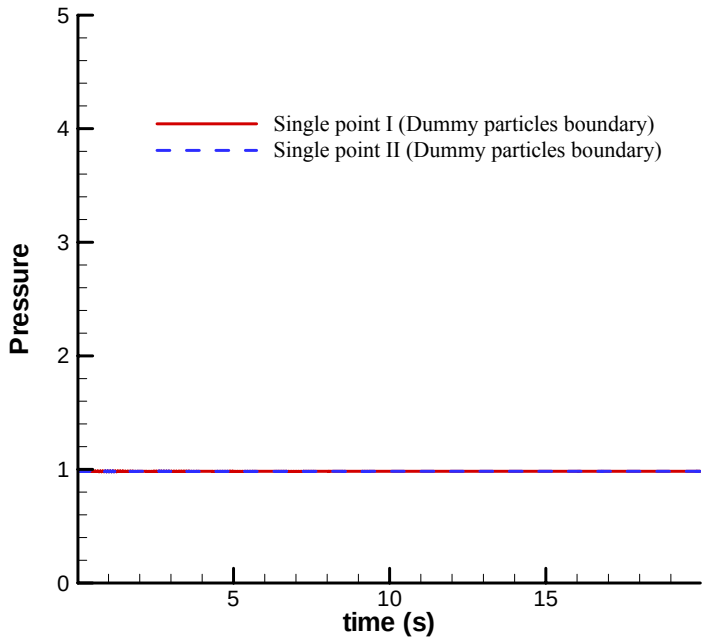

Fig 4.4 Pressure of particles with Dummy particle boundary

The theoretical value of pressure on the bottom of the tank is ρgD, where ρ is the density of the fluid, g is the gravity and D is water depth. In Fig 4.3 and 4.4, the dummy particles or ghost particles can provide very accurate and stable values of pressure (Normalized by $P/\rho gD$) in time series.

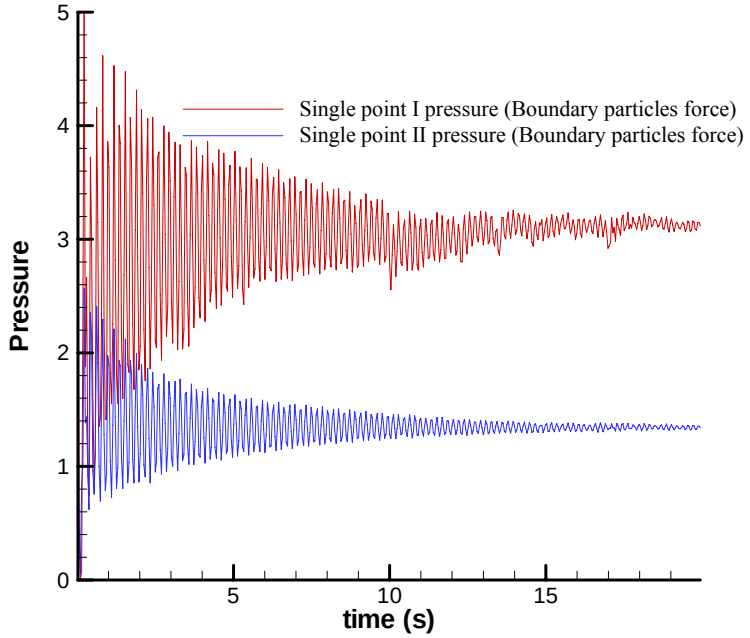

Fig 4.5 Pressure of particles with Boundary particles force

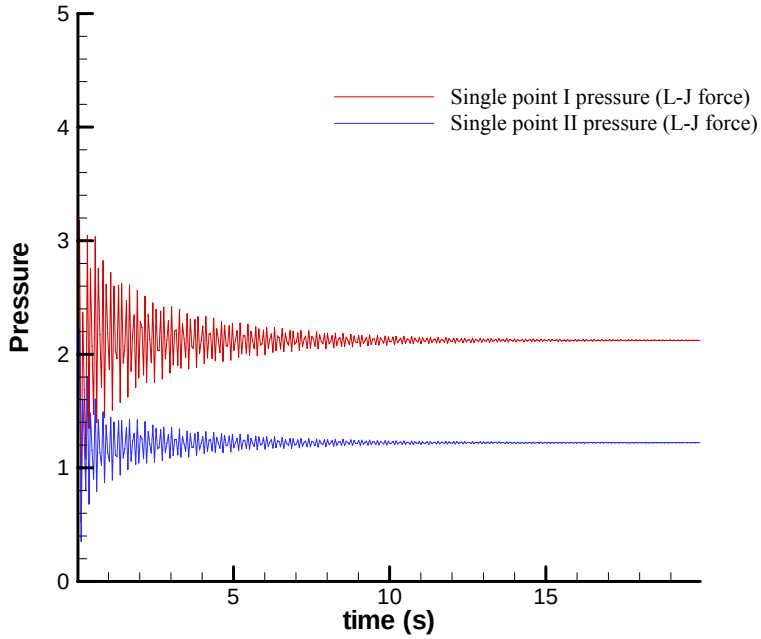

Fig 4.6 Pressure of particles with L-J force

In the simulations using Boundary particles force and L-J force with typical chosen parameter as solid boundary conditions (Fig 4.5-4.6), the pressure values of particles on the bottom were found oscillatory and much larger than theoretical value. The artificial forces that only depend on the distance between fluid particle and boundaries

will significantly disturb the particles that are very close to boundary. Although initialization of particles with damping can reduce the oscillation and the error of single fluid particle depends on the chosen parameters, the particles close to boundaries are inevitably irregular (Fig 4.7-4.9).

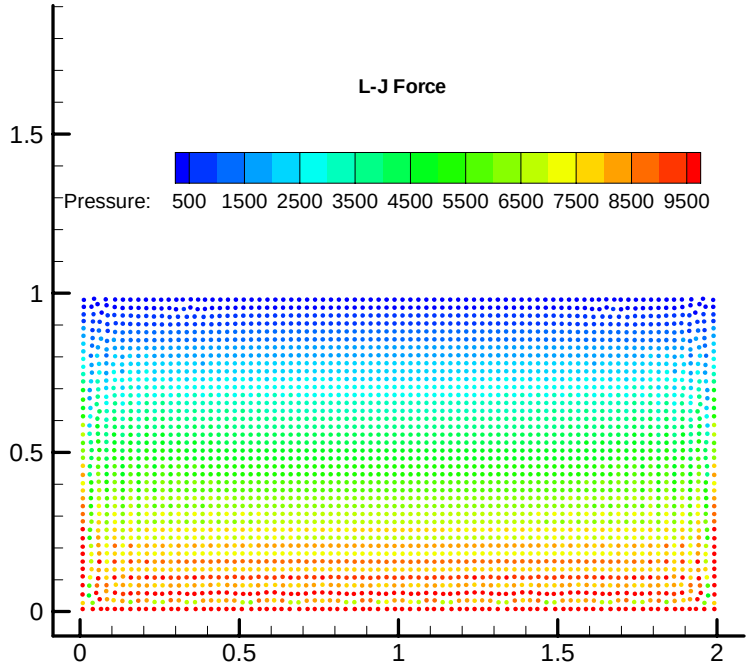

Fig 4.7 Particles position at time t=10s (L-J force)

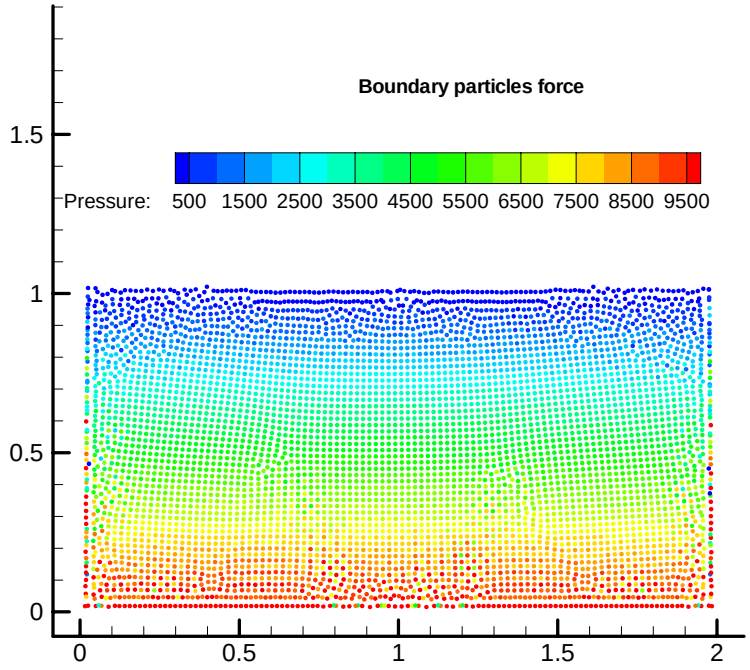

Fig 4.8 Particles position at time t=10s (Boundary particles force)

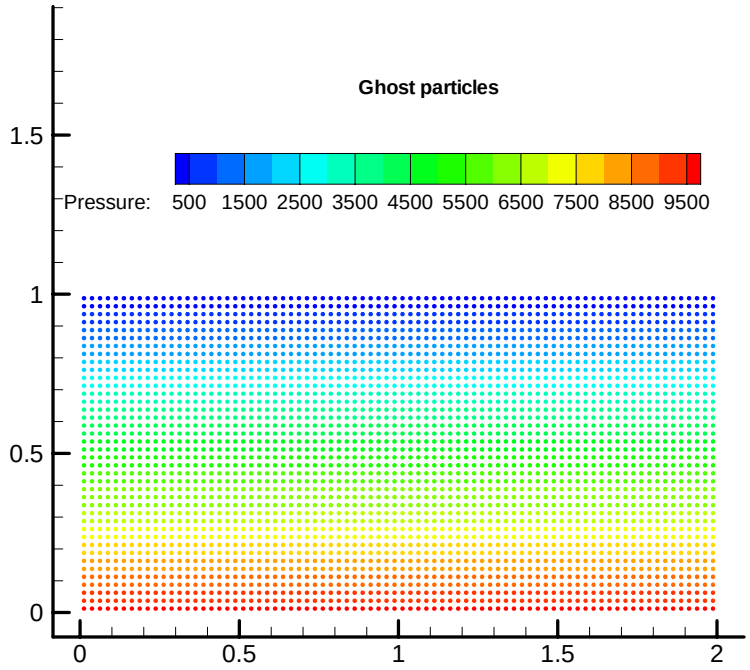

Fig 4.9 Particles position at time t=10s (Ghost particles)

However, if the pressure is evaluated with integral of neighbor particles instead of a single particle, the value of pressure is still correct (Fig 4.10).

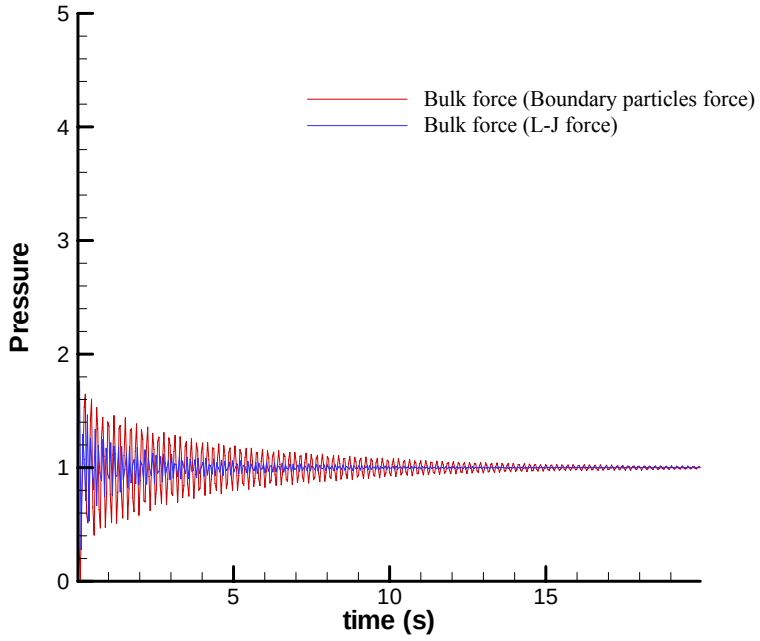

Fig 4.10 Bulk force of static tank (Boundary particles force and L-J force)

The second case is illustrated by considering 2D flow generated after the breaking of a dam, as sketched in Fig 4.11. This case concerns the accuracy of flow evolution and impact force under different boundary conditions. A vertical wall is placed at a given distance from the broken dam, and the fluid flowing along the dry deck then impacts against it eventually. The simulations were performed four times with different boundary conditions.

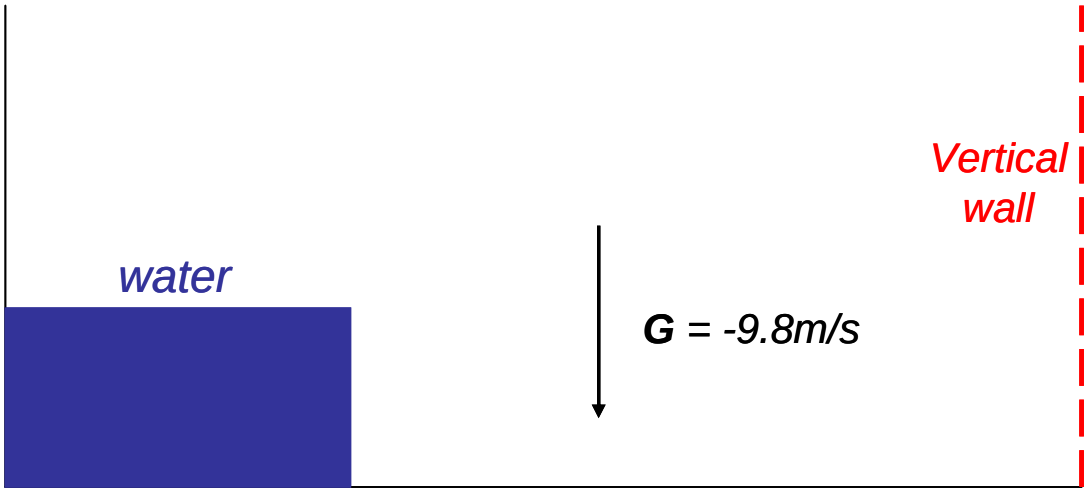

Fig 4.11 Dam break problem and impact against a vertical rigid wall

Firstly we study this case before fluid impact. Fig 4.12 gives the propagation in time of the water-front toe after the dam break. All boundary conditions offer the numerical results which agree with each other very well. As expected, although L-J force and Boundary particles force significantly disturb the fluid particles close to boundaries, the total fluid evolution is still acceptable.

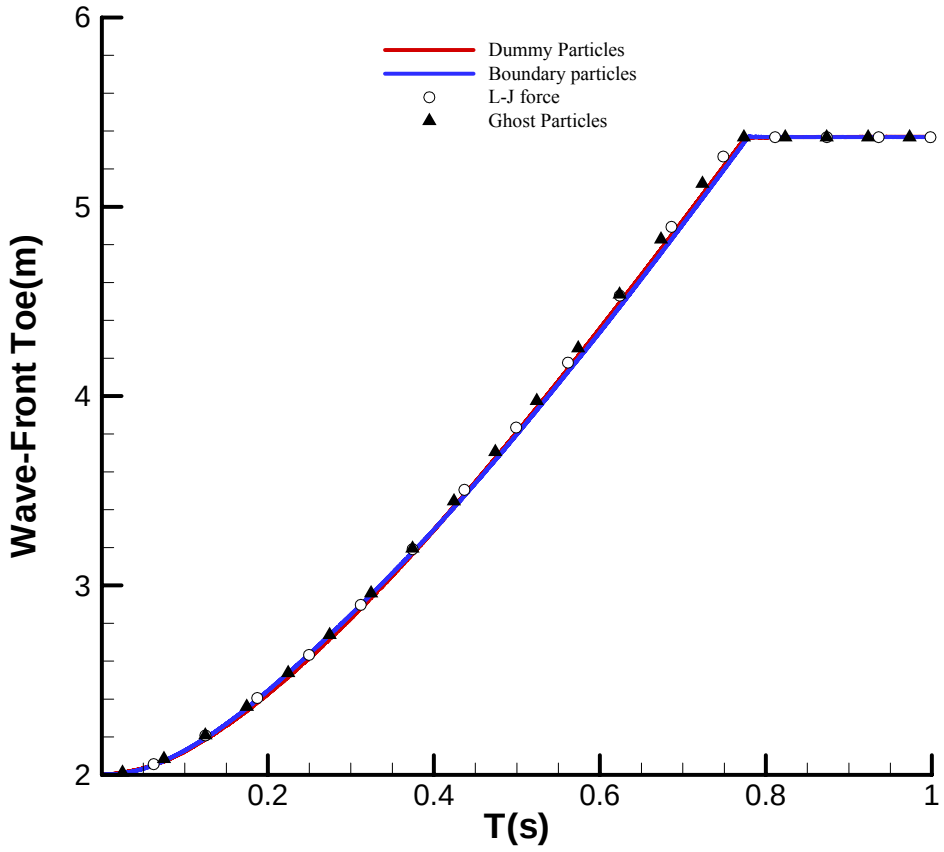

Fig 4.12 time evolution of wave front toe

In the research of nonlinear free surface flow, the interaction between solid and fluid is one of the most critical issues such as sloshing and slamming. In order to compare the stability and accuracy of four boundary conditions, impact forces on the vertical wall are evaluated.

The integral of pressure along the wall is commonly used to evaluate the response force due to fluid. However, it is not simple to catch the pressure value on the wall in particles method. There are three strategies that can be utilized to solve this problem. The first idea to extract the local pressure is kernel function convolution at the desired boundary point i

$$P(x_i) = \sum_{j=1}^{N} \frac{m_j}{\rho_j} P(x_j) W(x_i - x_j, h) \tag{4.8}$$

However, only few particles contribute in this procedure which gives some crude results.

The second strategy coming to the mind is to increase the number of particles. Aiming at estimating the local pressure at a given point M (Fig 4.13), the value is extracted by averaging the fluid particles in the near boundary area around M. The distance is typically chosen as $2h - 5h$

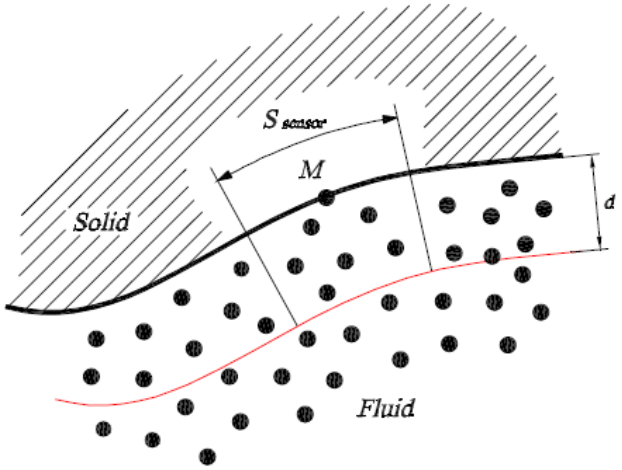

Fig 4.13 Sampling area

Then, the impact force on the wall is

$$F_w = \int_{wall} P_M dS_{sensor} \tag{4.9}$$

In meshless method, the solid boundary condition is always carried out with additional constraint force from boundaries to avoid fluid penetration. The third method to evaluate the force on the boundary is deduced from the summation of additional constraint forces.

Moreover, because of the explicit algorithm adopted in SPH method the pressure shows oscillations in time series, the larger number of particles distributed can reduce the amplitude of the oscillations. In our tests, 51,200 particles are used and the second (pressure integration) and the third (summation of boundary force) strategies are

adopted for comparison (Fig 4.14-4.21)

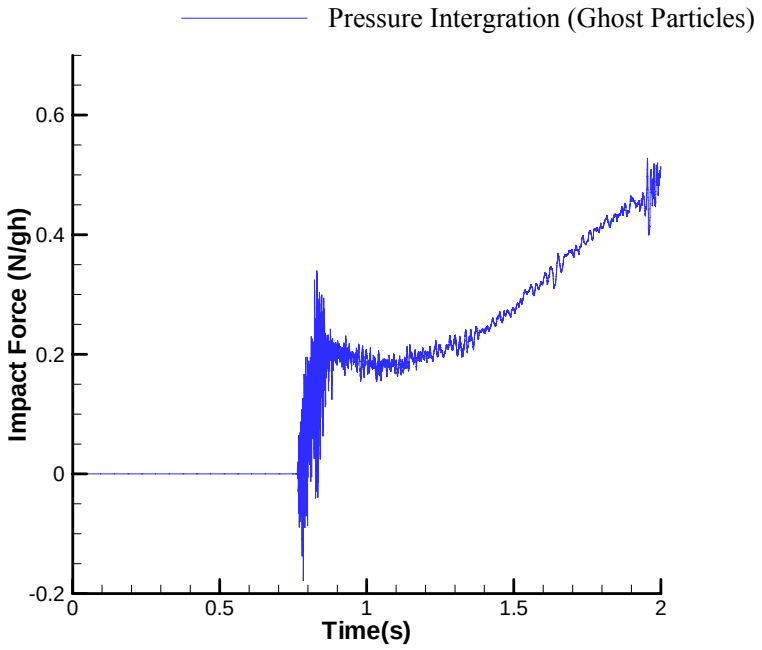

Fig 4.14 Pressure Integration (Ghost Particles)

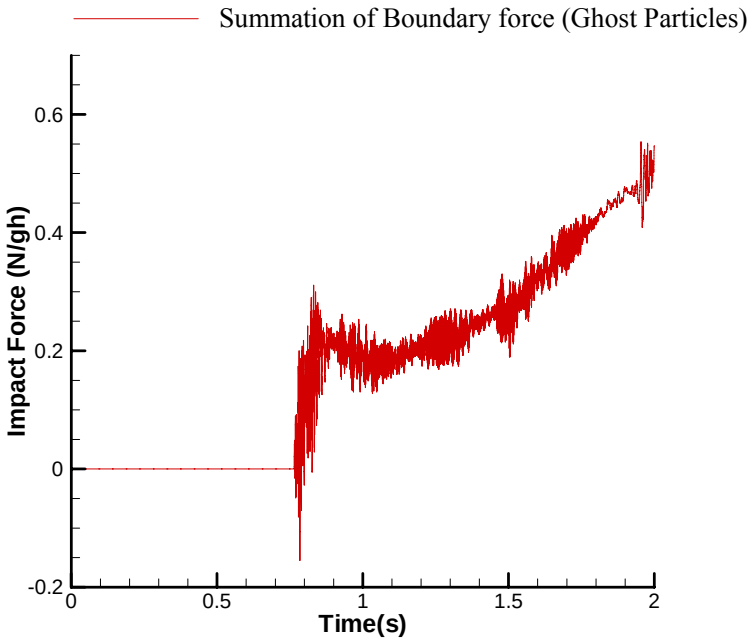

Fig 4.15 Summation of Boundary force (Ghost Particles)

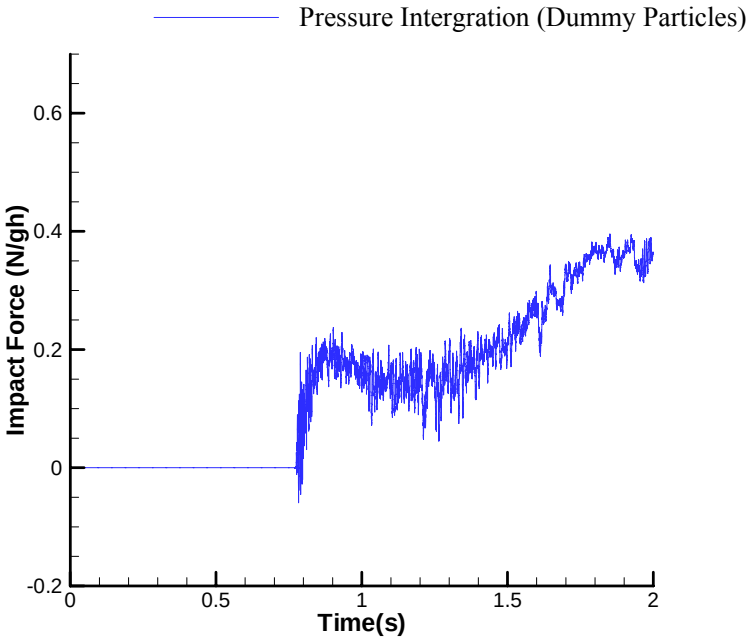

Fig 4.16 Pressure Integration (Dummy Particles)

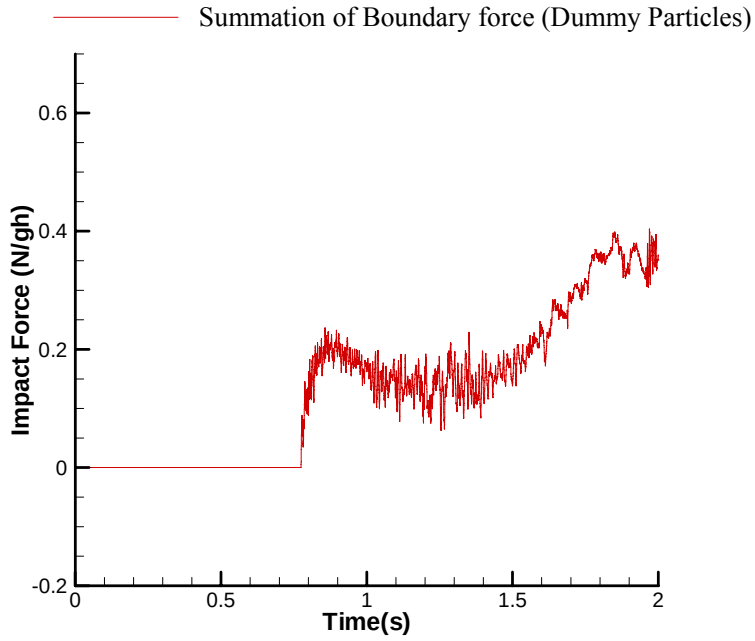

Fig 4.17 Summation of Boundary force (Dummy Particles)

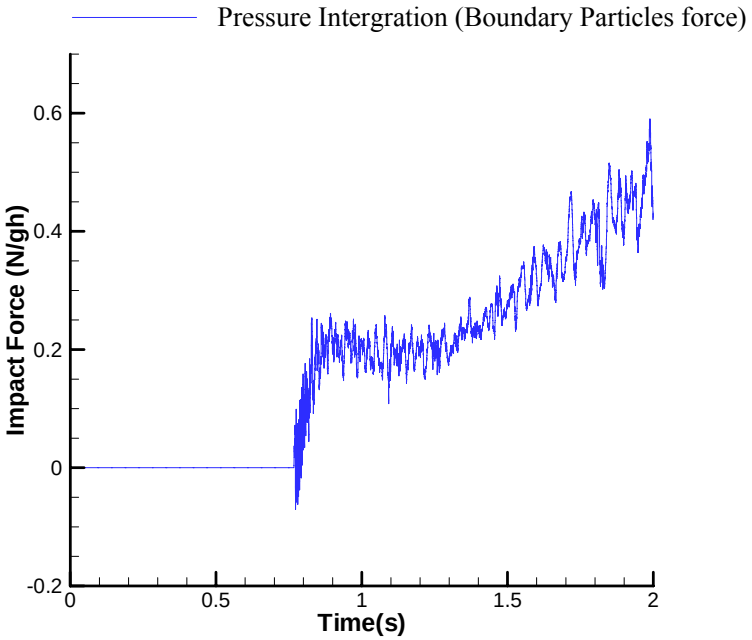

Fig 4.18 Pressure Integration (Boundary Particles force)

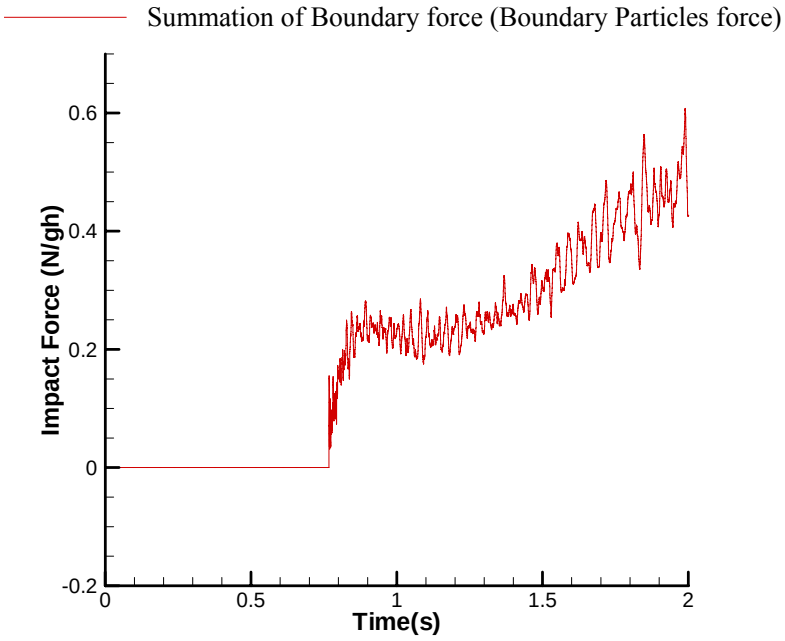

Fig 4.19 Summation of Boundary force (Boundary Particles force)

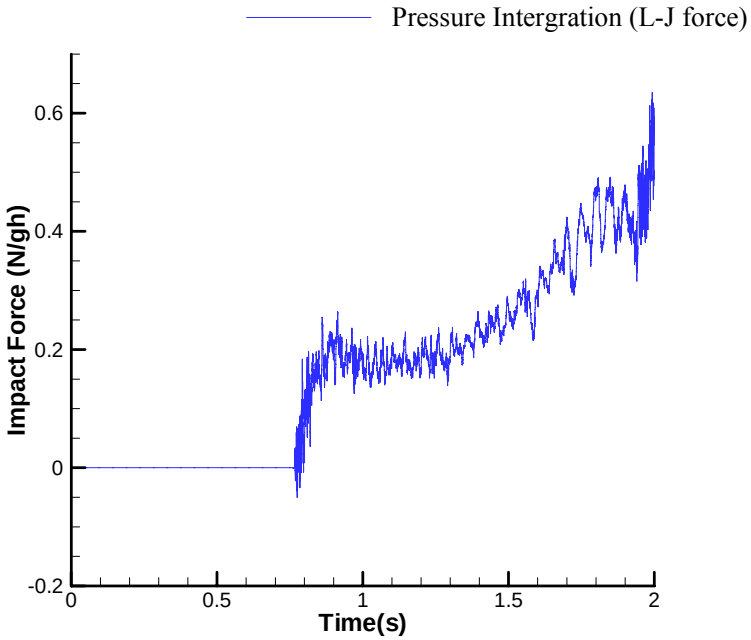

Fig 4.20 Pressure Integration (L-J force)

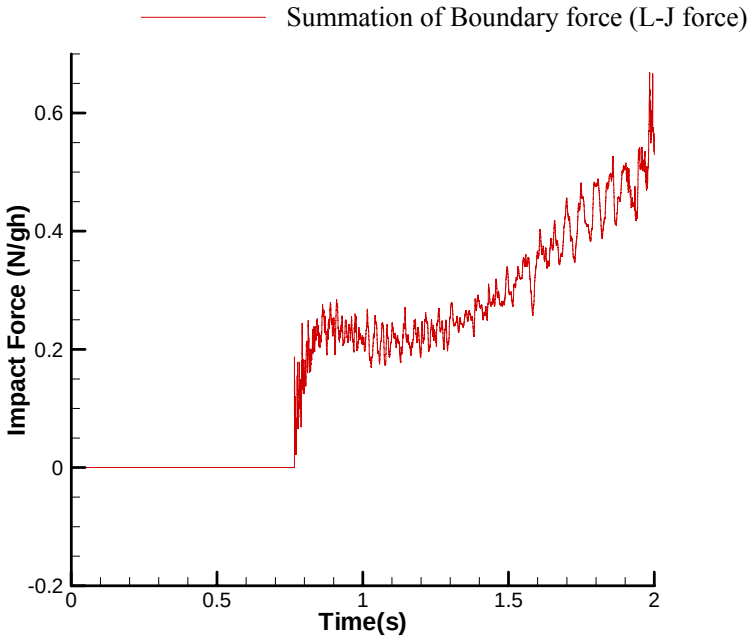

Fig 4.21 Summation of Boundary force (L-J force)

In comparison between Fig 4.14-4.21, Ghost particles and dummy particles shows additional steady impact force on the wall, but dummy particles have underestimated the value of impact force. This is because dummy particles imply non-slip boundary condition. Moreover, comparing Fig 4.14 and Fig 4.15 using ghost particles as

boundary condition, pressure integration gives additional smooth results than summation of boundary force. As a conclusion, ghost particles method is adopted as the solid boundary condition in latter study cases and pressure integration proves to be good technique to extract local pressure.

4.5 Approximated boundary for ghost particles

As previously outlined, ghost particles give steady and accurate results of local pressure but it will be difficult to handle the complex geometry (Fig 4.22). For instance, corrections have to be enforced to avoid an excess or loss of ghost mass on the convex or concave corner.

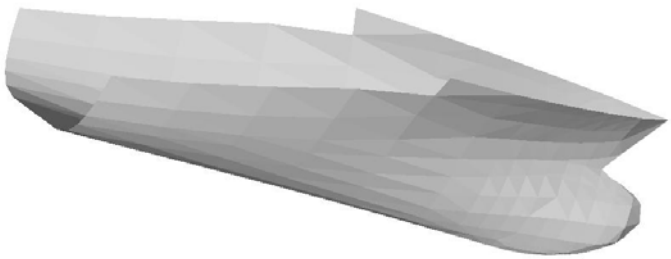

Fig 4.22 Complex 3D geometry

Ghost particles imply the knowledge of the local normal to the desired boundary, taking into account the position of the particle to be mirrored. However, in general case with complex curved surface, the mirror particle is very difficult to obtain. Here a method is proposed to extend the application of ghost particle technique to general geometry. The 3D boundary is decomposed into flat triangular panels. These panels are used to allow the capture of the particles to be mirrored easily. Equations (4.6, 4.7)

are still used at this time to prevent particles from penetrating the boundaries.

Consider a curved face (Fig 4.23), it is firstly discretized into many pieces of faces which are considered as flat face such as section 1 and section 3. The corner (section 2) between two flat faces may lead to excess ghost mass when mirroring fluid particles. However, if the number of flat faces is large enough, the corner will be negligible. Moreover, the flat face will be very approximate to curved face.

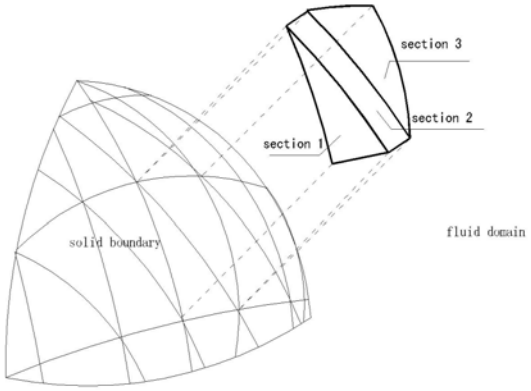

Fig 4.23 Approximation of complex geometry

This pre-processing of geometry is made by Gambit and the results are transferred to SPH code. The procedure to capture ghost particles on flat face is simple and each fluid particle is mirrored only once on the solid boundary.

To validate this specific method, the simple case is studied where a simple 2D circle immersed vertically into calm water. The circle made it possible to derive the exact ghost particles, and to compare with the approximated straight line. Compared with exact ghost particles, five different numbers of approximate pieces are proposed. The immersed part of the circle is divided into 2, 10, 40 and 200 pieces. The total vertical forces are monitored and compared with exact ghost particles and shown in Fig 4.24 - 4.28 respectively.

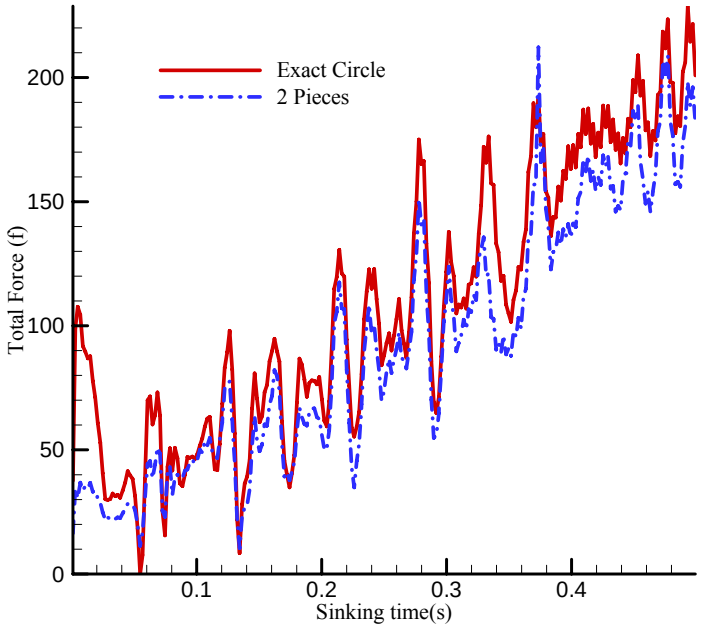

Fig 4.24 Total vertical force (2 pieces and exact)

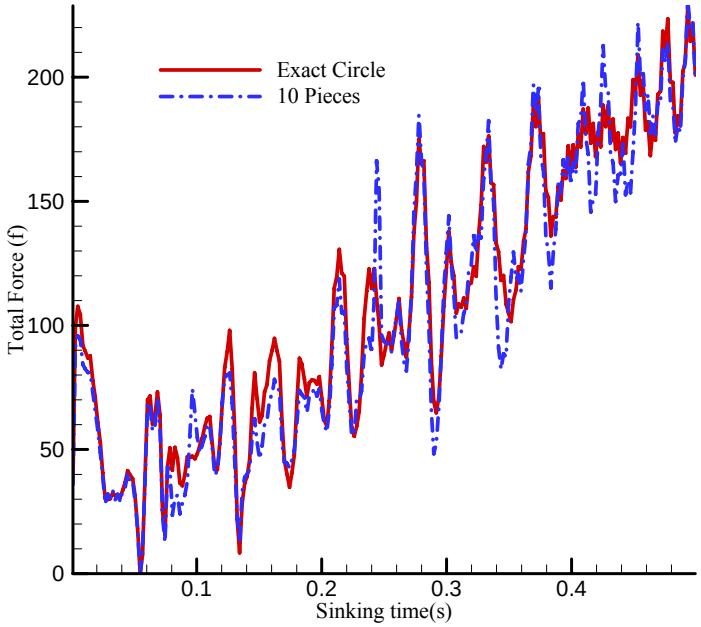

Fig 4.25 Total vertical force (10 pieces and exact)

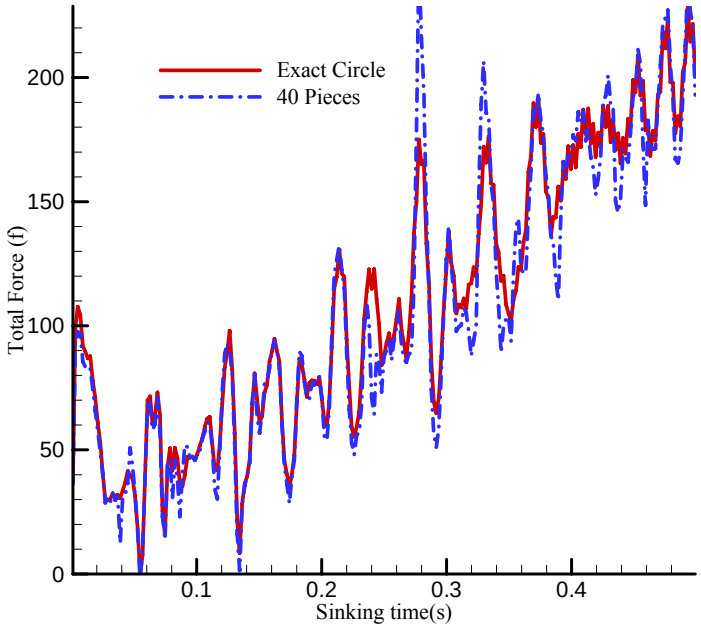

Fig 4.26 Total vertical force (40 pieces and exact)

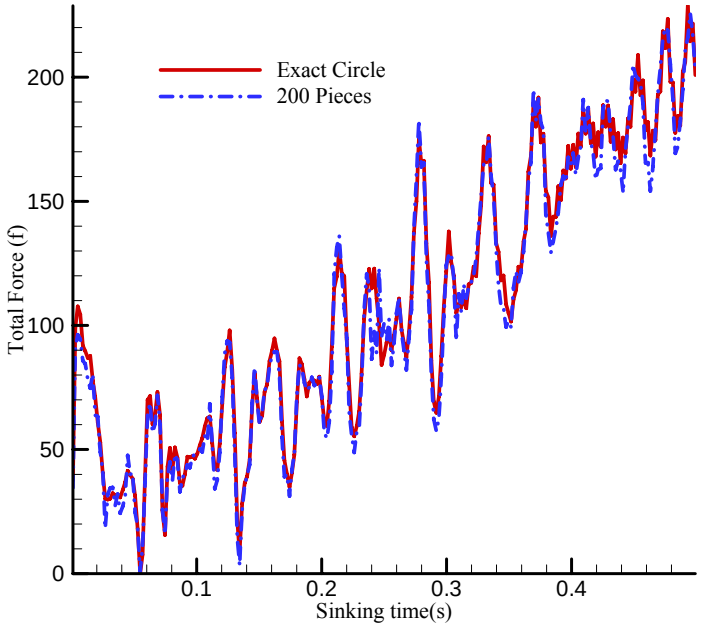

Fig 4.27 Total vertical force (200 pieces and exact)

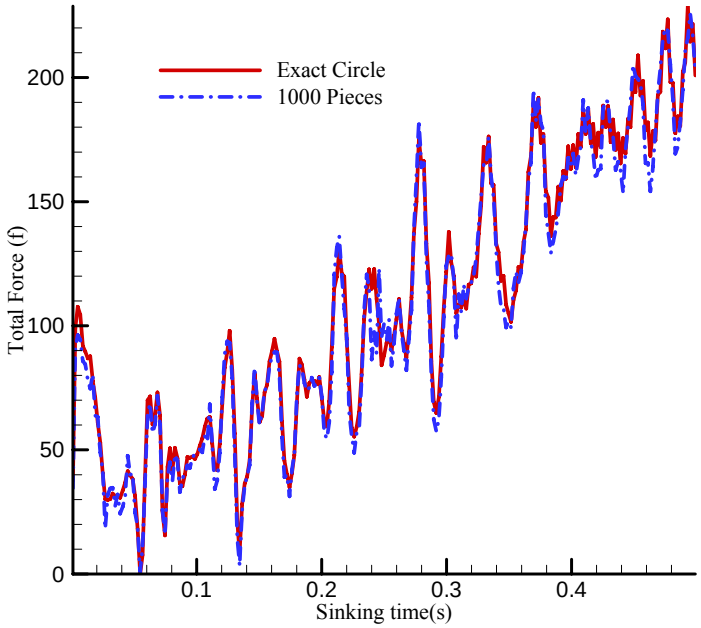

Fig 4.28 Total vertical force (1000 pieces and exact)

As great number of pieces is used to approximate the circle, the results are found to be very close to the 'exact one'. Despite of the quality of this simulation (oscillation caused by too small number of particles used), the initial distance between fluid particles is about 1/500 of immersed arc length, 200 pieces could provide identical results to the exact one, the maxima error of force at every single time step is less than 95% (Fig 4.29)

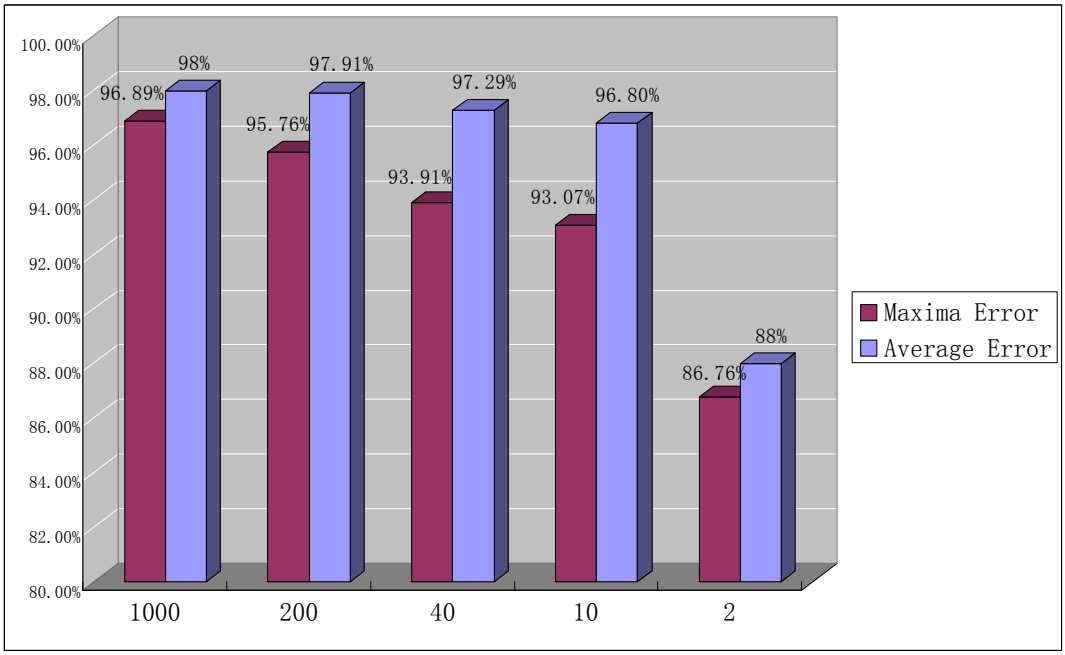

Fig 4.29 Average error and maxima error of total force compared to 'Exact circle boundary' (From left to right 1000, 200, 40, 10, 2 pieces)

5 Time evolution and Parallel SPH

5.1 Time stepping and evolution

The numerical integration of the ordinary differential equations for the physical variables at each particle can be carried out by standard methods with a time-step control that involves the courant condition, the force terms, and the viscous diffusion term. The time step should be defined following Courant Friedrichs Levy (CFL) condition based on the local smoothing length and local sound speed.

One of the most popular integration schemes applied to SPH is the Predictor Corrector Scheme. The following equations are used to obtain the field quantities at the next time step

$$\tilde{v}^{1/2} = v^0 + \frac{\Delta t}{2} f^0$$
$$\tilde{x}^{1/2} = x^0 + \frac{\Delta t}{2} v^0$$
$$\rho^{1/2} = \rho(\tilde{x}^{1/2})$$
$$f^{1/2} = f(\tilde{x}^{1/2}, \tilde{v}^{1/2}, \rho^{1/2}, ...)$$
$$v^{1/2} = v^0 + \frac{\Delta t}{2} f^{1/2}$$
$$x^{1/2} = x^0 + \frac{\Delta t}{2} v^{1/2}$$
$$x^1 = 2x^{1/2} - x^0$$
$$v^1 = 2v^{1/2} - v^0 \qquad (5.1)$$

Here, the superscripts refer to the time step index, and f is the force per unit mass.

Another scheme applied in codes is the fourth order *Runge-Kutta* method:

$$v^* = v^0 + \frac{\Delta t}{2} f^0$$

$$x^* = x^0 + \frac{\Delta t}{2} v^*$$

$$\rho^* = \rho(x^*)$$

$$f^* = f(x^*, v^*, \rho^*, ...)$$

$$v^{**} = v^0 + \frac{\Delta t}{2} f^*$$

$$x^{**} = x^0 + \frac{\Delta t}{2} v^{**}$$

$$\rho^{**} = \rho(x^{**})$$

$$f^{**} = f(x^{**}, v^{**}, \rho^{**}, ...)$$

$$v^{***} = v^0 + \Delta t \cdot f^{**}$$

$$x^{***} = x^0 + \Delta t \cdot v^{***}$$

$$\rho^{***} = \rho(x^{***})$$

$$f^{***} = f(x^{***}, v^{***}, \rho^{***}, ...)$$

$$v^1 = v^0 + \Delta t \frac{f^0 + f^* + 2f^{**} + 2f^{***}}{6}$$

$$x^1 = x^0 + \Delta t \cdot v^1$$

$$\rho^1 = \rho(x^1) \tag{5.2}$$

The time step should be chosen to accommodate the CFL condition. In SPH

$$\frac{h}{\Delta t} > c \tag{5.3}$$

However, if viscosity is present, it should be taken into account:

$$dt = \beta \min[\frac{h}{c_i(1 + 0.6\alpha)}] \tag{5.4}$$

In Equation 5.4, c_i is the speed of sound of the $i\text{-}th$ particle. The minimum dt is evaluated over all the particles. Subsequently, the resulting ordinary differential equation system can be integrated in time by schemes such as *Runge-Kutta*, *Leap-Frog* or any *Predictor-Corrector*, to ensure at least second order convergence in

time. The exact choice of coefficient β depends on the scheme chosen and it can be varied slightly. 2.5 is chosen for forth order *Runge-Kutta* method and 0.3 in *Predictor-Corrector* in codes.

5.2 Parallel SPH

In general, SPH calculation demands a lot of memory resources and enormous computer processing power.

Firstly, SPH method usually involves a large number of particles to be geometrically enough to model the deformation of fluid body. In three dimensional cases, the SPH model may involve several millions of particles.

Secondly, the evolution of the particle information should be very time consuming. Besides the governing equations themselves, neighbor search, boundary treatment, and interactions between particles manifold the complexity of the problem.

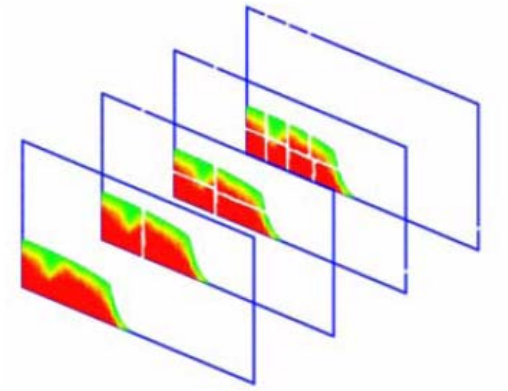

Fig 5.1 Parallel SPH

For these reasons, standard MPI technique is adopted for parallel SPH code. MPI stands for “Message Passing Interface”. It is a library of functions (in C) or subroutines (in FORTRAN) that could be inserted into the source code to perform

data communication between processes.

The first step in designing a parallel algorithm is to decompose the problem into smaller problems. Then, the smaller problems are assigned to processors to be solved simultaneously. In SPH code, most of the calculation costs occur in neighboring search. Each particle's acceleration is due to the neighbor particles. Therefore, domain decomposition is adopted here. Fluid domain are divided into pieces of the same approximate size and then mapped to different processors. Each processor then only process the portion of the data that was assigned including neighbor search, acceleration, densities update and so on. Of course, the processes may need to communicate periodically in order to exchange data.

The main goal of parallel program is to obtain an enhanced performance over the serial version. With this in mind, there are several issues to be considered when designing parallel code in order to obtain the best performance possible within the constraints of the problem being solved. These issues are

- **Load balancing** is the task of equally dividing work among the available processes. It is easy to accomplish because the same operations are being performed by all the processes (on different pieces of domain) if the number of particles are similar. Sometimes, calculation domain is difficult to decompose into equal pieces. For example: Variable smooth length, irregular fluid domain. Large number of pieces is divided and different processes could load the data by order.

- **Minimizing communication**

  Total execution time is a major concern in parallel programming because it is an essential component for comparing and improving all programs. Three components make up execution time:

  1. Computation time

2. Idle time
3. Communication time

Computation time is the time spent on performing computations. If load balancing is optimized, the job would be ideally expected to be finished in 1/Nth the time if there are N processors working on a problem.

Idle time is the time a process spends waiting for data from other processors. In SPH code, following the neighbor search, acceleration and density calculation, all the work will be left to one process while all other processes are in an idle state. However, this particular part only includes data collection and particle motion updating which only occupy 1%~3% of the total calculation.

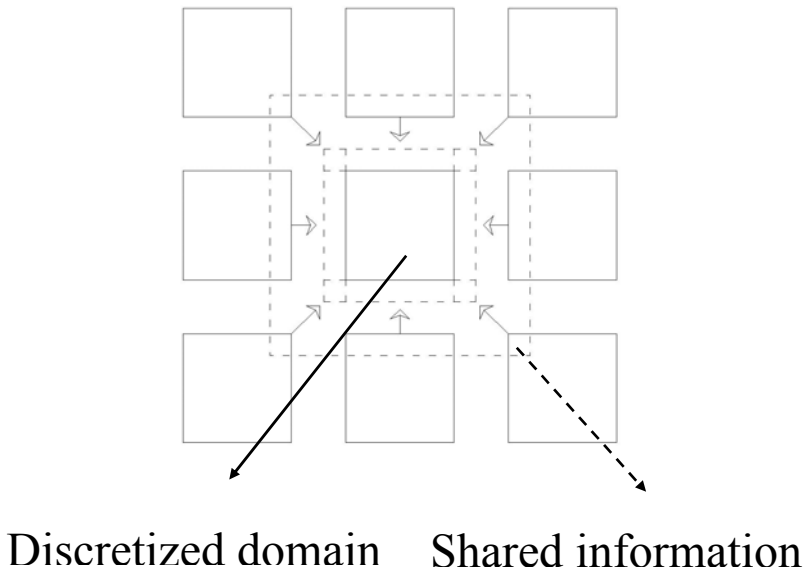

Fig 5.2 Discretized domains and shared information

Finally, communication time is the time it takes for processes to send and receive messages. Thanks to the explicit algorithm in SPH code, communication could be only processed once at each time step if we assign the data to each process including necessary '*shared information' (Fig 5.2)*

6 Verification and Validation

In this chapter, the features of present SPH solver are outlined. Using these techniques, SPH method shows stability and efficiency when dealing with fluid hydrodynamics. After that, the developed SPH method is verified and validated through the comparison with experiments or other numerical solvers. These test cases are discussed: 1) 2D dam break aim at validating the method with standard free surface flow using both one-phase and two-phase SPH model; 2) 2D wedge slamming

6.1 Features of Present SPH solver

The main features involved in present code are outlined below

- Parallel code based on the MPI technique

Computation ability is always the bottleneck of the CFD method. Parallelization is the best option in order to solve this problem. In our code, the MPI technique is adopted for parallelization. As the SPH method adopts an explicit algorithm in interactions, the efficiency of parallelization is higher than traditional CFD tools (VOF).

- Automatic domain discretization and fluid particles initialization

As a well used method, the discretization strategy is developed to simulate different cases including both 2D and 3D, the number of processors, different hydrodynamics problems and real time updating for high efficiency.

Similar to the other CFD method based on grid, SPH should pre-process the initial condition of fluid by the collocation of the fluid particles in the domain. If the geometry of calculation domain is complex or the fluid is not uniform, pre-process

software Gambit is firstly used to discretize the domain and the output mesh file can be simply transferred to particles information (Fig 6.1).

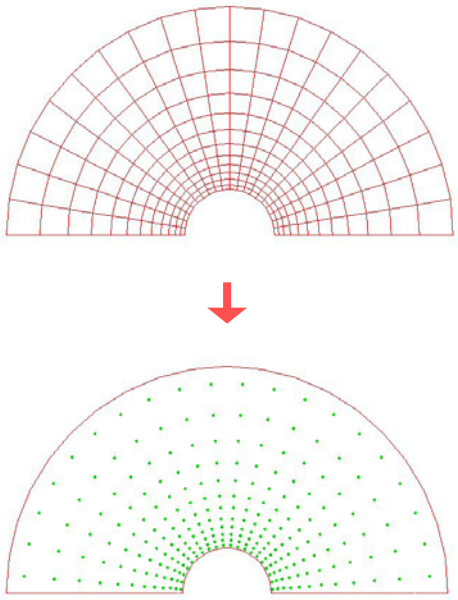

Fig 6.1 Top: Mesh file, Bottom: Particle information

- Complex solid boundary condition technique

SPH has difficulties in handling the presence of solid boundaries.

1.) The first attempt to deal with solid walls involved exerting forces on the fluid (Monaghan 1994). This idea is based on the fact that, at a micro scale, it is clear the body is made of particles, i.e. atoms or molecules. In the reality, the forces due to such particles are relevant within a distance of the order of the atom dimension. Numerically, they are approximated as forces acting within distances comparable to the resolution length of the simulation.

2.) The boundary particles (Morris 1997) can be used to model both fixed and moving bodies. The main drawbacks of such a technique are: (i) it causes pressure-wave disturbances at the beginning of the numerical simulation and (ii) it is not suitable to calculate accurately the local hydrodynamic loads induced on the

structures.

3.) An alternative to this approach is to model the body presence by introducing a layer of "ghost particles" along the body and outside of the physical domain (Cummin & Rudman 1999). The density, pressure and velocity of such particles are deduced from those of the real particles adjacent to the solid boundary. With this technique the local loads on the body can be accurately calculated however, close attention is necessary when dealing with the complex geometries of the structures.

'Ghost particle' is mostly used in the code to deal with the solid boundary condition. This technique implies that the knowledge of the local normal is required on the desired boundary, taking into account the position of the particle to be mirrored. However, in general case with complex curved surface, the mirror particle is very difficult to obtain. At this time, a method is proposed to extend the application of ghost particle technique to general geometry. The 3D boundary is decomposed into flat triangular panels. These panels are used to allow the capture of the particles to be mirrored easily. Software known as 'Gambit' is used to transform the boundary into tiny flat panels. This process is called the 'approximate solid boundary' and has been proven to correctly simulate complex geometry problems.

In addition, extra boundary particle control is used to prevent particle penetration because of tensile instability. Equation 4.6 and 4.7 are used at this moment to solve this problem.

- Variable smoothed length

In the context of astrophysics studies, Monaghan introduced spatially varying resolutions in which the smoothed length adapts according to the local number and

density of particles (Monaghan 1992). Various studies aiming to improve the efficiency of this extension to SPH have been carried out (Hernquist & Katz 1989, Nelson & Papaloizou 1994). This technique has been an interesting tool for more general use in the field of fluid mechanics because in many cases we do not need the high resolution everywhere but in sensitive areas (Oger 2005). In this thesis, the variable smoothed length technique is created by modifying momentum equations to satisfy conservation requirements. Using this technique, the computation cost of cases becomes more acceptable. Additionally accurate results are produced in the cases of wedge entry and ship hull slamming.

- Wave height and local pressure evaluation method

The interpolation of local particle volume method is adopted to extract correct wave height information.

Many of the general fluid problems require the knowledge of local pressure on solid boundaries. However, the standard SPH method suffers from lack of stability which leads to irregular pressure in specific points. To extract accurate local pressure, we tried the technique called 'kernel function interpolation' on space and time history.

- Coupling tank motion with hydrodynamics

The captive tank motion or free tank motion are complied in the code using the same explicit fourth order Runge-Kutta method as fluid domain evolution.

The tank boundary is assumed to be not deformable. In each step, free motion of the tank will be predicted by the 6 DOF forces and moments due to hydrodynamics. Instead of the integral of pressure, the forces in 6 directions are calculated by summing up the particles' interactions between fluid particles and mirroring particles.

$$\vec{F} = m_b \sum_N m_a (\frac{P_b}{\rho_b^2} + \frac{P_a}{\rho_a^2} + \Pi_{ab}) \nabla_a W_{ab} + M\vec{G} \tag{6.1}$$

Where a fluid particle a is close to boundary and gives its mirror particle b internal force with viscous effect. $M\vec{G}$ is the external force of the tank.

Roll, pitch and yaw moment could be deduced easily after defining the gravity centre of the tank.

- Code structure

The simplified algorithm structure of SPH Parallel code is described in fig 6.2.

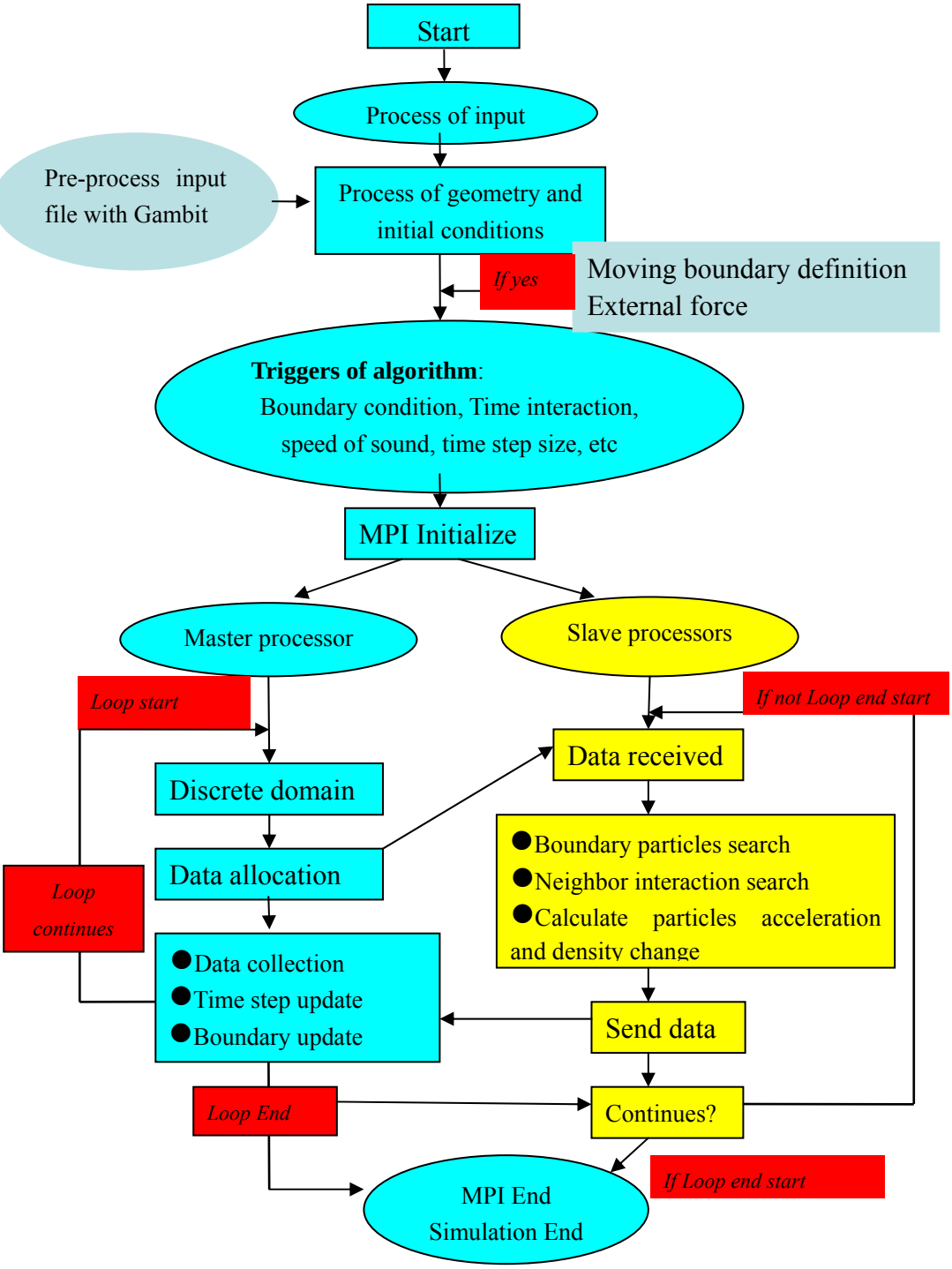

Fig 6.2 Code structure

6.2 Dam break

Following the specification of solid boundary condition in the case in Chapter 4 (dam break, Fig 4.11), the present SPH solver is tested with the experimental setup (fig 6.3) to verify the techniques mentioned in previous chapter. One-phase model and multi-phase model of SPH are both tested and the results are compared with the one that had been experimented. In the experiment, two height sensors are set up on the right bottom of the tank. Sensor I and Sensor II are 1.653 and 0.825 respectively away from the right vertical wall.

Another pressure sensor has been used and this is located on the bottom of the vertical wall. The height of the sensor is 0.2 meters.

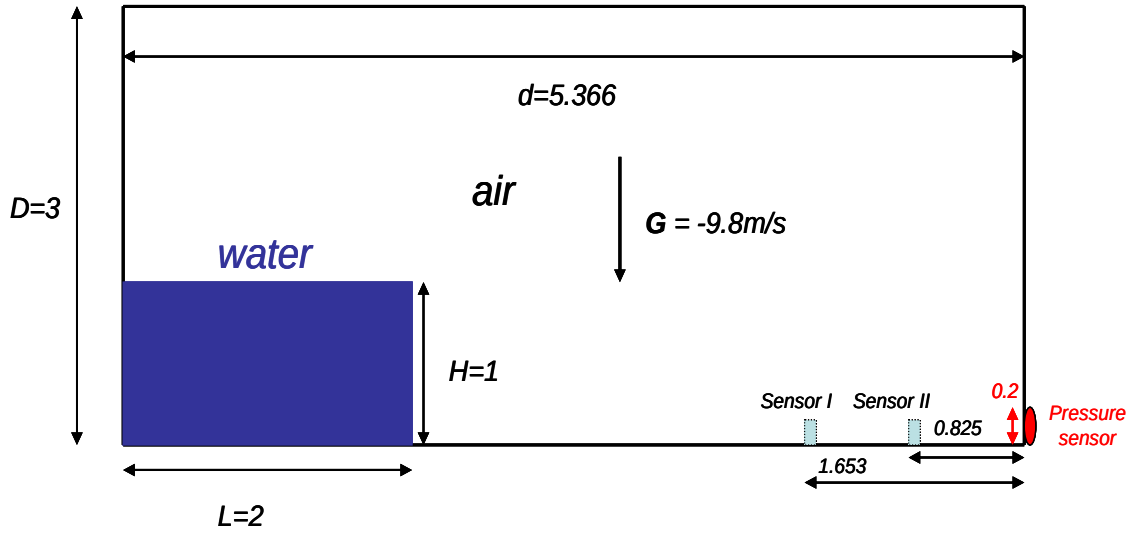

Fig 6.3 Dam-break problem and impact against a vertical rigid wall Geometric parameter H = 1, L = 2, D = 3, d = 5.366

Fig 6.4 shows the single phase of SPH evolution after the dam has been released. The particles' density is usually initialized as reference value or hydrostatic value. This is illustrated in Fig 6.4 (top right). Unlike the mesh-based method, where the pressure values will converge according to continuum equation and momentum equation, SPH

use explicit algorithm to avoid the resolver of Pressure Poisson Equation, and the initial disturbance will cause the pressure oscillation as sound wave. However, the problem can be solved if we initialize the pressure of particle as t^{0+} results from VOF (LES) method. Moreover, Cummin and Rudman (1999) conducted incompressible SPH method by solving Pressure Poisson Equation. Incompressible SPH code is also developed and the density of particles is initialized here by one tiny time step calculation in incompressible SPH code (Top left one in Fig 6.4). It is called 'cold start'.

There are more comments on incompressible SPH method here. Because Pressure Poisson equation is solved in incompressible SPH, the results are steady and there is no oscillation phenomenon for the pressure. The implicit algorithm leads to increased interactions in each time step and at the same time, allows larger time step, so the efficiency of incompressible SPH is still high. However, the particles on free surface have to be captured and defined as reference pressure in order to solve the Pressure Poisson equation. In conclusion, one of the most significant advantages of SPH method is lost particularly in the nonlinear free surface flows.

The speed of sound is defined as $10\sqrt{2gH} = 44.27m/s$ according to Equation 3.46, artificial viscosity $\alpha = 0.03$, the number of particles is about 20,000. The details of numerical parameters are shown in Table 2 as below

Dimension	2D
Number of fluids	One-phase
Fluid Density	1000 Kg/m3
Viscosity	Artificial viscosity 0.03
smoothed length	1.3h, constant smoothed length
Tensile stability	No

Solid boundary condition	No slip, ghost particles
Kernel function	Cubic spline kernel (2h)
Gravity	-9.81 m/s²
Kernel correction	MLS correction
Sound speed	44.27m/s
Initial particle distance	6.25mm
Total number of particles	51200
Number of particles in X-direction	320
Number of particles in Y-direction	160
Time evolution algorithm	fourth order *Runge-Kutta*
Duration of simulation	3 s
Recorded Time step (extracted data)	0.1s

Table 2: Numerical parameters of SPH for 2D dam break

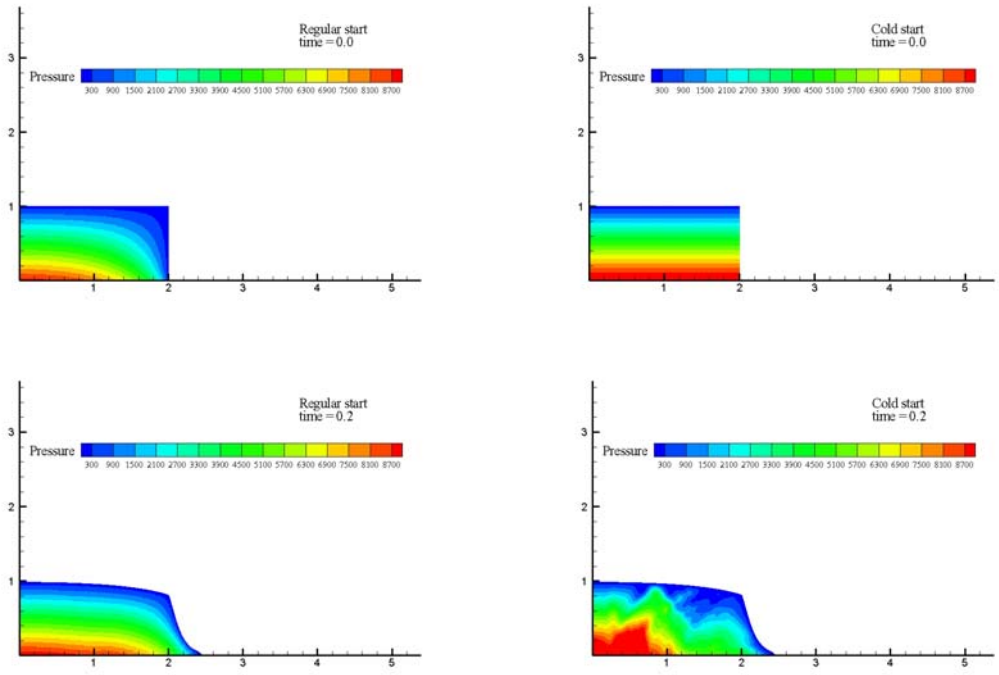

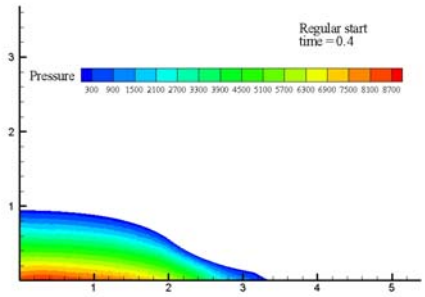
Regular start
time = 0.4
Pressure
300 900 1500 2100 2700 3300 3900 4500 5100 5700 6300 6900 7500 8300 8700
1
2
3
4
5

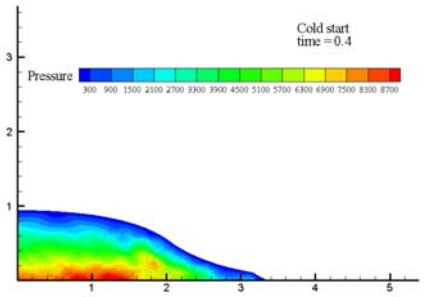
Cold start
time = 0.4
Pressure
300 900 1500 2100 2700 3300 3900 4500 5100 5700 6300 6900 7500 8300 8700
1
2
3
4
5

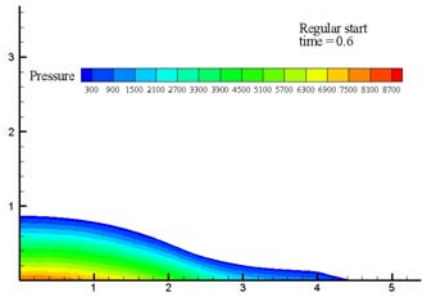
Regular start
time = 0.6
Pressure
300 900 1500 2100 2700 3300 3900 4500 5100 5700 6300 6900 7500 8300 8700
1
2
3
4
5

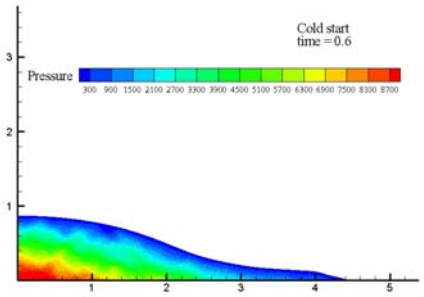
Cold start
time = 0.6
Pressure
300 900 1500 2100 2700 3300 3900 4500 5100 5700 6300 6900 7500 8300 8700
1
2
3
4
5

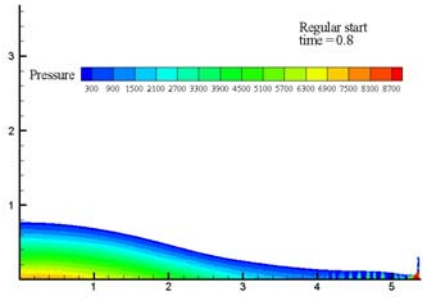
Regular start
time = 0.8
Pressure
300 900 1500 2100 2700 3300 3900 4500 5100 5700 6300 6900 7500 8300 8700
1
2
3
4
5

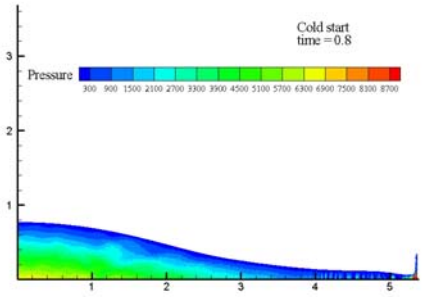
Cold start
time = 0.8
Pressure
300 900 1500 2100 2700 3300 3900 4500 5100 5700 6300 6900 7500 8300 8700
1
2
3
4
5

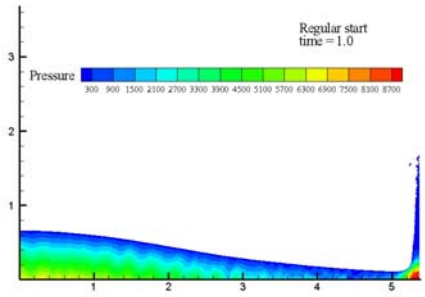
Regular start
time = 1.0
Pressure
300 900 1500 2100 2700 3300 3900 4500 5100 5700 6300 6900 7500 8300 8700
1
2
3
4
5

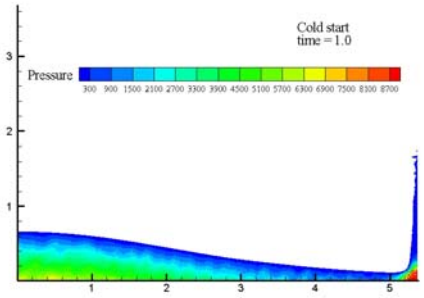
Cold start
time = 1.0
Pressure
300 900 1500 2100 2700 3300 3900 4500 5100 5700 6300 6900 7500 8300 8700
1
2
3
4
5

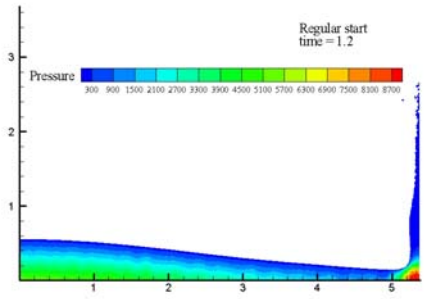
Regular start
time = 1.2
Pressure
300 900 1500 2100 2700 3300 3900 4500 5100 5700 6300 6900 7500 8300 8700

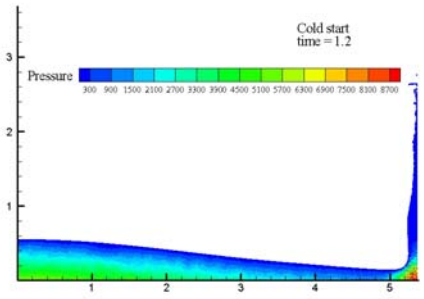
Cold start
time = 1.2
Pressure
300 900 1500 2100 2700 3300 3900 4500 5100 5700 6300 6900 7500 8300 8700

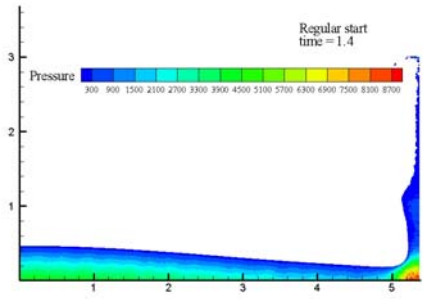
Regular start
time = 1.4
Pressure
300 900 1500 2100 2700 3300 3900 4500 5100 5700 6300 6900 7500 8300 8700

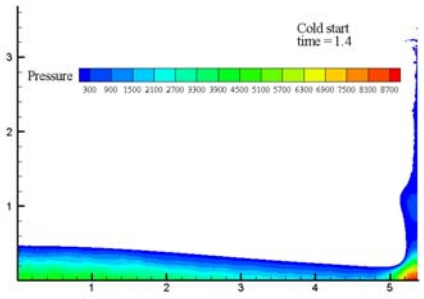
Cold start
time = 1.4
Pressure
300 900 1500 2100 2700 3300 3900 4500 5100 5700 6300 6900 7500 8300 8700

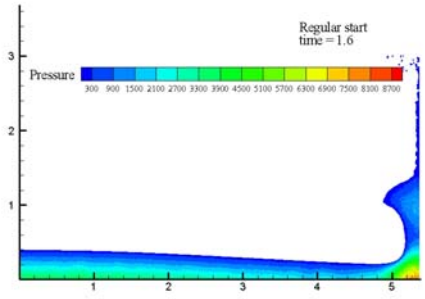
Regular start
time = 1.6
Pressure
300 900 1500 2100 2700 3300 3900 4500 5100 5700 6300 6900 7500 8300 8700

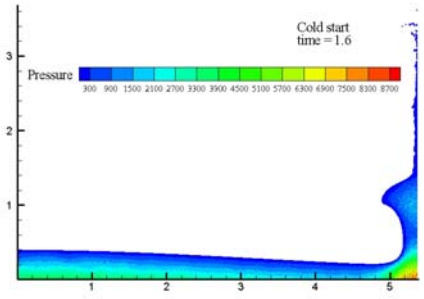
Cold start
time = 1.6
Pressure
300 900 1500 2100 2700 3300 3900 4500 5100 5700 6300 6900 7500 8300 8700

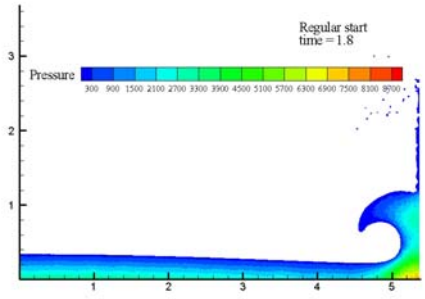
Regular start
time = 1.8
Pressure
300 900 1500 2100 2700 3300 3900 4500 5100 5700 6300 6900 7500 8300 8700

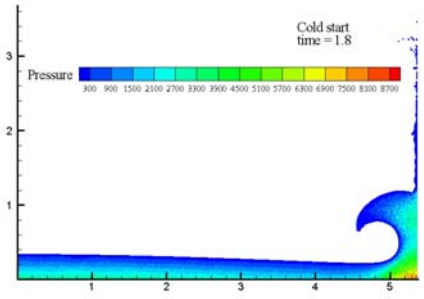
Cold start
time = 1.8
Pressure
300 900 1500 2100 2700 3300 3900 4500 5100 5700 6300 6900 7500 8300 8700

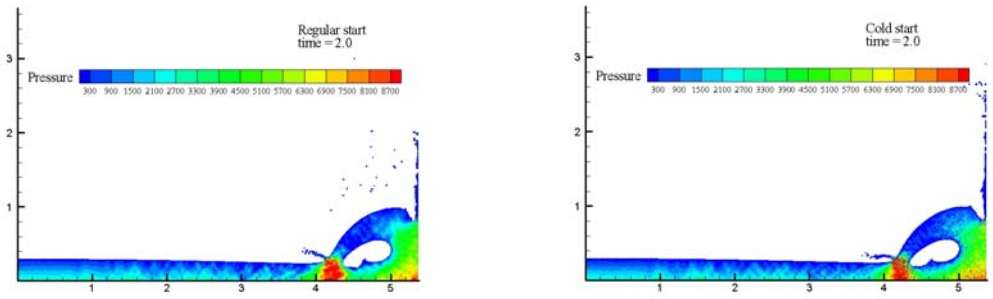

Fig 6.4 Regular start (left) and cold start (cold start)

Fig 6.4 shows the difference between regular start and cold start for flow evolution. The pressure contour is very smooth in the case with cold start and sound wave is observed in the case with regular start. The amplitude of sound wave depends on the initial disturbance and the frequency depends on the speed of sound defined in SPH. After one second simulation, the sound wave disappears because of the energy dissipation that occurred due to the artificial viscosity. Additionally, the latter pressure contours agrees very well.

To validate the fluid evolution of SPH results, commercial software Fluent (SIMPLE+VOF) is used for comparison in time series (Fig 6.5).

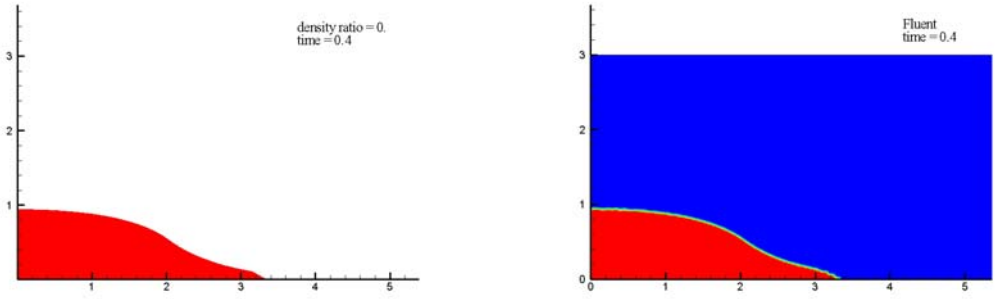

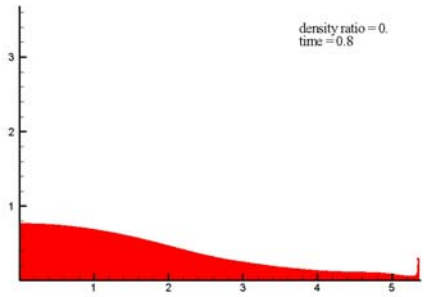
density ratio = 0.
time = 0.8

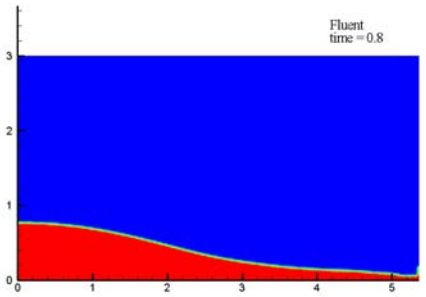
Fluent
time = 0.8

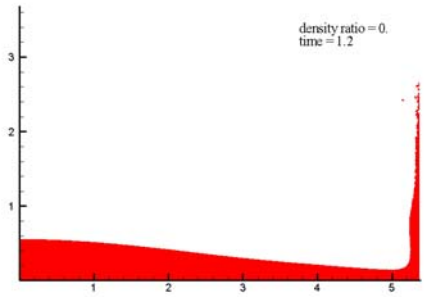
density ratio = 0.
time = 1.2

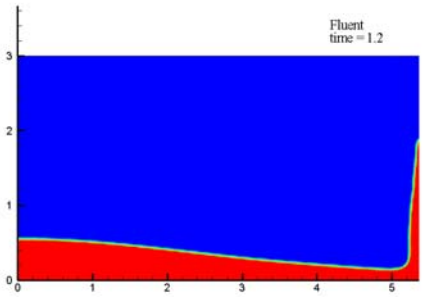
Fluent
time = 1.2

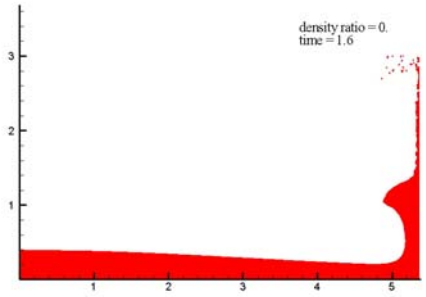
density ratio = 0.
time = 1.6

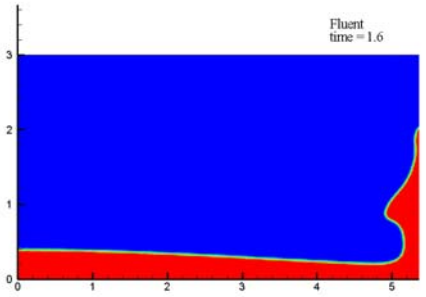
Fluent
time = 1.6

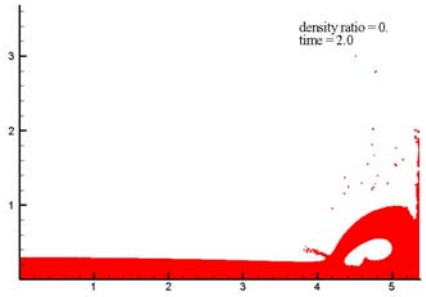
density ratio = 0.
time = 2.0

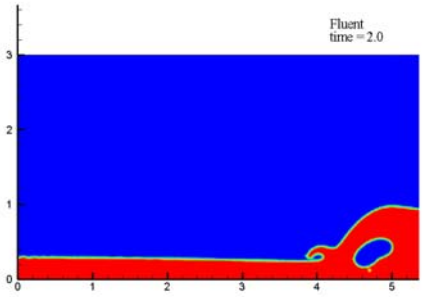
Fluent
time = 2.0

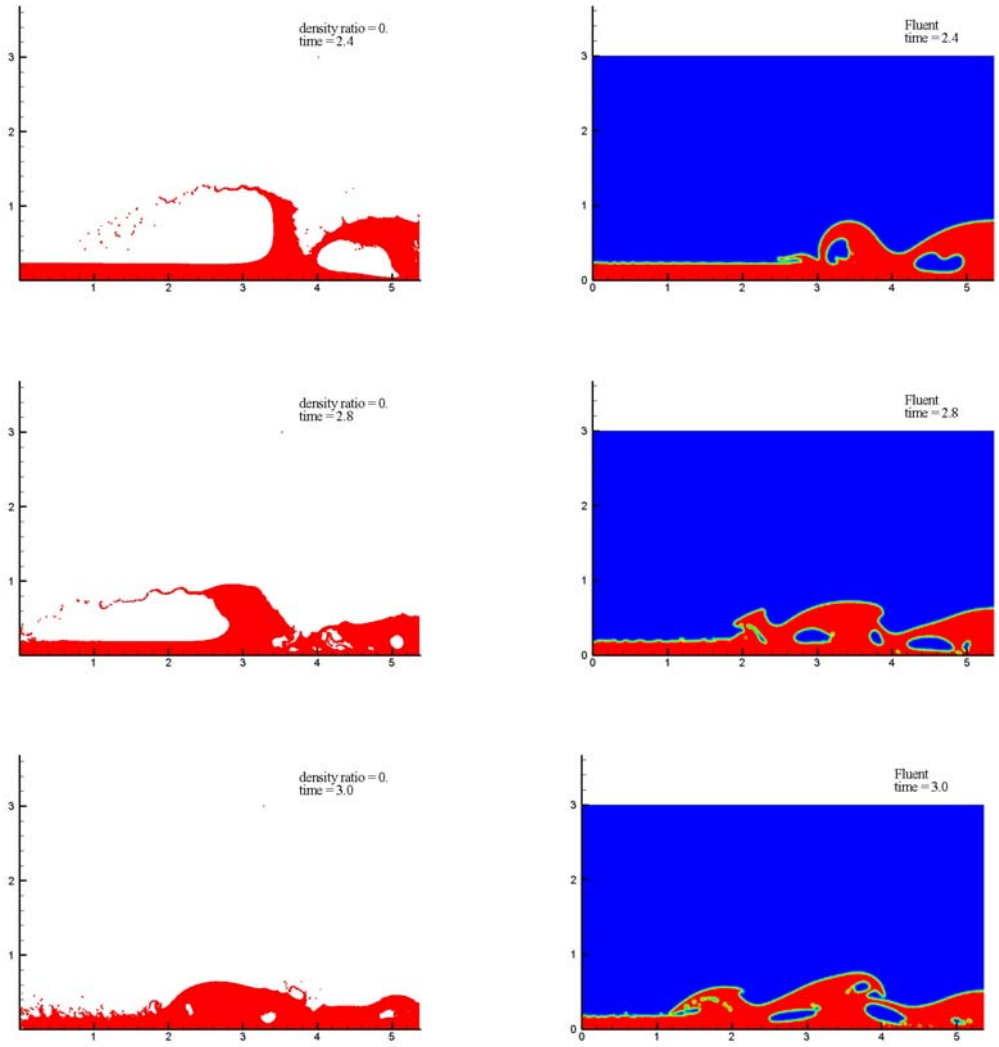

Fig 6.5 One-phase SPH results (left) and Fluent results (right) From top to bottom: time = 0.4, 0.8, 1.2, 1.6, 2.0, 2.4, 2.8, 3.0s

The results before the flow impacting on the wall are in good harmony between SPH code and Fluent. In the latter results when the time is 2.4~3.0s, the surface shape shows a difference. Firstly, the cavity in SPH results at time 2.4s is larger than the results of Fluent. It is because one-phase model of SPH implies that the second phase's air is vacant and the air entrapment is neglected. Furthermore, SPH shows more fragmentations than VOF method. These fragmentations can be considered as breaking waves caused by the impact of flows on the rigid wall or the impinging of the backward plunger on the underlying layer of water. Regardless of the accuracy and the quality of breaking wave described numerically, SPH has the advantage of

producing complex interface than VOF method. In addition, VOF method suffers the problems of constructing the correct interface. Although many strategies were proposed for VOF method such as geometry re-mesh technique, it requires very fine meshes.

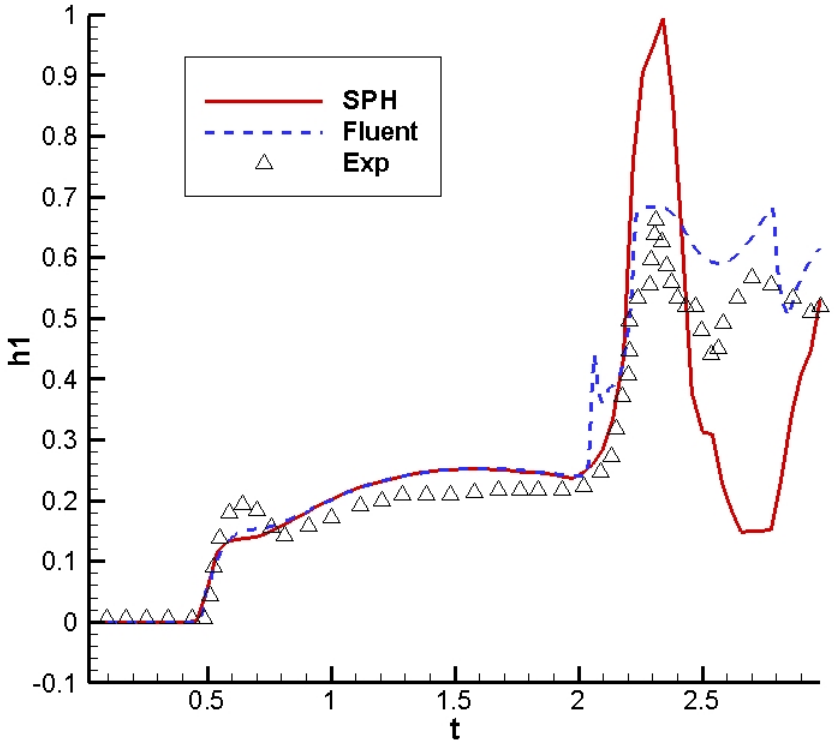

Fig 6.6: Height h of the water at height sensor I

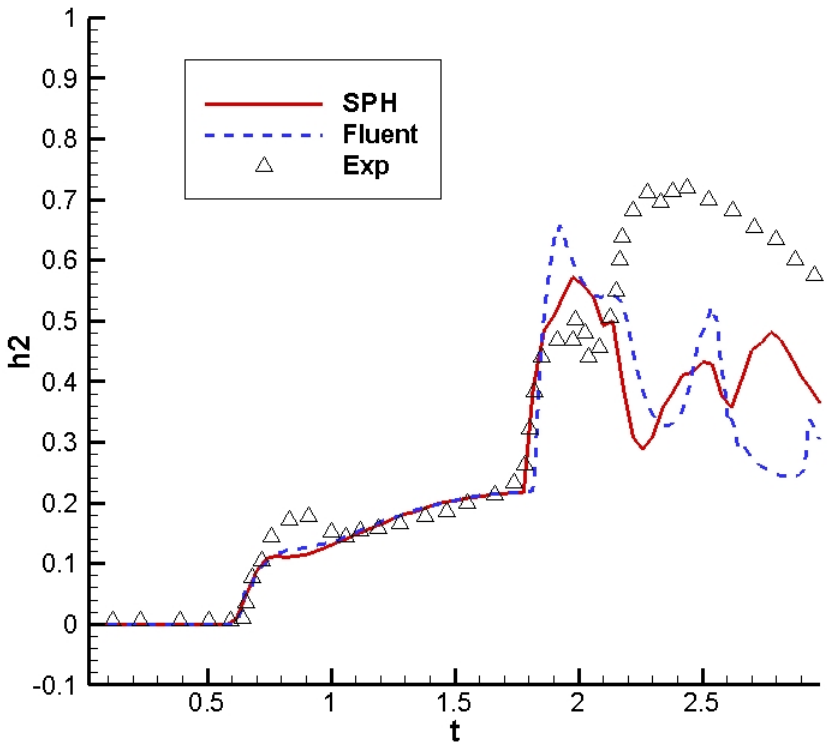

Fig 6.7: Height h of the water at height sensor II

Fig 6.6 and Fig 6.7 shows the time evolution of water height measured by the height sensor I and II respectively. The SPH case (red solid line) and FLUENT case (blue dash line) were compared with the experimented measurements from Zhou (1999). In the experiment, standard capacitive wave gauge was setup which is sensitive to the wet portion of the wire. The difference between numerical and experimental results were observed from time =0.5s to 1.0s because the flow evolution in the experiment was characterized by the sudden rise of the water level due to the transition from dry-deck to wet –deck on the wave gauge. Moreover, the numerical results of SPH and Fluent complement each other before the flow begins to have an impact on the wall. Discrepancy of water height was found after time = 2s which was due to the difficulty of predicting the cavity and breaking wave.

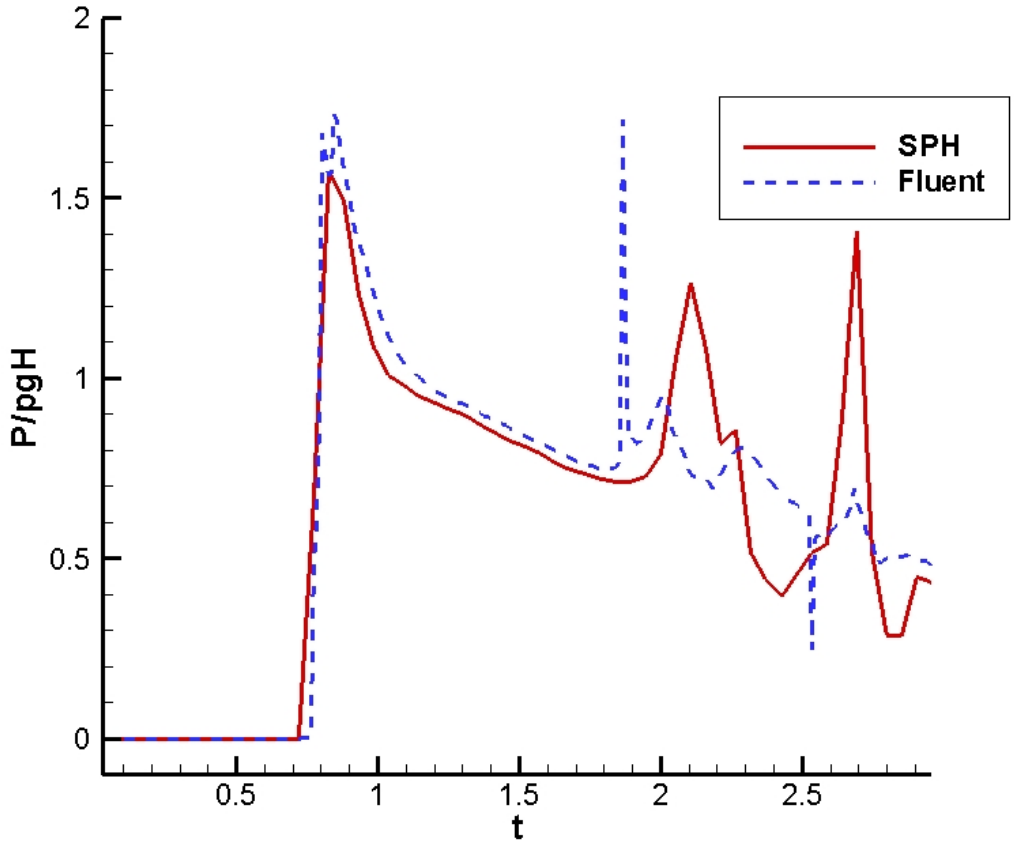

Fig 6.8: Pressure evolution on the pressure sensor on the vertical wall

The normalized pressure $P/\rho gH$ was measured in fig 6.8. Pressure integration method was used to evaluate the pressure of SPH. For comparison, the pressure measured from SPH method was filtered by averaging the value every 20 time steps (about 0.02s). The results before time = 1.8s agree very well with VOF method. The backward plunging water front induces the second pressure peak on the vertical wall at time = 1.8s, but limited information about the experiments does not allow a better discussion.

In many circumstances, violent fluid-structure interactions lead to air entrapment and multi-phase flows. The dynamics of the entrapped air in the impacting cases is an important part in FSI problems and has contributed to large and oscillated pressure

during the process. Therefore, neglecting the influence of air entrapment may cause incorrect results. The simulations are reproduced with the participation of the second phase particles. Fluid density is defined as ρ_1 and the second phase density is ρ_2. In one-phase simulation, the second phase is vacant which means $\rho_2 / \rho_1 = 0$. Three density ratios are simulated in two-phase SPH model: $\rho_2 / \rho_1 = 0.001$ (air-water case), $\rho_2 / \rho_1 = 0.01$ and $\rho_2 / \rho_1 = 0.1$ shown in fig 6.9

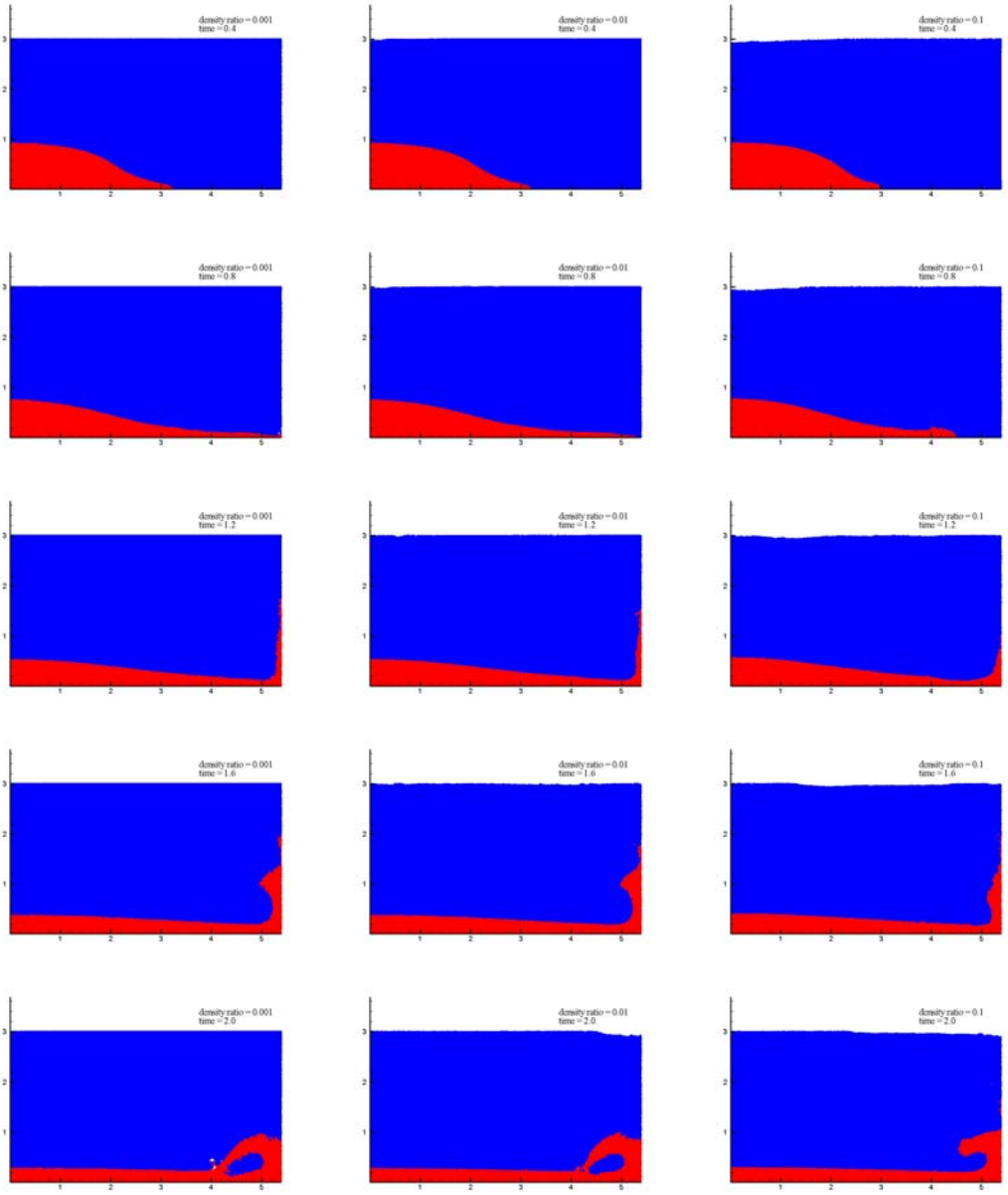

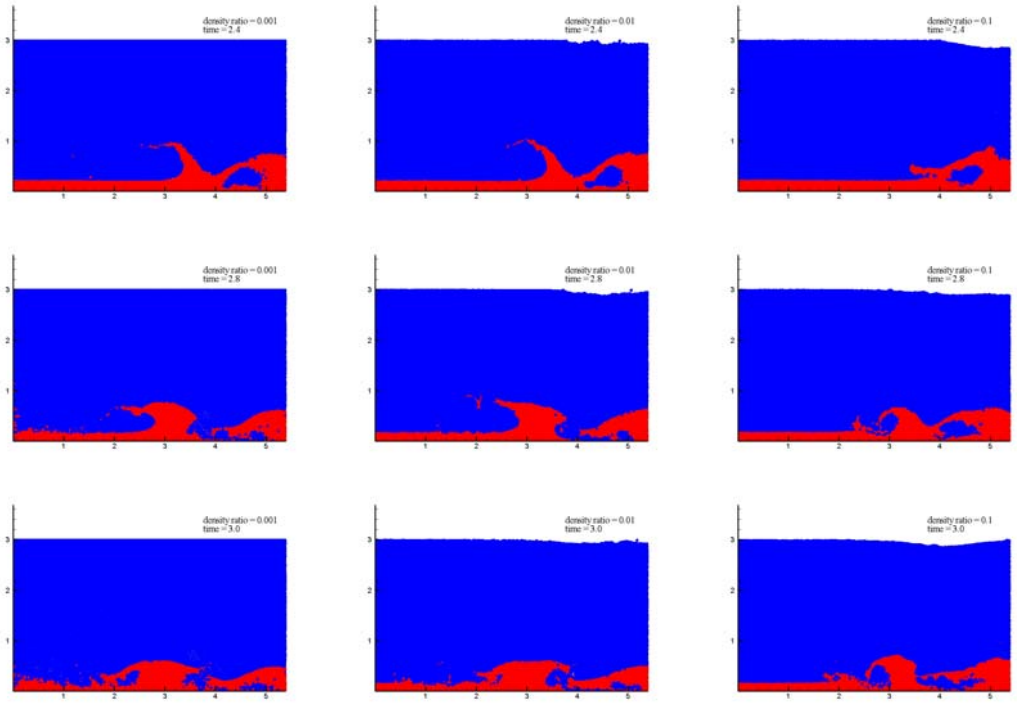

Fig 6.9 Two-phase SPH model with density ratio 0.001(left), 0.01(center), 0.1(right) From top to bottom time = 0.4, 0.8, 1.2, 1.6, 2.0, 2.4, 2.8, 3.0 s

SPH has shown its outstanding capability and expansibility to multi-phase model. The main features of the flow evolution compliment very well with the different density ratios in Fig 6.9. Before the impact, an obvious difference can be observed where the greater the ρ_2, the greater the water motion was impeded which was expected. Consequently, the water-front velocity decreases when the density of the second phase fluid increases. In fig 6.10, the evolution of front wave is compared with different density ratio of two phases.

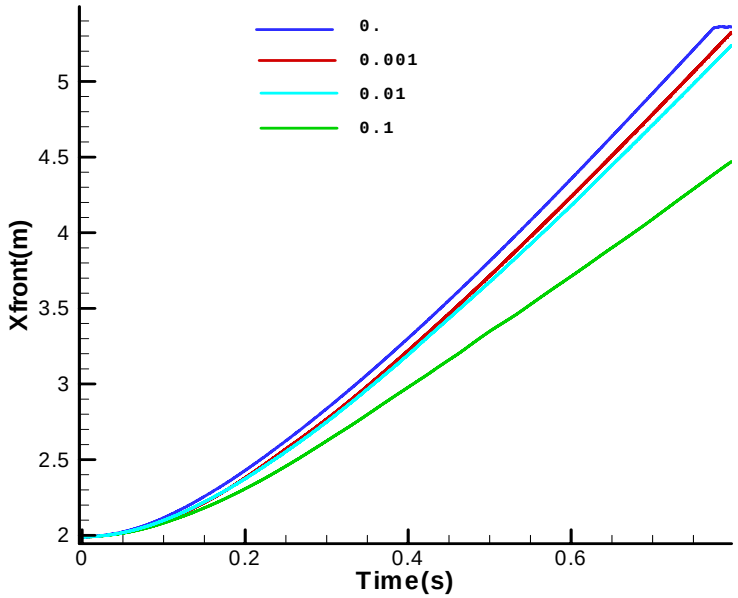

Fig 6.10 Time evolution of front wave with different density ratio

With regards to the low density ratio (0.001) of two-phase simulations, the speed of sound of the light phase would be very large to retain the stability of flow interface which means that calculation time will increase rapidly because the time step size depends on the speed of sound.

Regarding the water-air interface, typical values were adopted as $\gamma_1 = 7, \gamma_2 = 1.4$. According to the equation of state (Equation 3.45 and Equation 3.46), the speed of sound in the water is defined as $c_1 = 44.27 m/s$, meanwhile the speed of sound in the air is define as $c_2 = 626 m/s$.

However, in SPH simulation especially in 3D simulations, the number of particle was too large to attain accurate results, low density ratio of two phases like air and water will result in constraints within the calculation cost.

6.3 Wedge slamming

Description of wedge entry

Slamming is one of the leading hydro-elastic problems which have constantly defied designers' understanding of ship behaviors at sea. It is just as difficult to measure this phenomenon in model tests as it is to simulate it properly. Since the first studies by von Karman (1929) and Wagner (1932), slamming force prediction problems have been plentifully studied. It is a persisting field of research in ship hydrodynamics to study the local pressure forces acting on its structures.

The width of the wedge is 0.5 m. The deadrise angle is 30° , wedge free drop with vertical velocity of -6.15m/s. When entering the water, the length of wedge is 1 m. (more detail in experiment carried out by Zhao [Water entry of arbitrary two – dimensional section with and without flow separation, in: 21st Symposium on Naval Hydrodynamics, 1997])

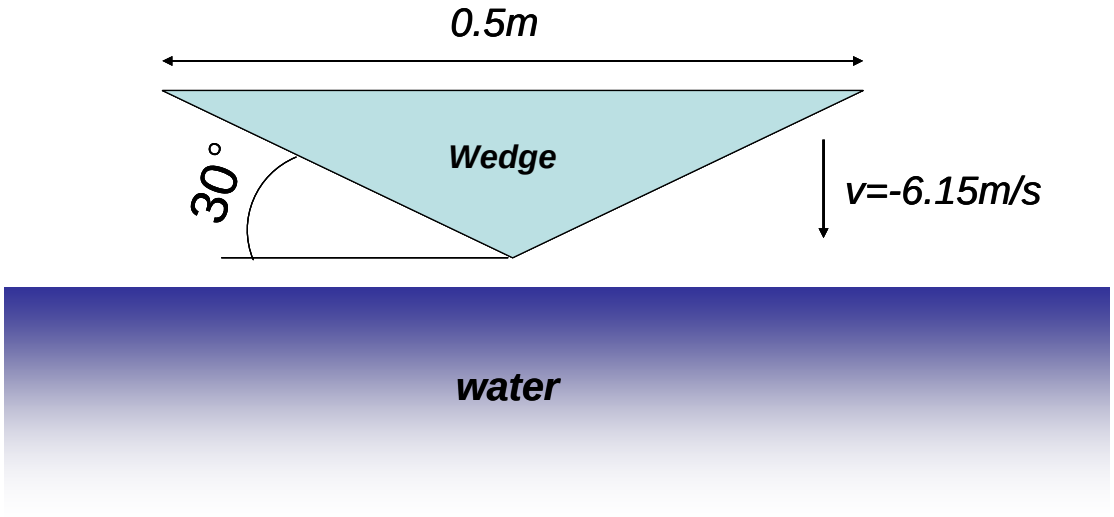

Fig 6.11 wedge slamming experiment setup

At time = 0s, the wedge was dropped on calm water with an initial vertical velocity of -6.15m/s. The impact generates two jets running out along the wedge with a large free

surface deformation, and a strong vertical force was imposed on the wedge. In the experiment, the length of this wedge was 1.0m (Fig 6.12), despite the three dimensional effects, the flow was regarded as two dimensional case in numerical simulation.

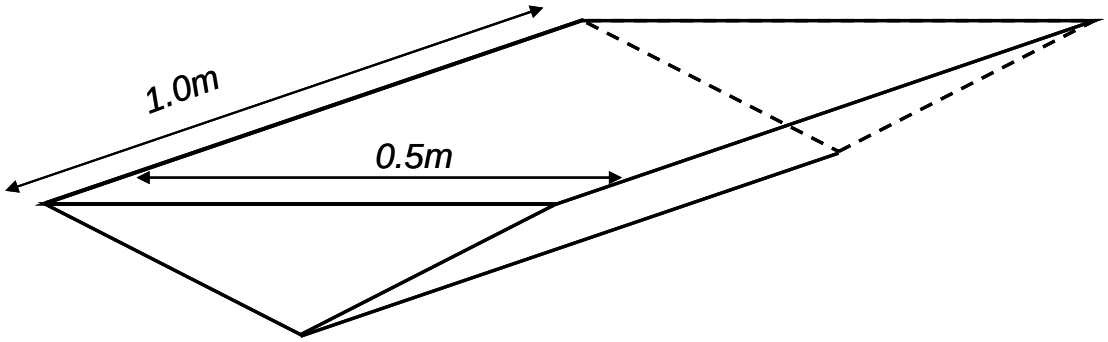

Fig 6.12 3D Wedge in the experiment

To compare the numerical with experimental results, in the SPH simulation the motion of the wedge is governed by the experimental motion of the test section. The measured velocity in experiments is reported in fig 6.13 as the captive wedge motion for SPH code.

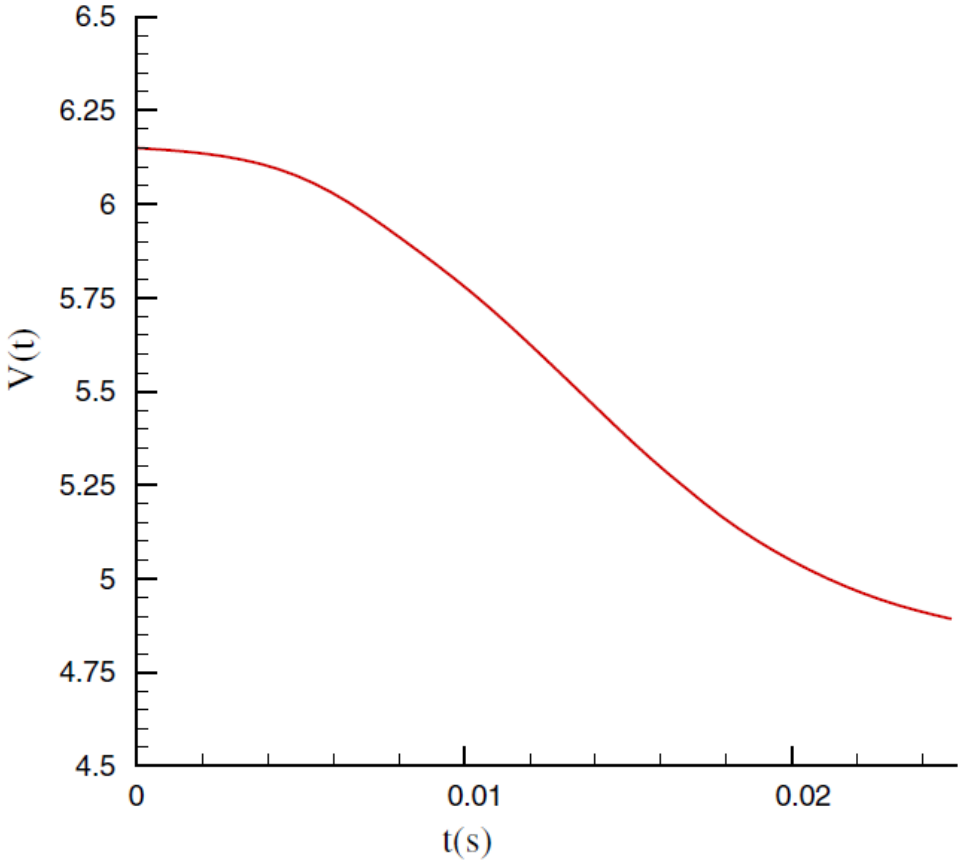

Fig 6.13Experimental vertical velocity time history

Numerical simulation with variable smooth length

In the SPH simulation, the calculation domain has to be adapted. In order to ensure nearly incompressible fluid with density change of less than 1%, the speed of sound was chosen as 80m/s for the water. When the wedge slammed on the water, the sound wave generated may have reached the boundary of the water and then reflected back on the wedge, In order to avoid this influence, the tank width and depth was chosen to be 3.6m and 2.0m respectively. The size was enough to predict the slamming before time = 0.025s.

In the first attempt, uniform fluid particles were distributed in the calculation domain. Regarding the efficiency of calculation, the initial particle distance 0.006m was used

in the simulation. The calculation time was only about half an hour on paralleled SPH code with four processors (2.4 GHz). However, the results of vertical force due to slamming show large oscillations in Fig 6.14.

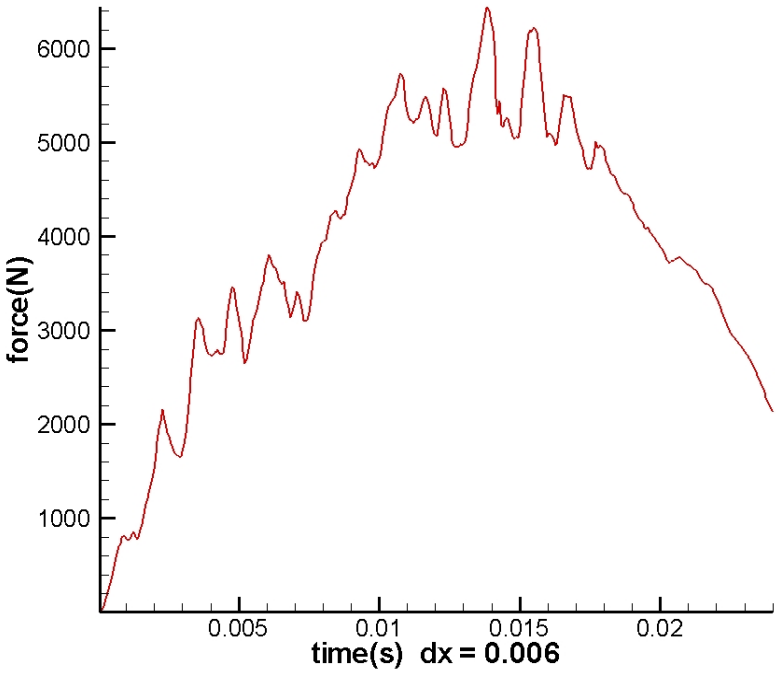

Fig 6.14 Vertical force with uniform particle distance 0.006m

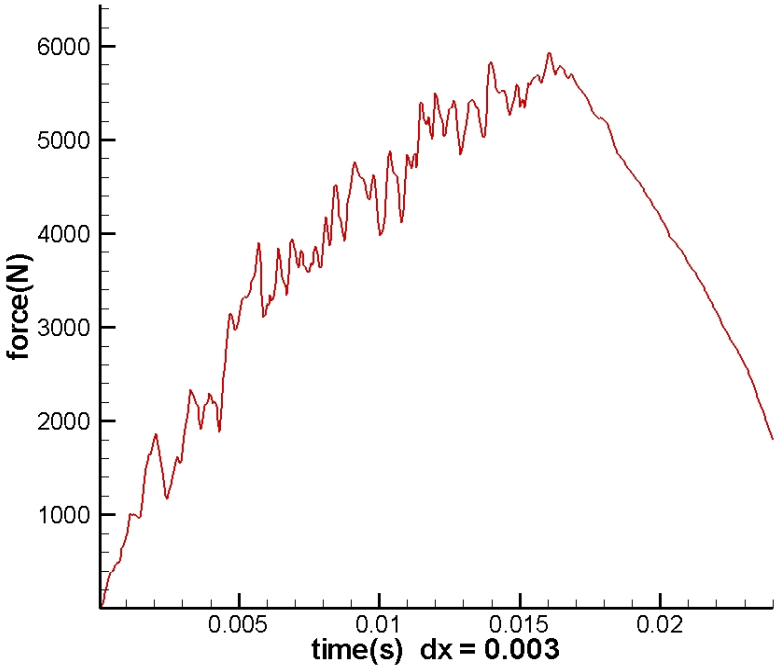

Fig 6.15 Vertical force with uniform particle distance 0.003m

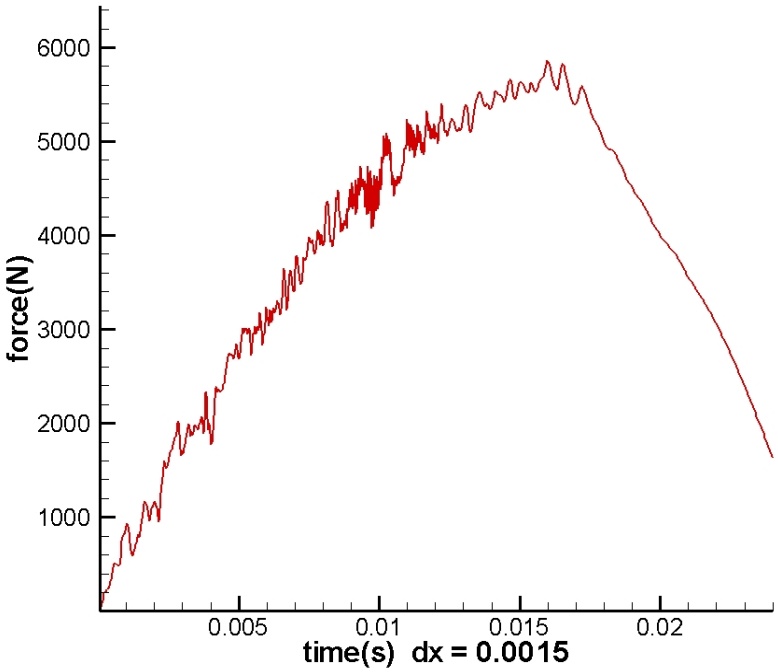

Fig 6.16 Vertical force with uniform particle distance 0.0015m

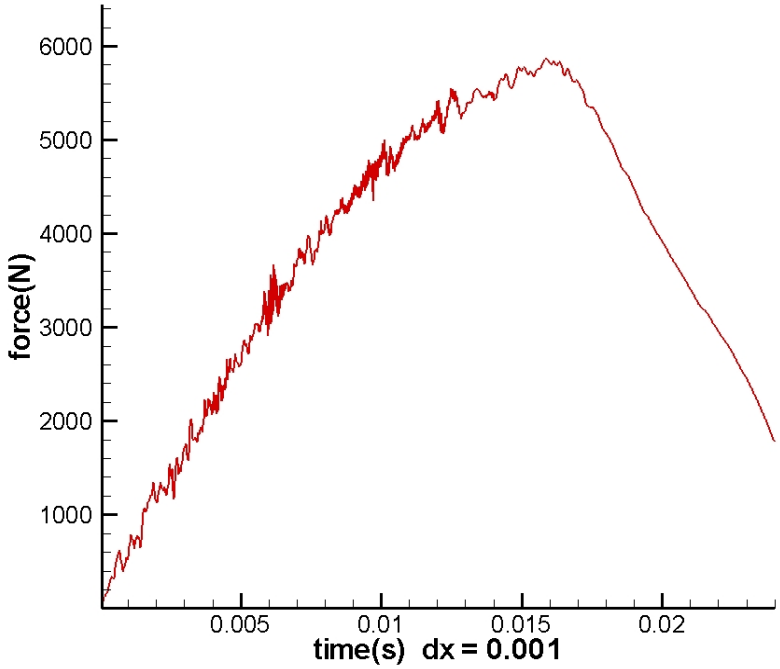

Fig 6.17 Vertical force with uniform particle distance 0.001m

In latter simulations, larger number of particles was used in the simulation. The results for initial particle distance were 0.003m, 0.0015m and 0.001m, which were given in fig 6.15, 6.16 and 6.17 respectively. Although the result was very sensitive in number of particles and coarser particles gave more oscillated results, all the evolution will be correct and totally controlled by momentum equations. Very fine particles with initial particle distance 0.001m are necessary to extract the correct local pressure (Fig 6.17). Whereas, the number of particles will be 720,000 for this case and the calculation time will take more than 4 days.

In order to reduce the calculation costs, variable smoothed length was adopted in the wedge entry test. As shown in Fig 6.18, the particles configured in the impacting area were very small in order to obtain accurate results. Out of this zone, particles were distributed so that smoothed length increases slowly. The ratio of neighbor particles was controlled to be less than 1.03 in order to prevent the error resulted from asymmetric force term between interaction particles in momentum equation.

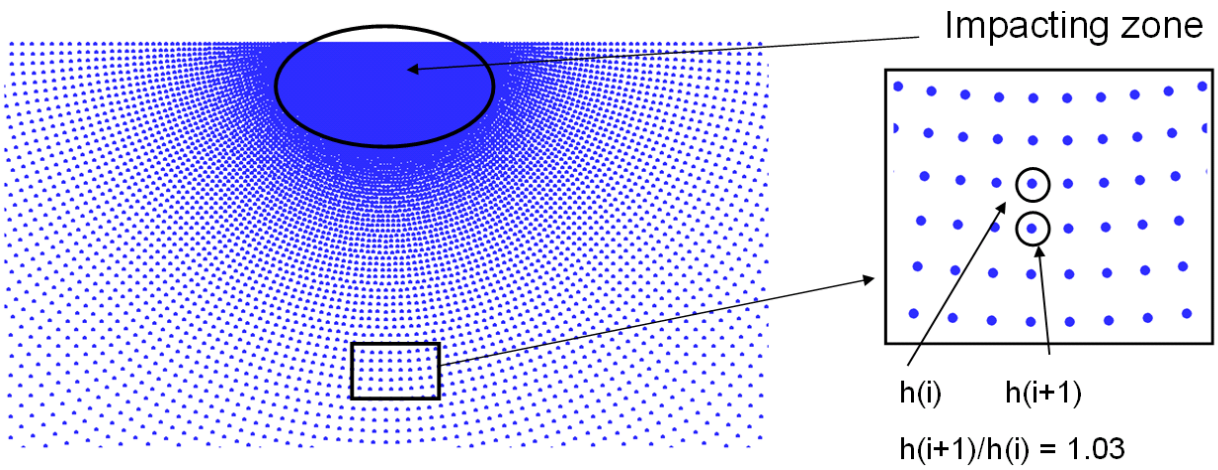

Fig 6.18 Variable smoothed length

The initial particle distance in impacting zone was 0.001m, but because of variable smoothed length the total number of particles are currently only about 176,000. The calculation efficiency was improved significantly (Fig 6.19) meanwhile the accuracy of results agree with experimental one very well.

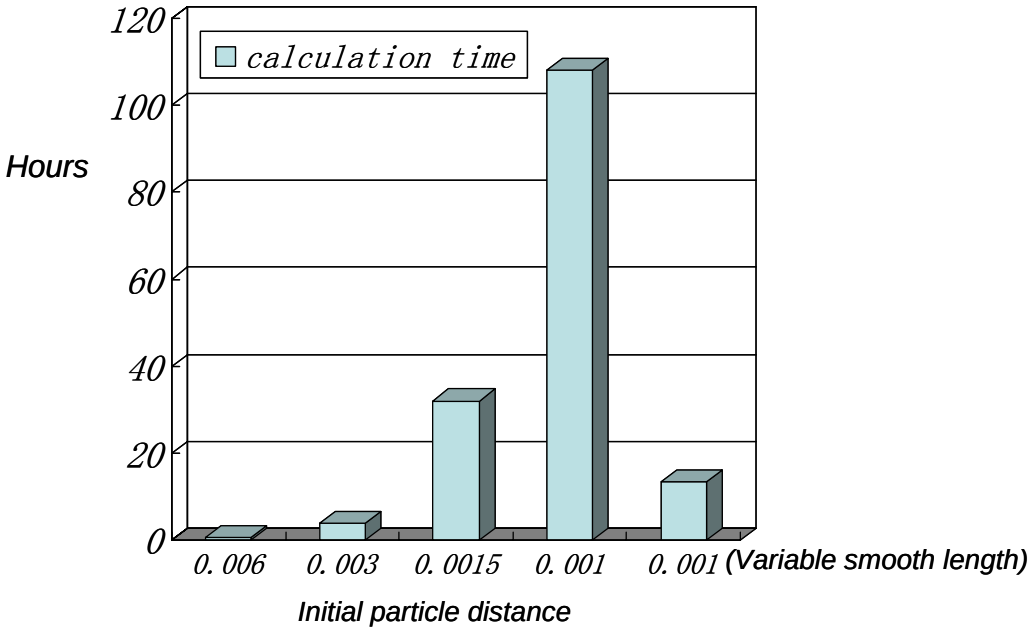

Fig 6.19 Calculation time comparison

The numerical parameters are set up for latter simulation in Table 3

Dimension	2D
Number of fluids	One-phase
Fluid Density	1000 Kg/m3
Viscosity	Artificial viscosity 0.01
smoothed length	1.3h, Variable smoothed length with ratio 1.03
Tensile stability	Yes
Solid boundary condition	No slip, ghost particles
Kernel function	Gaussian kernel (3h)
Gravity	-9.81 m/s²
Kernel correction	Shepard correction
Sound speed	80m/s
Initial particle distance	Min 1mm
Total number of particles	About 176,000
Number of particles in X-direction	Non-uniform
Number of particles in Y-direction	Non-uniform
Time evolution algorithm	fourth order *Runge-Kutta*
Duration of simulation	0.025 s
Recorded Time step (extracted data)	0.01s

Table 3: Numerical parameters of SPH for 2D wedge entry

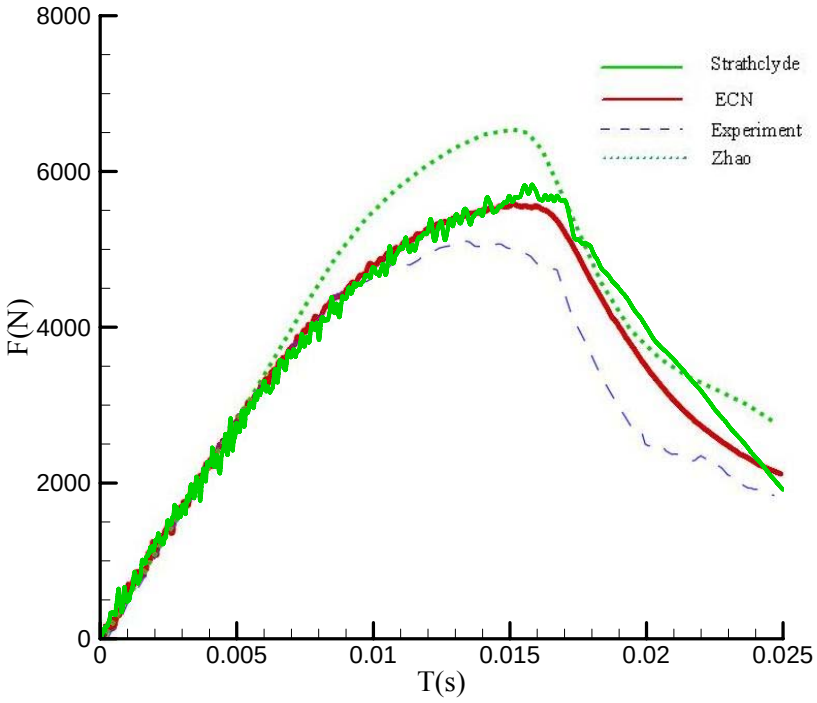

Fig 6.20 Total vertical forces (Green solid line: SPH of present thesis, Red solid line: SPH of ECN, Blue long dash: experiment, Green dots: Zhao's analytical result)

The results of vertical forces suggest that the water on the wedge were compared to CFD results by ECN, experimental results and analytical data given by Zhao et al. in Fig 6.20. The SPH slamming force time history was overestimated than experimental data when t > 0.01s, the same situations were shown in other results. This overestimation was due to the three dimensional effects because the wedge length is 1 meter during the experiment but it is regarded as infinite length in numerical simulations. Nevertheless, SPH results were in accordance with experimental and analytical curves.

Fig 6.21 provides pressure field near the impacting zone at time 0.1s and 0.2s. Boundary conditions: L-J force and ghost particles were tested in the simulations to validate their accuracies to extract local pressure. In this case, the results agree with each other very well. Both methods have demonstrated outstanding pressure field and

the similar large free surface deformation with the apparition of two jets were observed along the wedge boundaries.

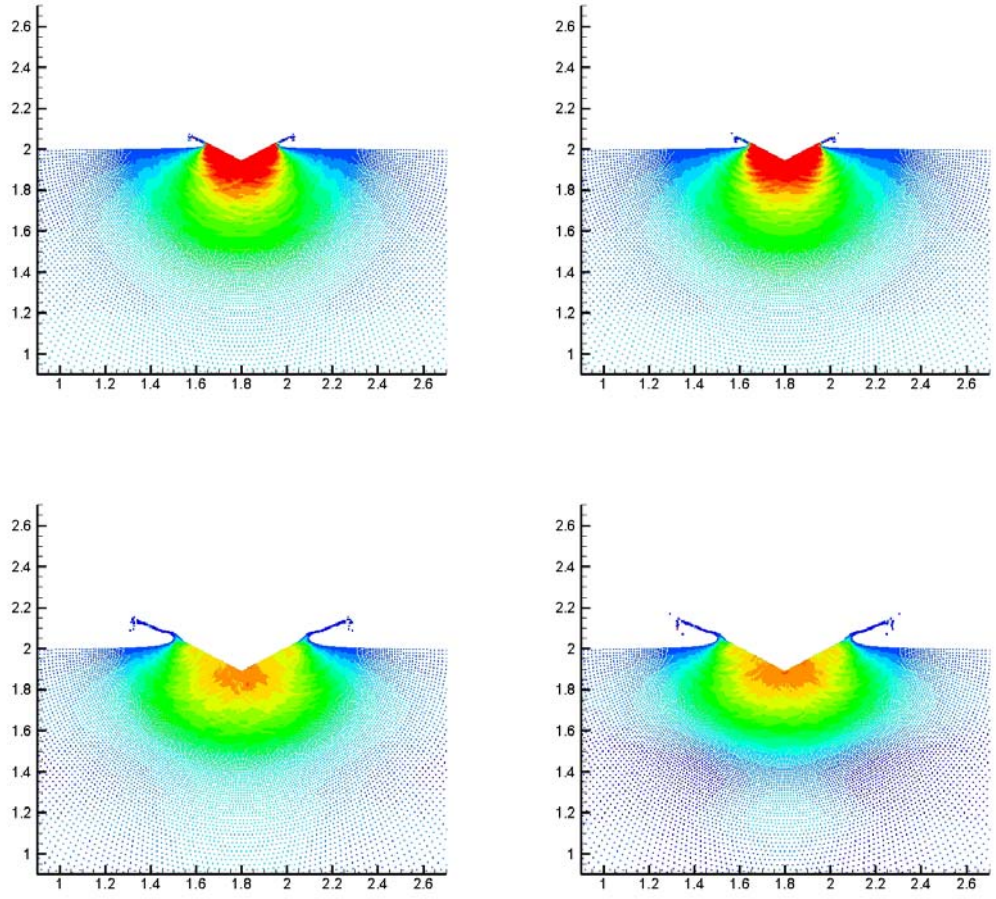

Fig 6.21: Top to bottom right: 0.1s, 0.2s Left to right solid boundary: Lernnard-Jone Force, Ghost particles Number of particles: 176,000 Pressure contour Range: 0~60k Pa

In order to study the efficiency of local pressure evaluation method in SPH, the validation was carried out by the experimental record. In the experiment, the wedge is fitted with piezoresistive pressure cells with a diameter of 4mm (P1-P5 in fig 6.22).

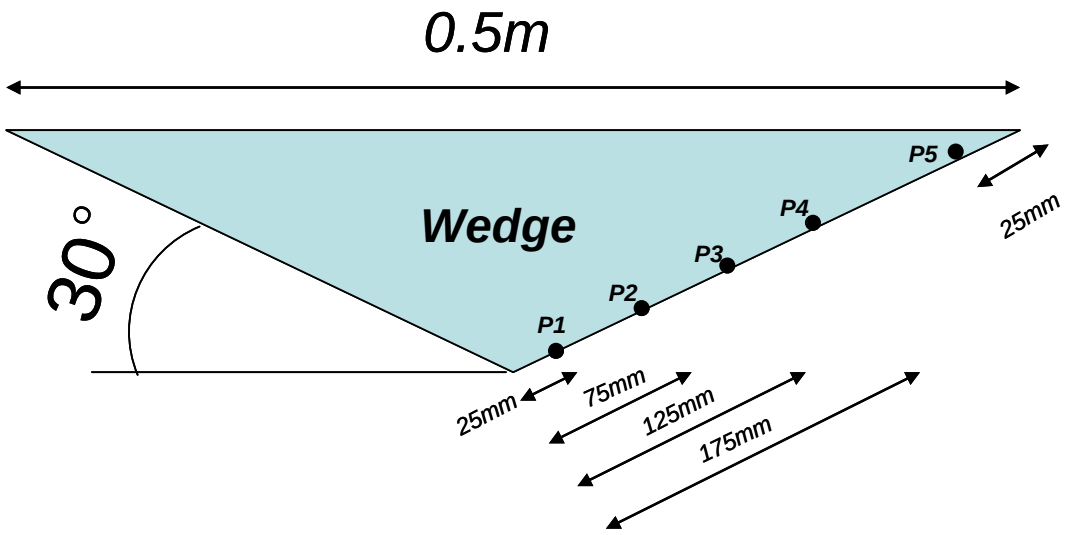

Fig 6.22 Pressure cell P1-P5 fitted on the wedge

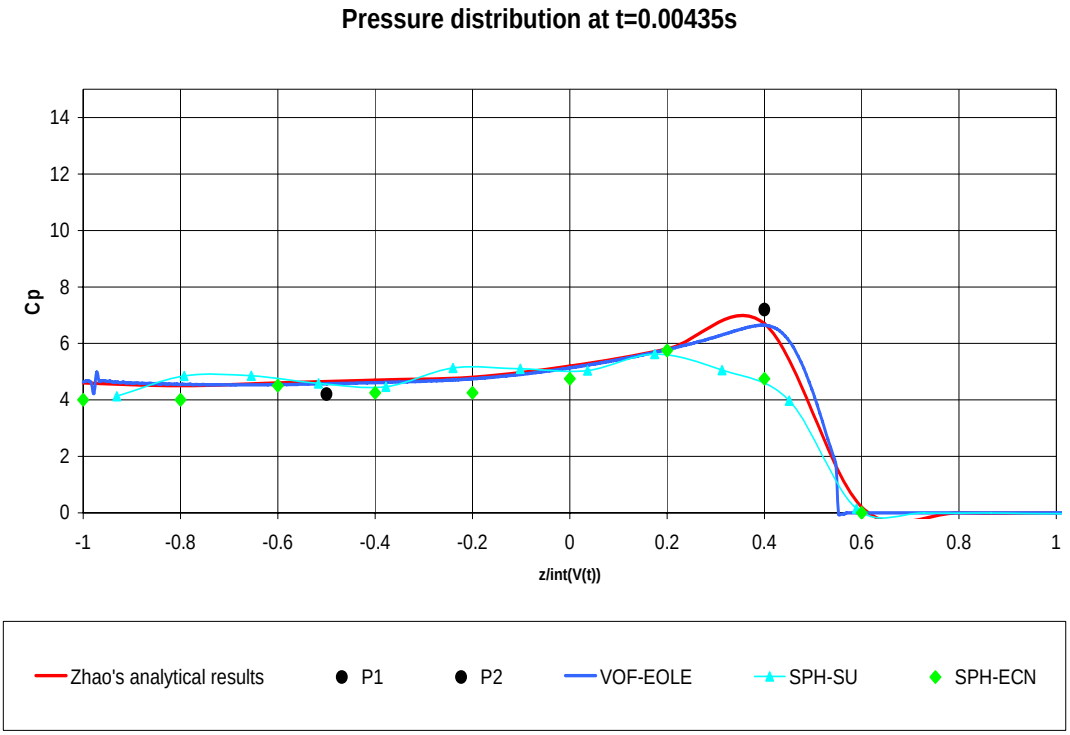

Fig 6.23 Pressure distribution at t = 0.00435s

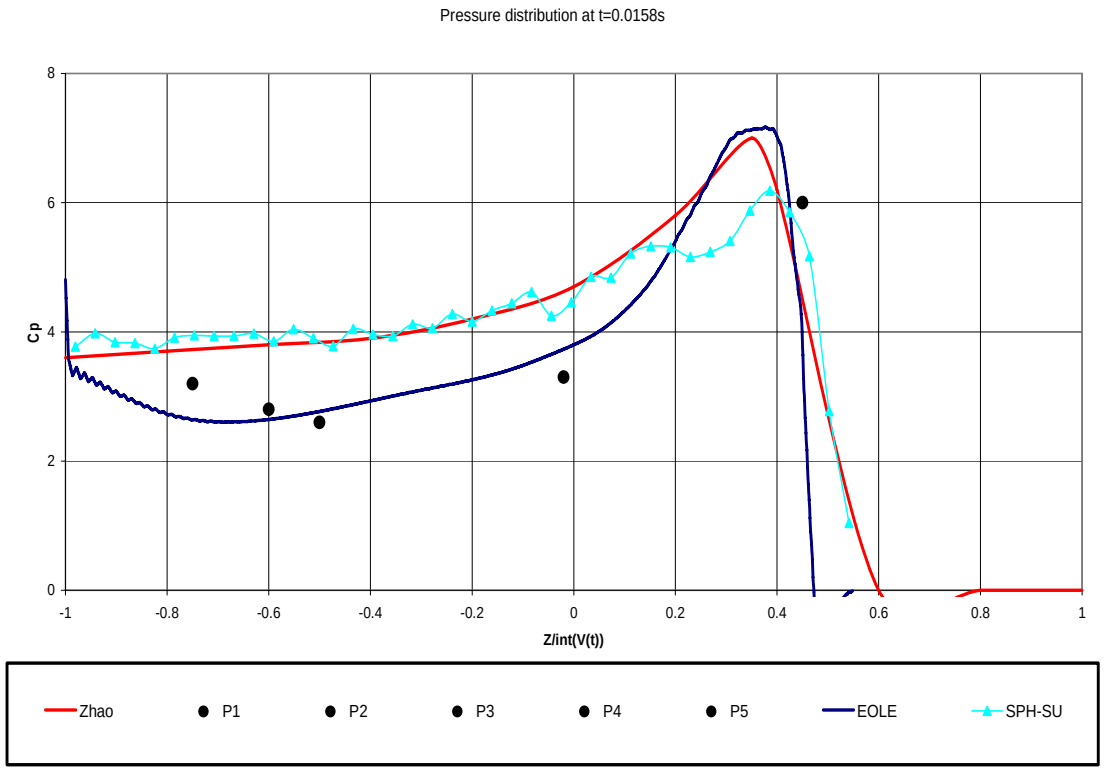

Fig 6.24 Pressure distribution at t = 0.0158s

In fig 6.23 and 6.24, positions of pressure cell P1-P5 and pressure values are normalized by Equations (6.2, 6.3) respectively.

$$Z/\text{int}(V(t)) = \frac{Z}{\int_0^t V(t)dt} \tag{6.2}$$

$$Cp = \frac{P - P_0}{0.5\rho V^2(t)} \tag{6.3}$$

Where P_0 is outside the pressure which is 0 in the SPH simulation, $V(t)$ is wedge vertical velocity given in fig 6.13. z is vertical coordinate on the wedge surface.

SPH results are compared with experiment by Zhao, VOF method by EOLE. At the instance time 0.00435, local pressure of SPH agrees with VOF, analytic and experimental results have been produced very well but it is underestimated at P2. This is supposed to be the compressible effects of SPH at the beginning of impact. However, this underestimation disappears instantly in 0.0158 seconds. In fig 6.24,

SPH results are in accordance with Zhao's results. However, both SPH and analytical results are overestimated when comparing with the experiments which are possibly due to the three dimensional effects. In conclusion, SPH method is capable of predicting acceptable local pressure in slamming.

7 Sloshing

Sloshing can be defined as dynamic load acting over a tank structure as a result of the motion of a fluid with free surface confined inside the tank. It is a highly nonlinear resonant phenomenon appearing in all marine structures containing liquids. This can lead to large local structural loads in the tank and has an important effect on the global ship motion. The effects of sloshing loads are of great importance when designing LNG carriers. It is necessary to develop numerical methods which can describe the fluid loading and coupling between ship motions and sloshing.

In this chapter, two dimensional and three dimensional sloshing problems are simulated with SPH method. The related sloshing effects are discussed with comparison by experiments.

7.1 Description of the problem

Due to the growth of the natural gas market, there is an increasing interest in floating production, storage and offloading system for offshore oil and gas. Moreover, the increasing size of LNG carrier sailing under extreme weather conditions (Barents Sea, North Atlantic) leads to the problem of sloshing which is of particular interest to the ships' designs that hold large liquid tanks. The prediction of loads caused by violent sloshing has been taken account as a part of approaches to safety at sea.

Consideration of internal liquid motions is important for the intact and stability of the (carrying liquid cargo) ships. The difficulty of the scaling of the experimental impact pressure has been extensively analyzed (Bass et al., 1985; Berg, 1987). In order to solve this problem, several studies on different numerical approaches to sloshing have been reported by Su Tsung-Chow (1992), Buechmann (1996), Tanizawa (1996), Chen

et al. (1997), Pawell (1997) and Faltinsen (1999).

Most of them used potential flow model for an incompressible fluid in irrotational motion, which can be used in many cases to model sloshing, in particular for smooth tanks and finite depths. However, dissipation and damping due to run-up and overturning of the fluid near the wall, wave breaking in the middle of the free surface, are issues for intermediate and shallow depths. Therefore, the development of feasible calculation methods to accurately predict sloshing loads should be based on CFD methods.

CFD approaches are used currently to resolve free surface flow problem such as VOF (Hirt and Nichols, 1981) and SPH method (JJ, Monaghan, 1994). In Lee et al. (2007), a solver based on VOF method for free surface was used to study the impacting force due to sloshing. The SPH method has provided good results when used to simulate sloshing problems with high fragmentation on free surface (Landrini et al., 2003; Souto-Iglesias et al., 2004, 2006).

Two cases are studied in this chapter to analyze the effect of sloshing in the tank for which a series of experimental tests have been conducted as well: 1) Two dimensional sloshing in the tank partially filled with water with captive excitation horizontal motion; 2) Three dimensional sloshing with the tank excited by irregular waves. SPH method was developed to simulate these cases and the comparisons are presented and discussed. Although the study (Lee et al., 2007) showed that gas cushioning was significantly affecting the impact phenomenon, the simulations have been performed with one-phase algorithm. The reason was mainly due to the costs connected with two-phase formulation. An example of CPU time required by one-phase and two-phase solvers is present in Table 4 for the simulation of one period in the tank with 70% filling level.

	N_{water}	N_{air}	N_{total}	CPU time
one-phase	70000	0	70000	1 hour
Two-phase	70000	30000	100000	20.2 hours

Table 4: CPU time requirements for one-phase and two-phase SPH solvers

7.2 Benchmark results – Sloshing

Case 1 – 2D Sloshing test for rectangular model

Firstly, the simulations were carried out to investigate the features of resonance phenomenon of sloshing. The rigid tank shown in fig 7.1 was partially filled with 35% fluid. A harmonic sway motion of the tank was forced with the law $A\sin(wt)$. Experimental data were reported by Faltinsen (1974) and Olsen & Johnsen (1975). A wave height sensor was placed 0.05m from the right wall and the maximum wave elevation was recorded.

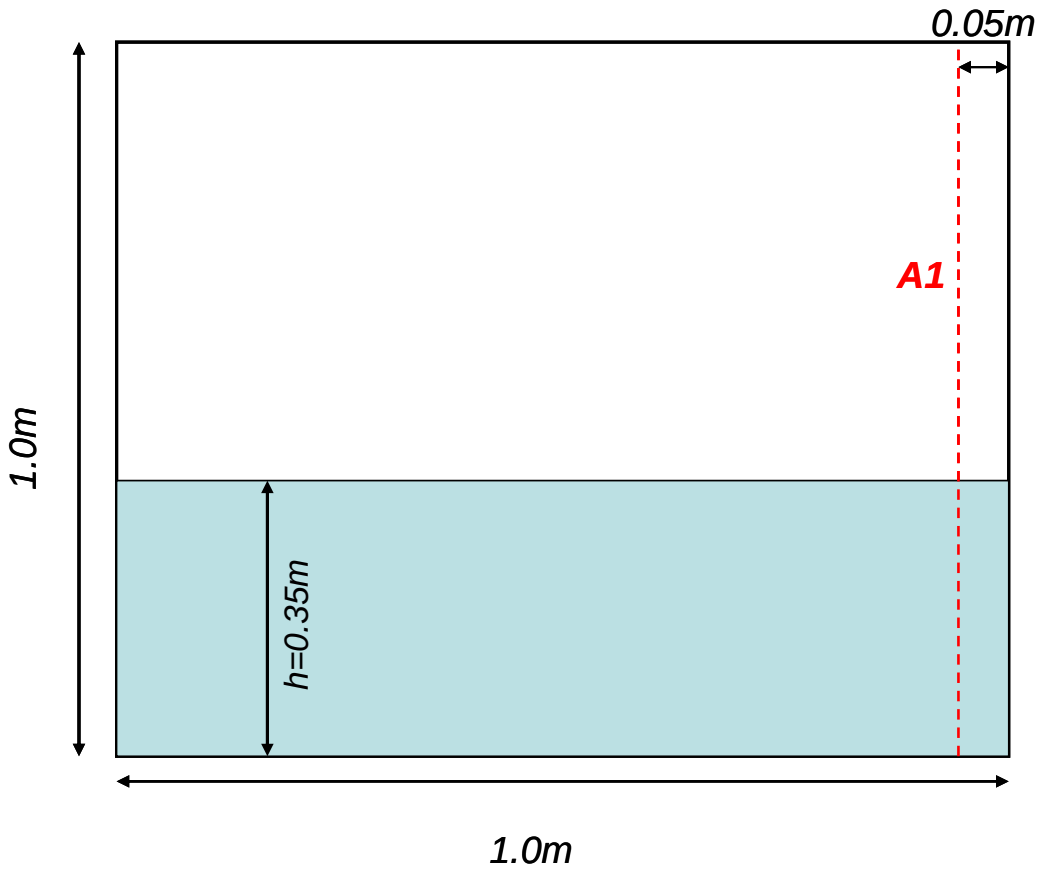

Fig 7.1 Tank model in the experiments by Olsen (1970)

In the experiments, the excitation amplitude $A = 0.05m$ and a series of excitation frequencies $T = \frac{2\pi}{w}$ were tested using the following constants where the length was $L = 1m$ fluid depth was $h/L = 0..35$ and the natural frequency was $T_1 = 1.27s$

In the numerical simulations, the forced sway amplitude increased smoothly then remained steady after 10T. The maximum wave elevation was recorded from 20T to 30T to obtain the steady-state value.

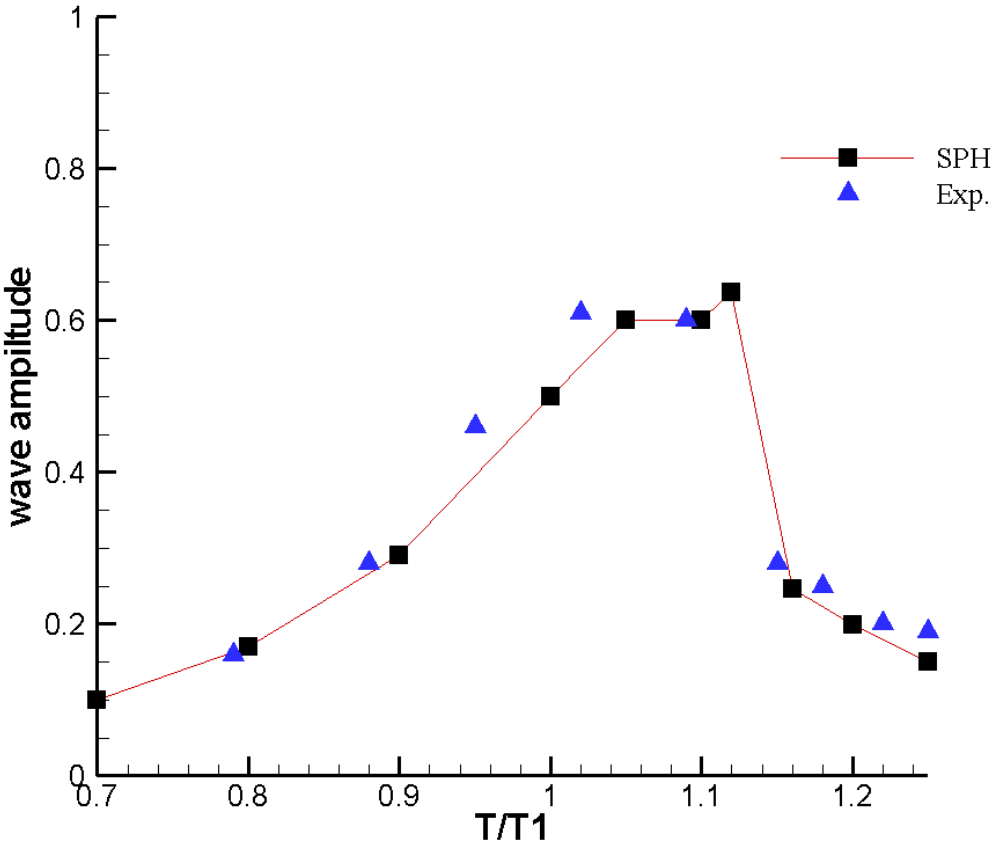

Fig 7.2 maximum wave amplitude at the wave height sensor A1

The maximum wave elevation amplitude was compared between SPH solution and the experiments. Generally, a good agreement was observed as a result.

The sloshing problem is one of the priority issues to shipyards and shipping companies. In order to study how the loads impacting on the structure in sloshing and to obtain the experimental results which can be used to verify numerical results, sloshing experiments were carried out by DSME (Daewoo Shipbuilding & Marine Engineering Co.Ltd 2005).

Experimental setup

The tank model was set on the table and it is allowed to move harmonically in horizontal direction by the shaking system. Pressure at the tank wall and the displacement of the table were measured. At the wall and top of the tank, 9 holes (C1~C9) were made to set the pressure sensor. Fig 7.3 shows rectangular model and its details.

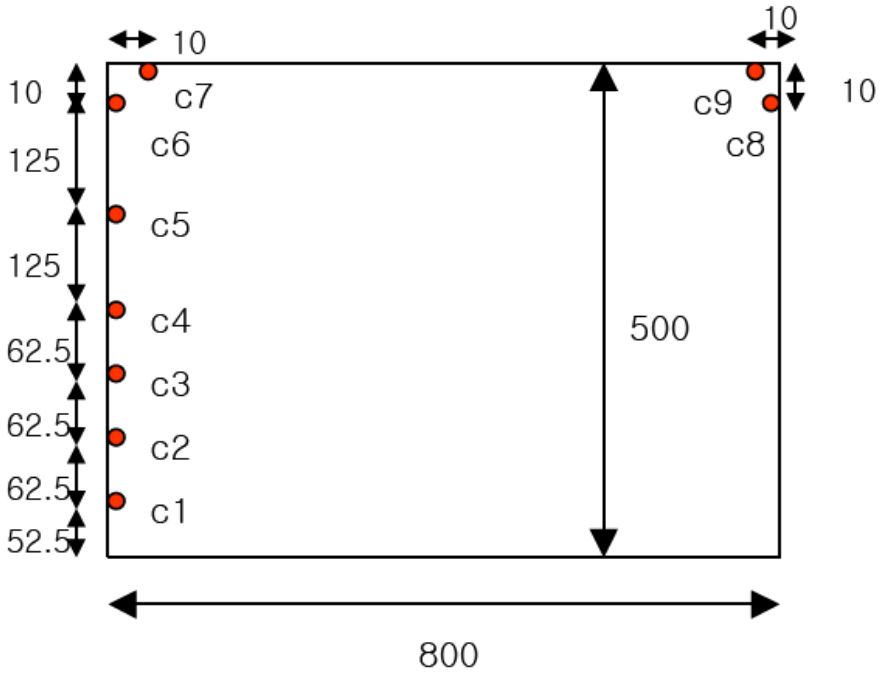

Fig 7.3 Sketch of tank with 9 pressure sensors (measurement: mm)

The direction of the tank motion is horizontal sway motion, and the motion type is harmonic. The tank position is defined as

$$X = \xi \sin(\omega \cdot t)$$

Where, ω is the excitation frequency, ξ is the excitation amplitude which is 20mm in experiments.

The excitation frequency ω is determined based on the natural frequency ω_n of the fluid motion in the tank and ω_n is obtained by the linear theory as follow

$$\omega_n^2 = \frac{\pi g}{L} \cdot \tanh(\pi \cdot \frac{h}{L})$$

Where g is the gravitational acceleration and h is the depth of a still water in the tank and L is the length of the tank.

In order to investigate the resonance of sloshing, $\omega/\omega_n = 1.0$ is adopted in SPH simulation when the filling level is 70%, $\omega = 5.8185$ (rad/sec). The tank forced motion is shown in Fig 7.4

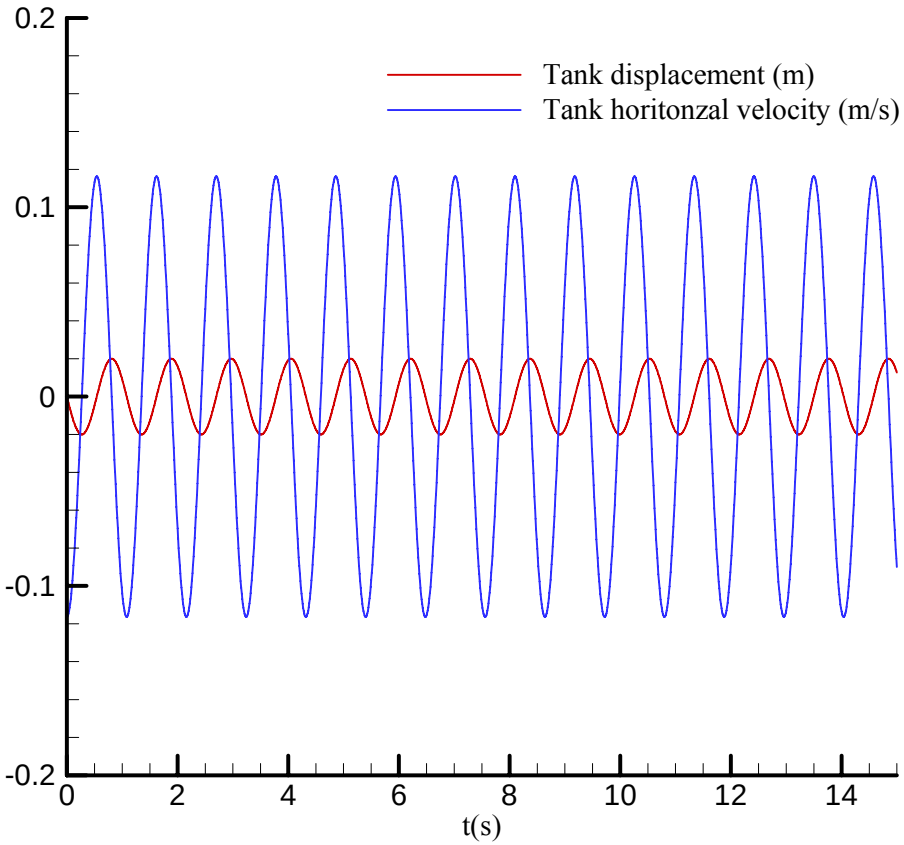

Fig 7.4 tank motion and velocity

The simulation time is about 15 seconds, which covers 14 periods of motion. Numerical parameters SPH in shown in Table 5 In order to compare experimental and numerical data, the snapshots at time series were compared with experimental video. Experimental data have been provided in the experimental report by DSME.

Dimension	2D
Number of fluids	One-phase

Fluid Density	1000 Kg/m3
Viscosity	Artificial viscosity 0.03
smoothed length	1.3h, constant smoothed length
Tensile stability	Yes
Solid boundary condition	No slip, ghost particles
Kernel function	Gaussian kernel (3h)
Gravity	-9.81 m/s²
Kernel correction	Shepard correction
Sound speed	40m/s
Initial particle distance	5mm
Total number of particles	11200
Number of particles in X-direction	160
Number of particles in Y-direction	70
Time evolution algorithm	fourth order *Runge-Kutta*
Duration of simulation	15 s
Recorded Time step (extracted data)	0.025s

Table 5: Numerical parameters of SPH for 2D sloshing

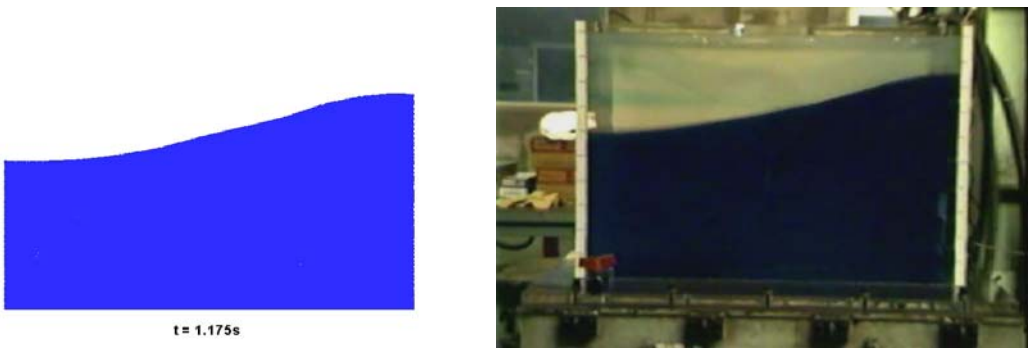

Fig 7.5 Evolution of fluid during sloshing at time = 1.175s

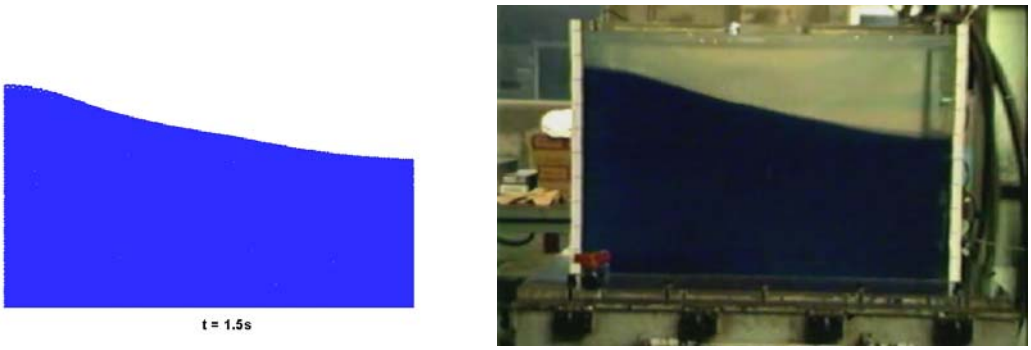

Fig 7.6 Evolution of fluid during sloshing at time = 1.5s

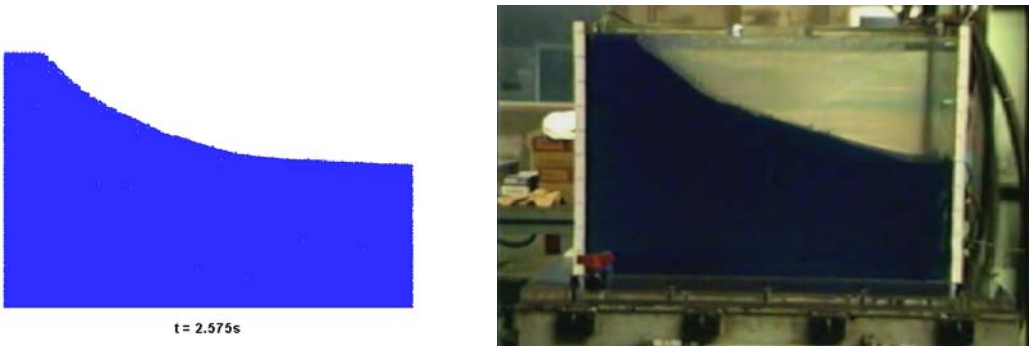

Fig 7.7 Evolution of fluid during sloshing at time = 2.575s

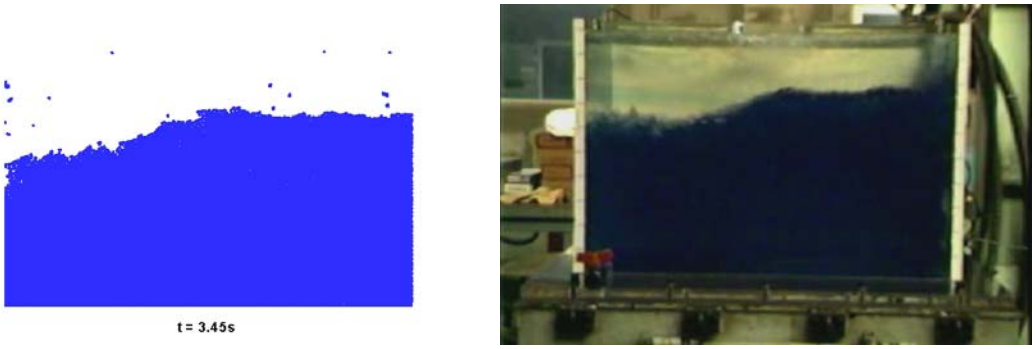

Fig 7.8 Evolution of fluid during sloshing at time = 3.45s

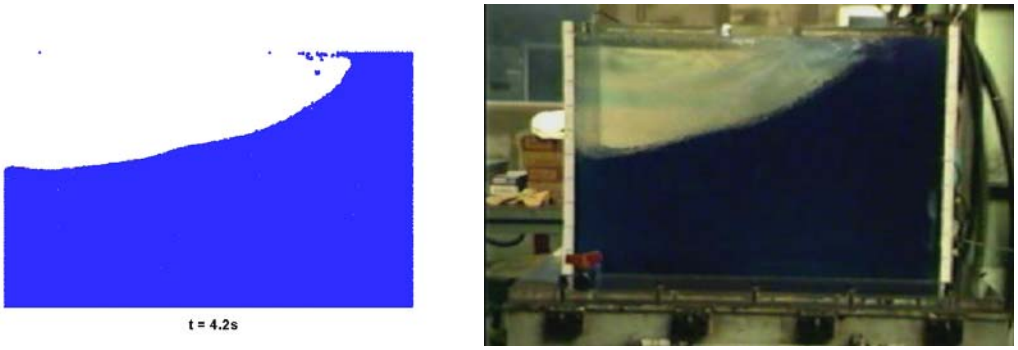

Fig 7.9 Evolution of fluid during sloshing at time = 4.2s

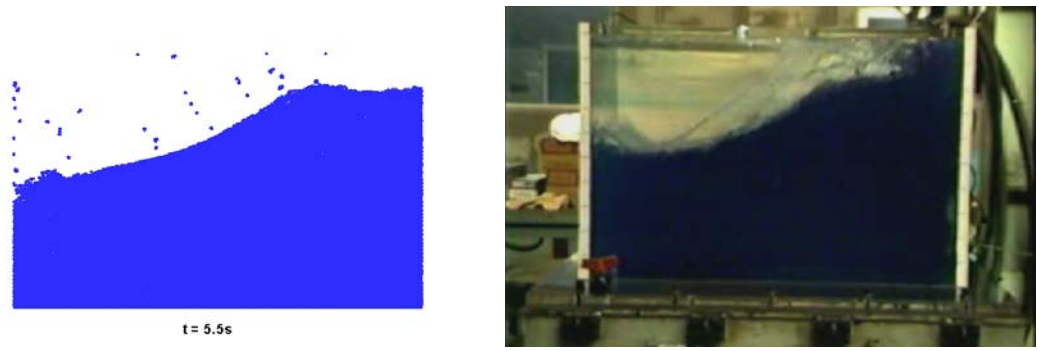

Fig 7.10 Evolution of fluid during sloshing at time = 5.5s

The free surface motion was splendidly reproduced in SPH simulations. The free surface shapes at different time series agree with the recorded experimental video very well even when the impacting and overturning of the waves occurred.

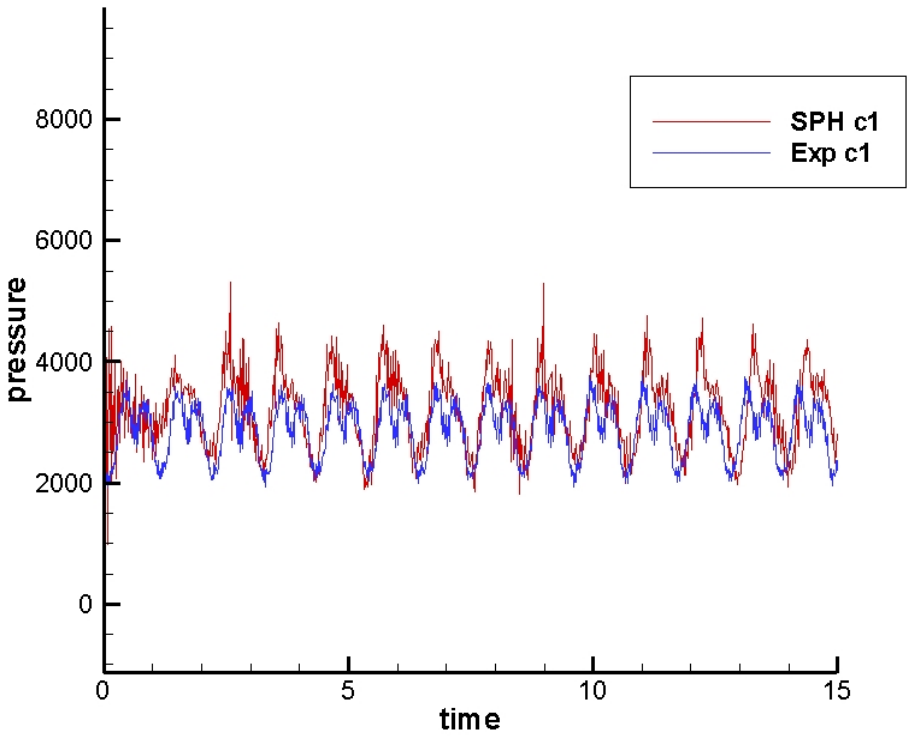

Fig 7.11 Experiment vs. SPH Pressure at sensor c1 in time series

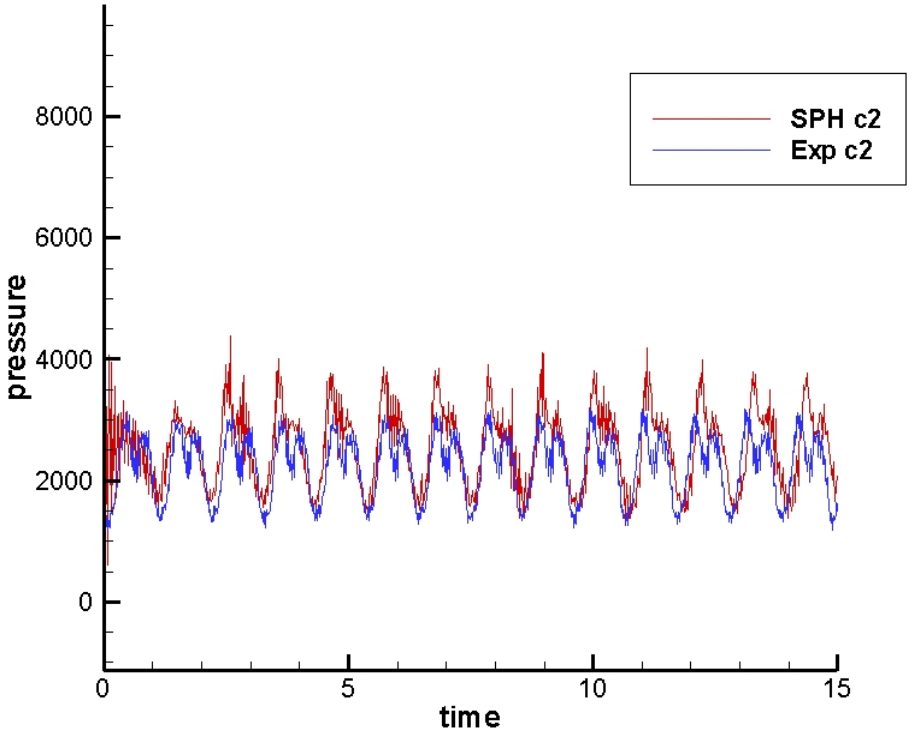

Fig 7.12 Experiment vs. SPH Pressure at sensor c2 in time series

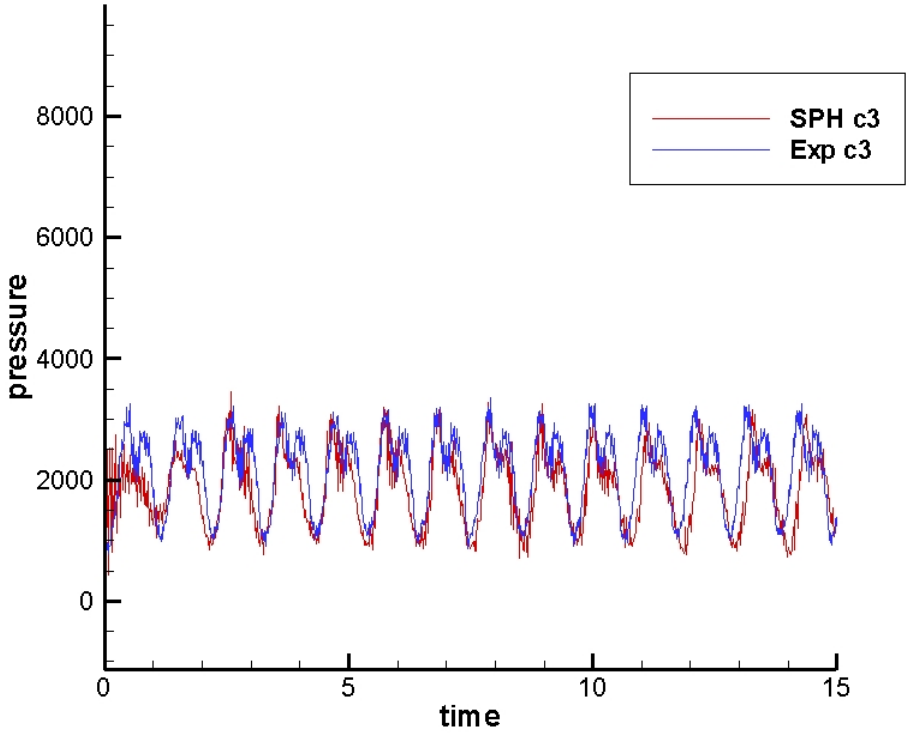

Fig 7.13 Experiment vs. SPH Pressure at sensor c3 in time series

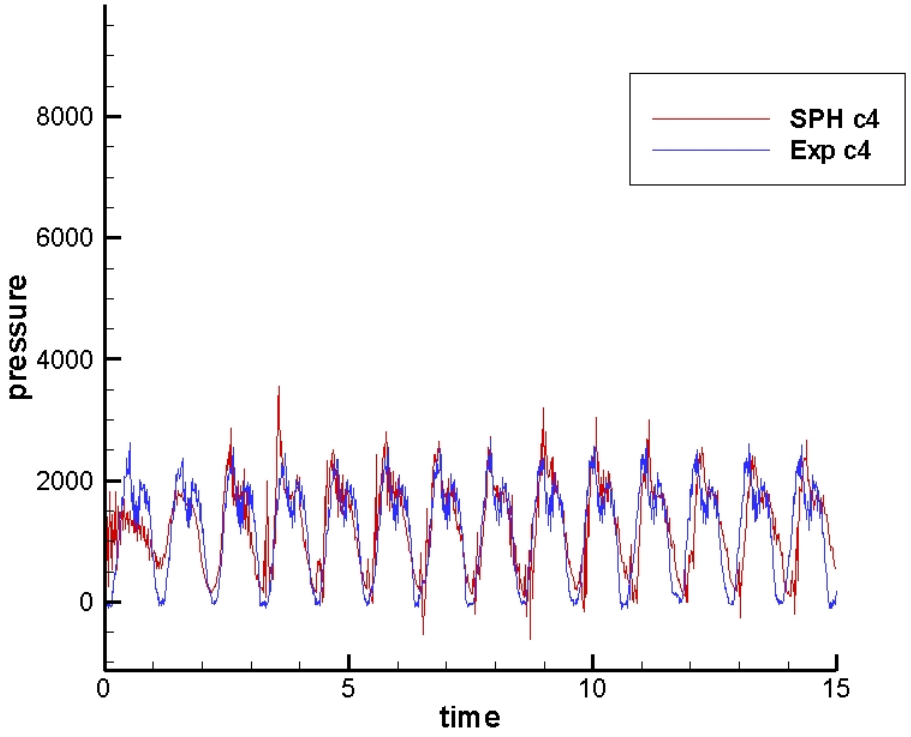

Fig 7.14 Experiment vs. SPH Pressure at sensor c4 in time series

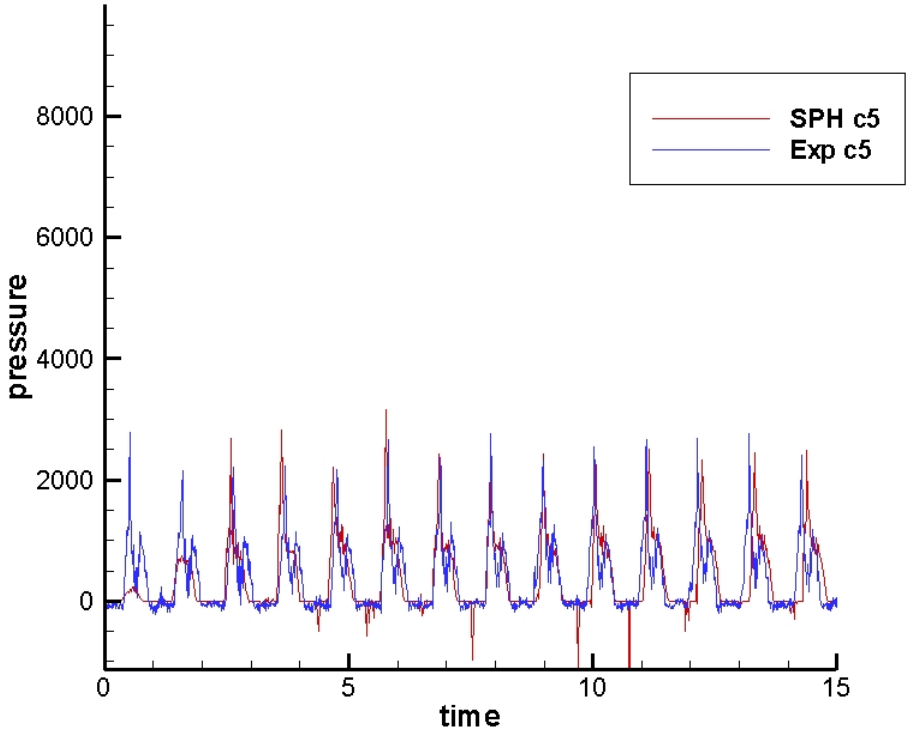

Fig 7.15 Experiment vs. SPH Pressure at sensor c5 in time series

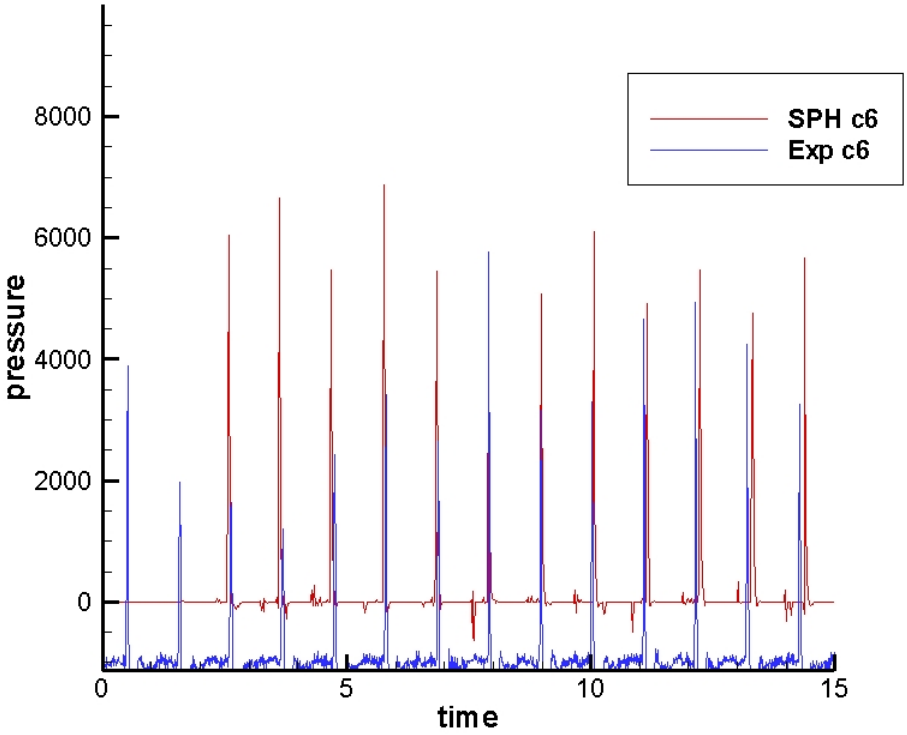

Fig 7.16 Experiment vs. SPH Pressure at sensor c6 in time series

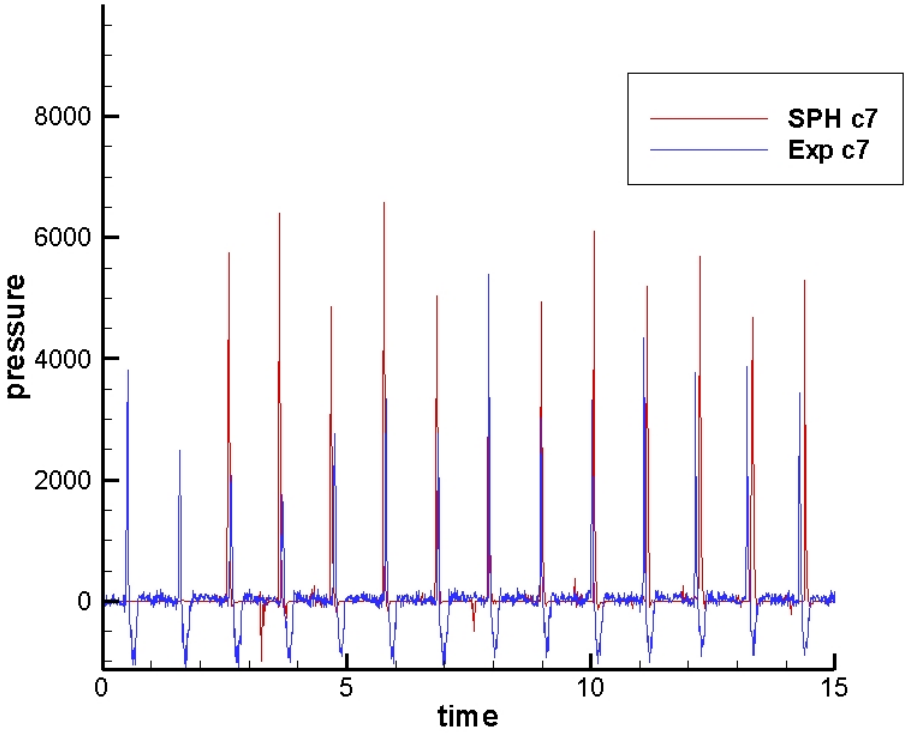

Fig 7.17 Experiment vs. SPH Pressure at sensor c7 in time series

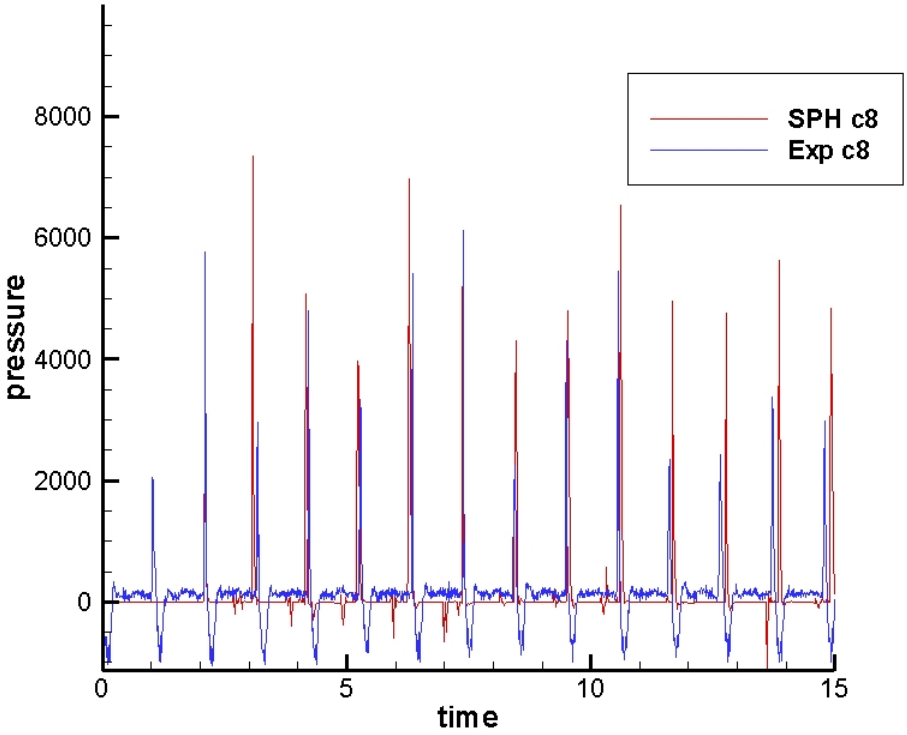

Fig 7.18 Experiment vs. SPH Pressure at sensor c8 in time series

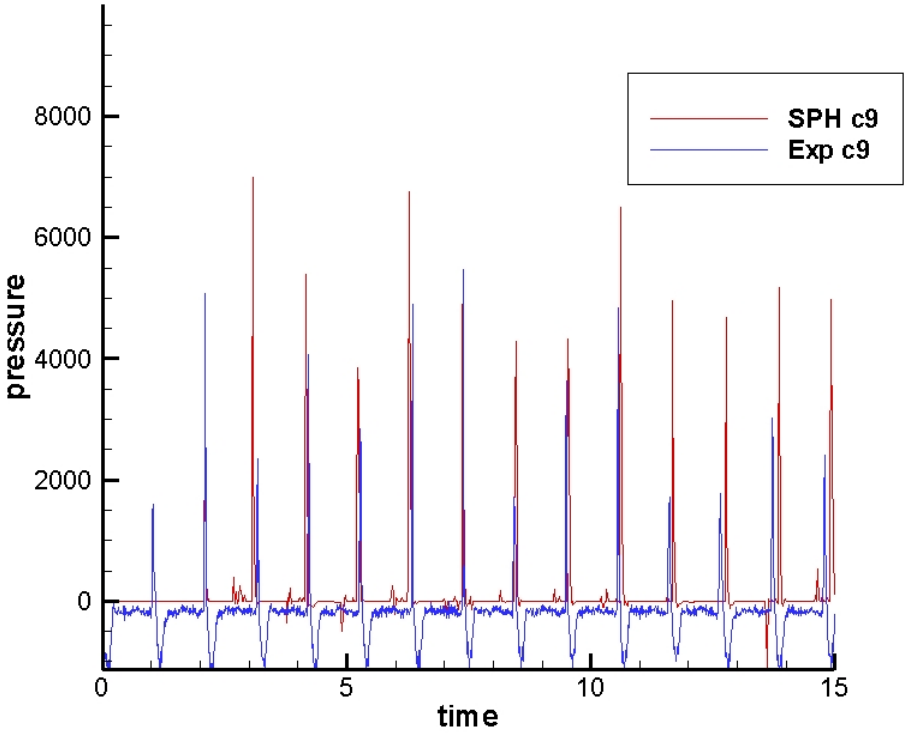

Fig 7.19 Experiment vs. SPH Pressure at sensor c9 in time series

The numerical oscillation comes from the speed of sound which was related to the weekly compressible approach adopted in SPH.

The overestimation of pressure peak value were observed on pressure sensor c6~c9 which were involved in impact event. Firstly, the impact pressure has a random character due to its strong dependence on the wave's shape just before the impact (Bass et al. 1985; Peregrine 2003). Another reason is probably due to the two-phase character of the impact phenomena as one-phase solver was used in numerical simulation.

The global shape of the pressure curve agrees with the experimental pressure very well for all the pressure sensors.

Case 2 – 3D sloshing

Tests (Principia) have been carried out in 2001 and 2002 by the GIS-Hydro in the wave basin of La Seyne/mer – France (BGO First facilities). The experimental set up consists of a rectangular barge model supporting two rectangular tanks partly filled with water. Regular and irregular wave tests results were available for the beam seas. Barge motions and internal wave elevations have been measured.

Benchmark tests are proposed hereafter based on these model tests both for pure sloshing conditions, imposing the measured barge motions, and for barge / tanks coupling.

The barge has the following features

Length	3m

Width	1m
Height	0.267m
Mass without tank	127 kg
Draft	0.108m
Molded volume	0.285m3
Centre of gravity above keel	0.237m
Gyration radius (in roll)	0.414m

Table 6: feature of barge

The model was installed in the basin in the middle of the testing section with its longitudinal axis parallel to the wave-maker line (only beam waves were considered).

The mooring system was ensured by 4 cables equipped by springs. The mooring lines were attached on the 4 corners of the barge at 0.262m height according to the keel. The natural sway period of the mooring system (direction of the waves) was 20s.

The reference point for the measurements of the translation of the barge motion was at the deck level (0.267 m above the keel level).

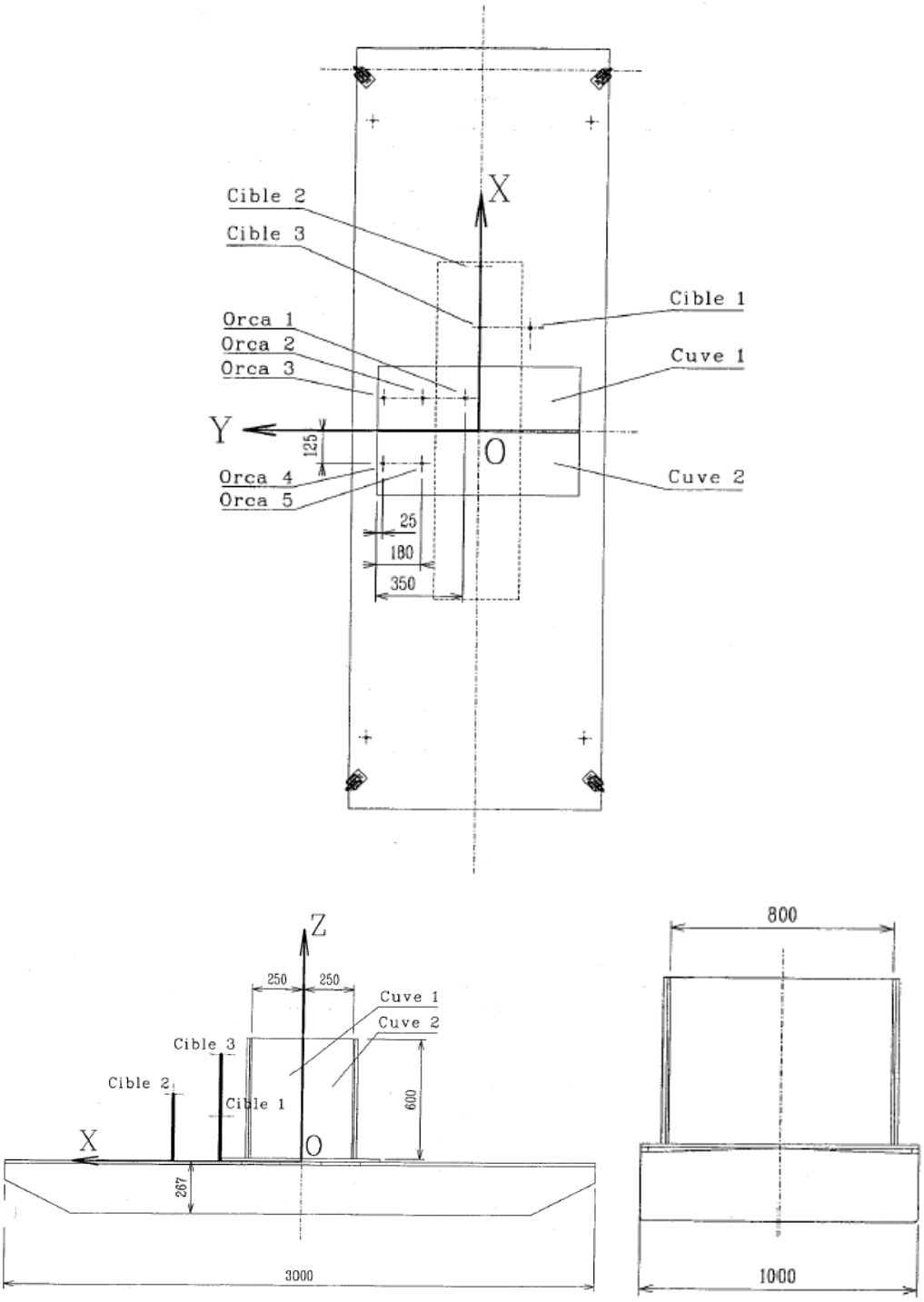

Fig 7.20 Sketch of the model

The two tanks were set on the deck of the barge, at mid-ship, with their length in the transverse direction. The elevation of the inner bottom of the tanks, with respect to the keel, is about 0.3m.

The following are the characteristics of the two rectangular tanks:

Length	0.8m
Width	0.25m
Height	0.6m
Mass	37kg

The water motion inside the tank was measured by 5 probes:

- 3 in the tank 2 (higher filling level) at 24mm, 180mm and 350mm from the wall closest to the wave-maker.
- 2 in the tank 1 at 25mm and 180mm from the corresponding wall.

Wave elevations were measured by 5 probes. All were set on the longitudinal axis of the basin at different spacing.

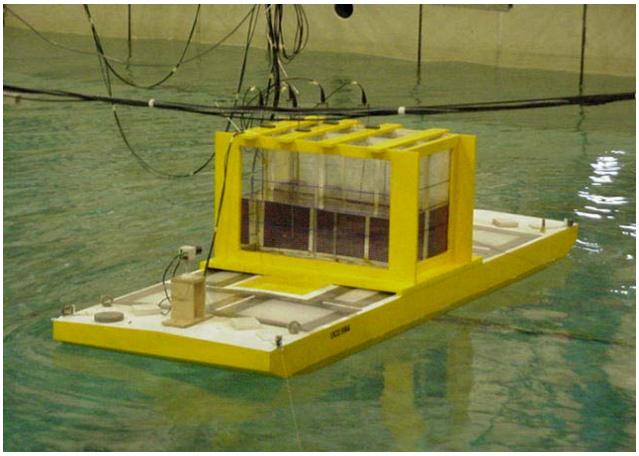

Fig 7.21 View of the model test set-up in BGO First

The tests were carried out in irregular waves. The sloshing in the tank was induced from the 6 DOF (Degrees of freedom) barge motions.

For the numerical model, the inputs were the initial height of the free surface, the 6DOF displacement of the tank (motions of the barge) and the position of the tank.

Test cases irregular waves	Motions of the barge	Filling level
Irreg 1	6 DOF	39cm
Irreg 2	6 DOF	19cm

The following figures show the 6 DOF movements of the barge (and the tank) in irregular waves.

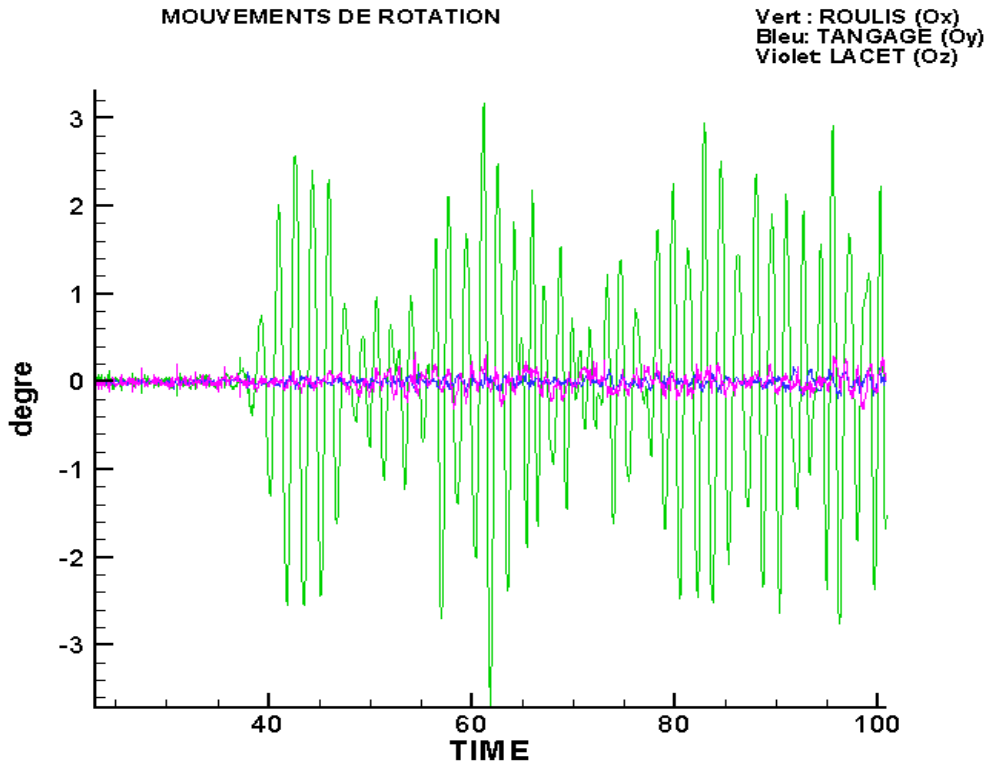

Fig 7.22 irregular waves – direction OY - Hs=6.1 cm, Tp=1.6 s Green: roll (OX) Blue: pitch (OY) Purple: yaw

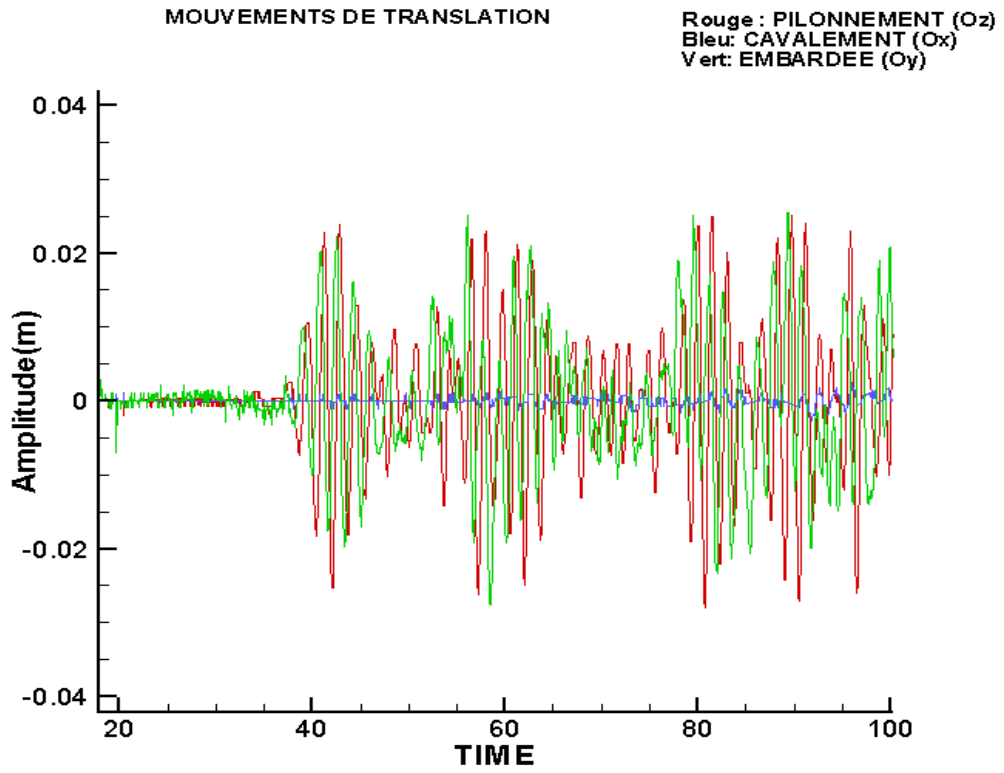

Fig 7.23 irregular waves – direction OY - Hs=6.1 cm, Tp=1.6 s Red: heave Blue: surge (OX) Green: sway (OY)

In the SPH simulation, one-phase model was considered to avoid expensive calculation assumption. Other parameters for SPH are shown in Table 7

Dimension	3D
Number of fluids	One-phase
Fluid Density	1000 Kg/m3
Viscosity	Artificial viscosity 0.03
smoothed length	1.3h, constant smoothed length
Tensile stability	Yes
Solid boundary condition	No slip, ghost particles
Kernel function	Gaussian kernel (3h)
Gravity	-9.81 m/s²
Kernel correction	Shepard correction

Sound speed	28m/s	20m/s
Initial particle distance	10mm	
Total number of particles	78000	38000
Number of particles in X-direction	25	25
Number of particles in Y-direction	80	80
Number of particles in Z-direction	39	19
Time evolution algorithm	fourth order *Runge-Kutta*	
Duration of simulation	100 s	
Recorded Time step (extracted data)	0.05s	

Table 7: Numerical parameters of SPH for 3D sloshing

The sloshing was computed using 2 methods: VOF and SPH. The following figures show the comparisons between the two methods and experiments, of free surface elevations at different probes, and for the two specified filling levels. The computed and measured transient flows were directly comparable because the initial conditions were identical for the two cases. The SPH results are shown below (Fig 7.24-7.34)

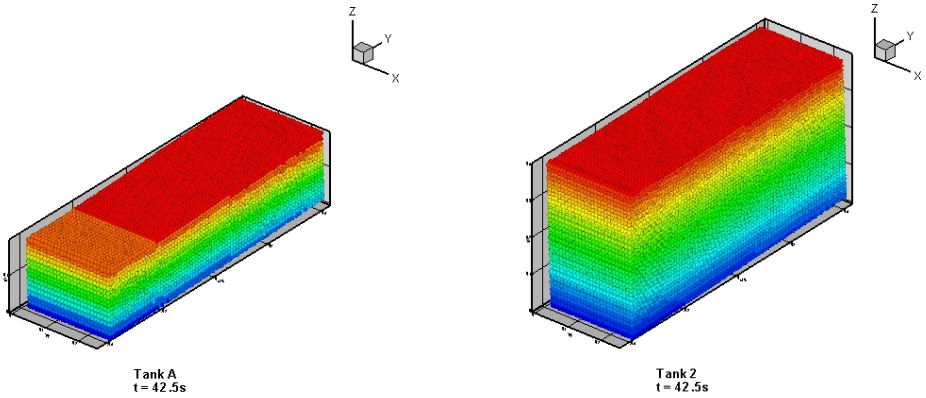

Fig 7.24 SPH snapshots at time t=42.5s (left: H=19cm, right: H=39cm)

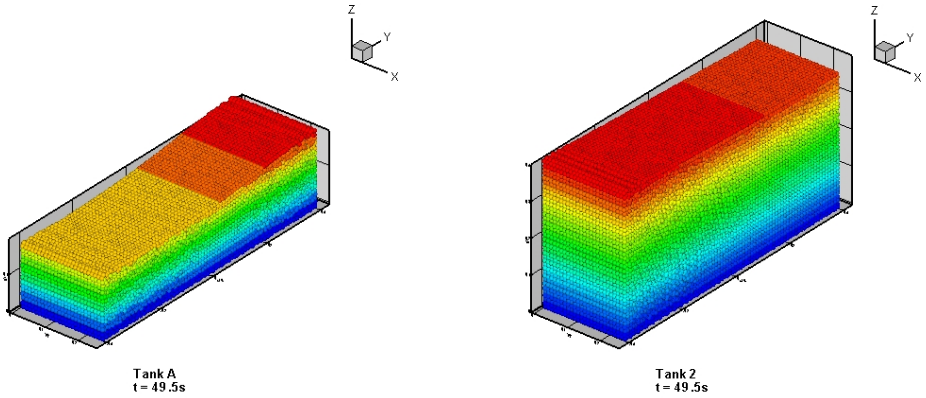

Fig 7.25 SPH snapshots at time t=49.5s (left: H=19cm, right: H=39cm)

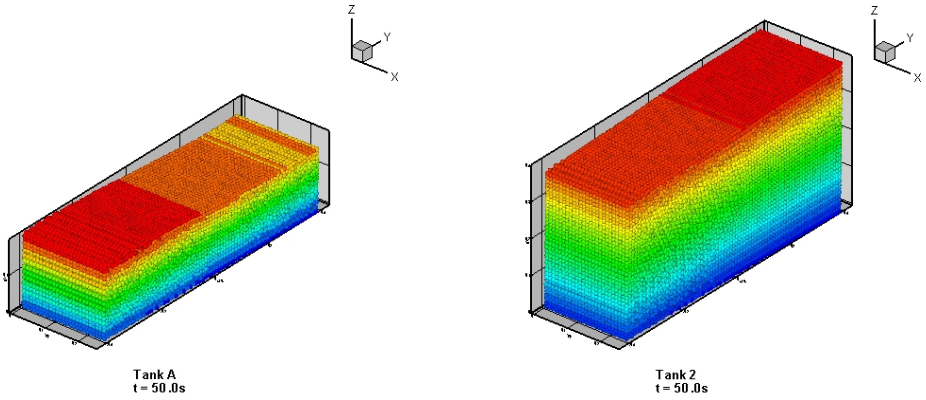

Fig 7.26 SPH snapshots at time t=50.0s (left: H=19cm, right: H=39cm)

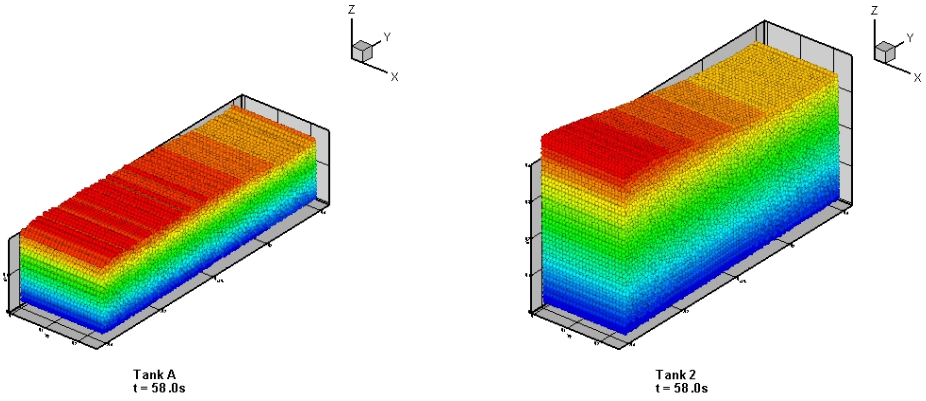

Fig 7.27 SPH snapshots at time t=58.0s (left: H=19cm, right: H=39cm)

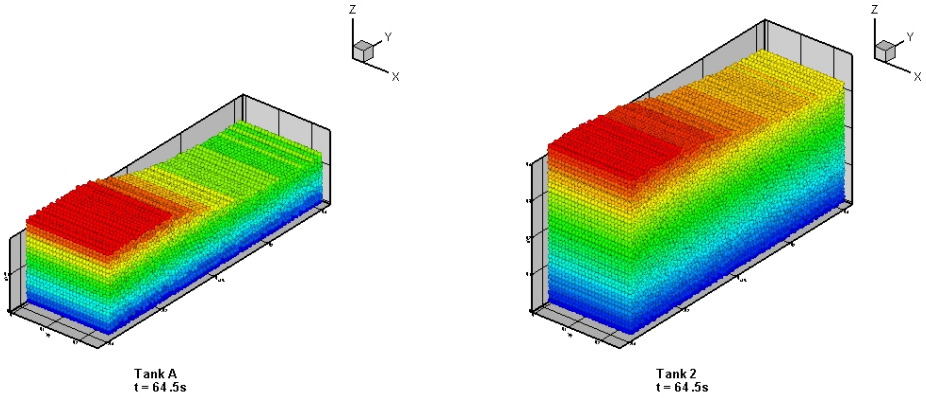

Fig 7.28 SPH snapshots at time t=64.5s (left: H=19cm, right: H=39cm)

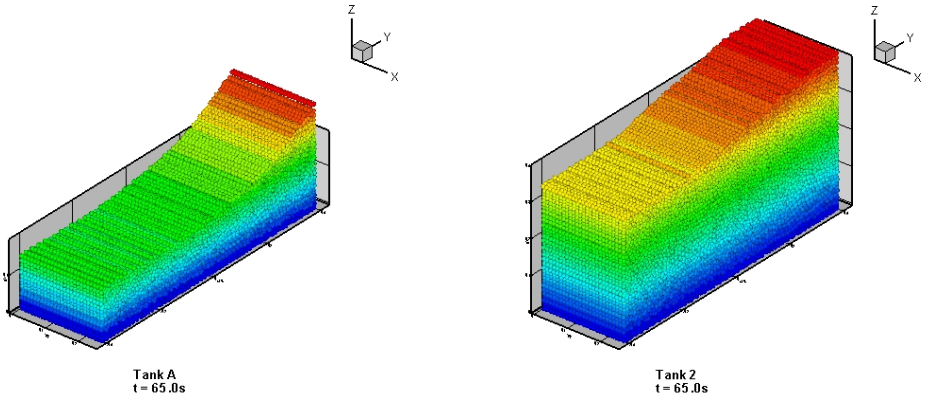

Fig 7.29 SPH snapshots at time t=65.0s (left: H=19cm, right: H=39cm)

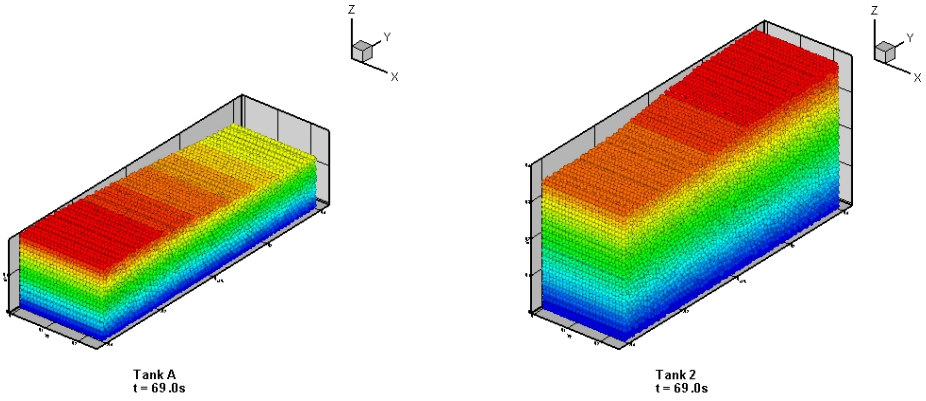

Fig 7.30 SPH snapshots at time t=69.0s (left: H=19cm, right: H=39cm)

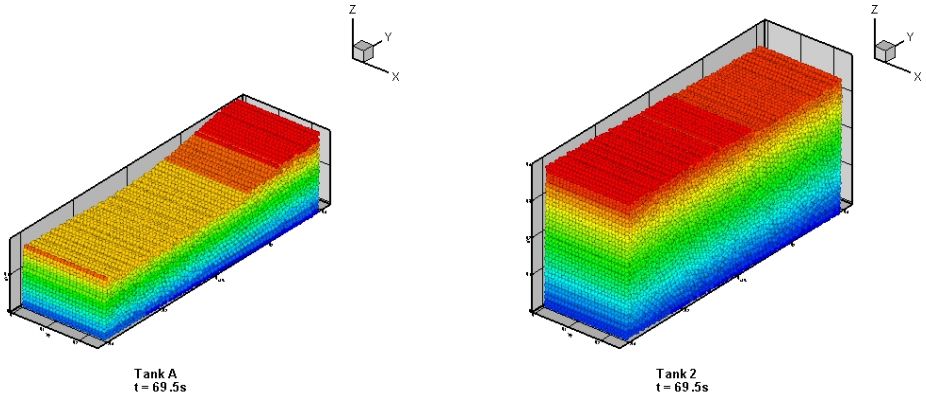

Fig 7.31 SPH snapshots at time t=69.5s (left: H=19cm, right: H=39cm)

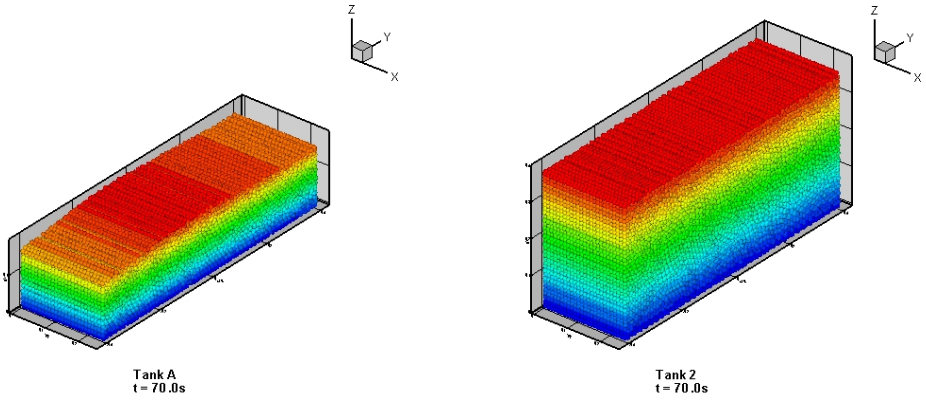

Fig 7.32 SPH snapshots at time t=70.0s (left: H=19cm, right: H=39cm)

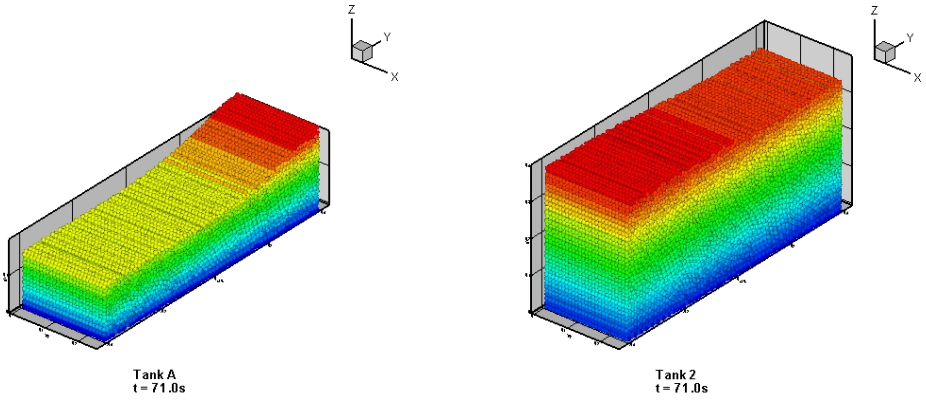

Fig 7.33 SPH snapshots at time t=71.0s (left: H=19cm, right: H=39cm)

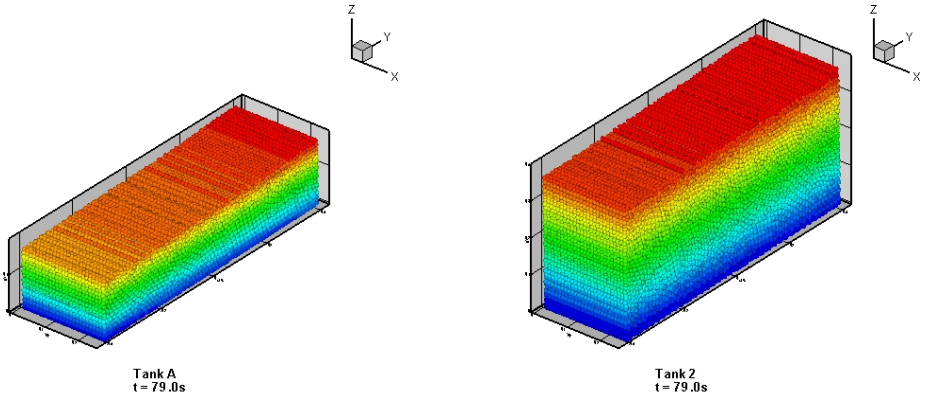

Fig 7.34 SPH snapshots at time t=79.0s (left: H=19cm, right: H=39cm)

The calculations were also performed with VOF method in the absolute reference frame. The 6 DOF tank motions (irregular wave) were imposed. The two-phase model using the VOF method for interface tracking was considered. The time-step is 0.004s. The mesh was coarse, especially in comparison with SPH and experimental results.

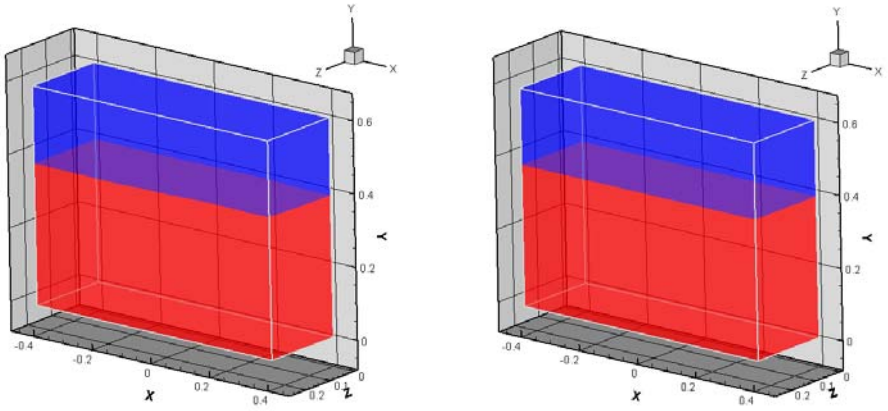

t = 0.0 s *t = 15.36 s*

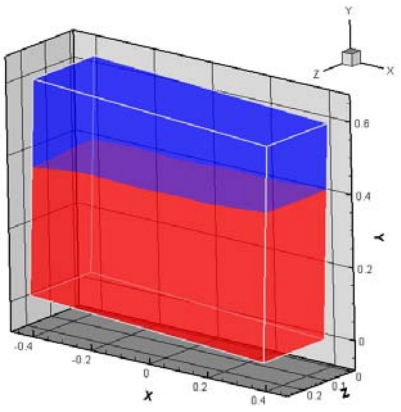

t = 29.759 s

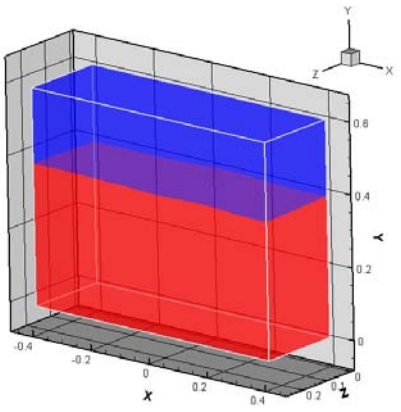

t = 42.558 s

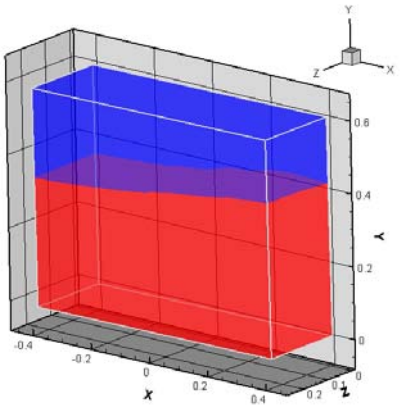

t=49.76s

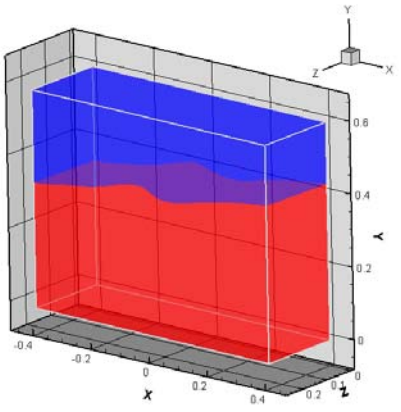

t=55.68s

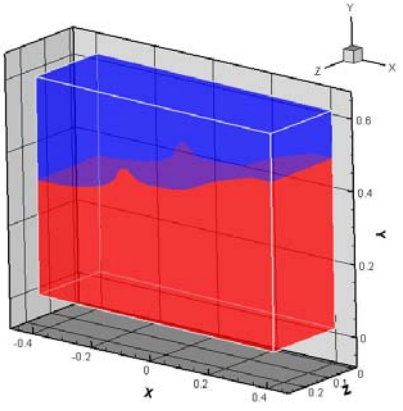

t=58.01s

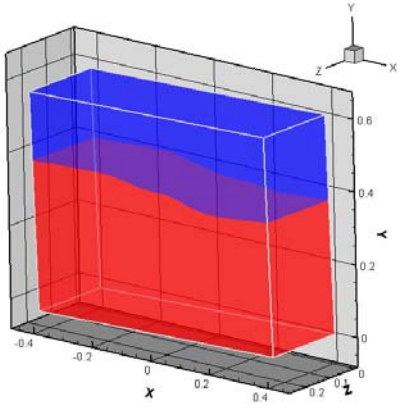

t=79.04s

Fig 7.35: sloshing in the tan k 2 - H=39cm

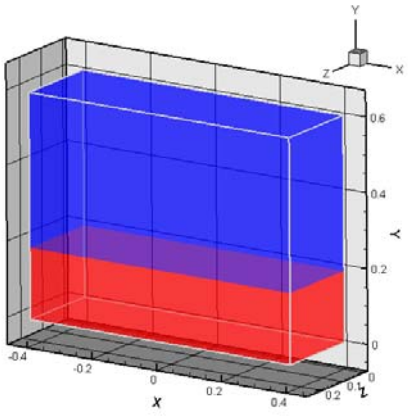

t=0.01s

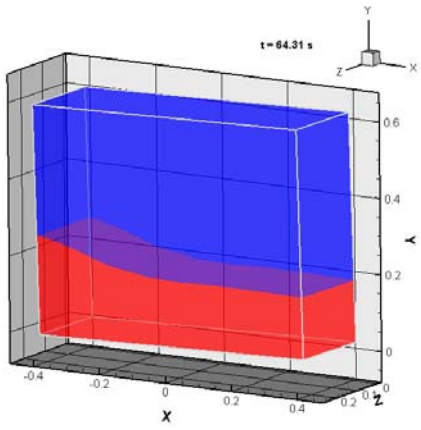

t=64.31s

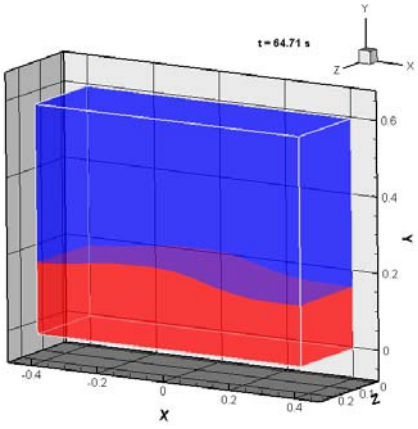

t=64.71s

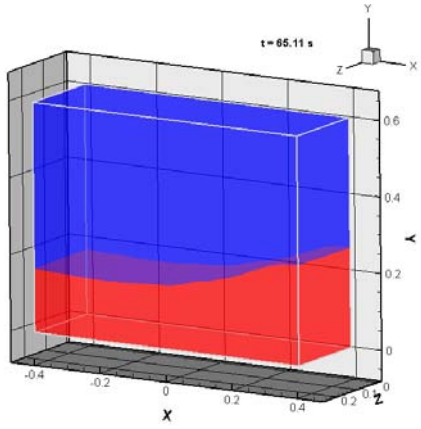

t=65.11s

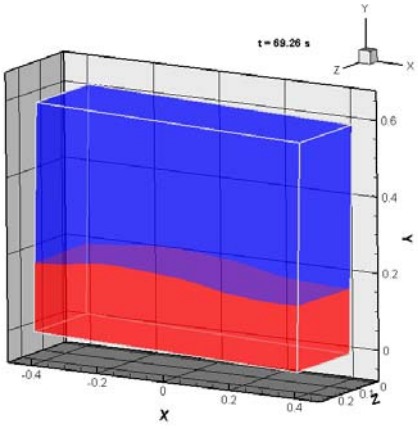

t=69.25s

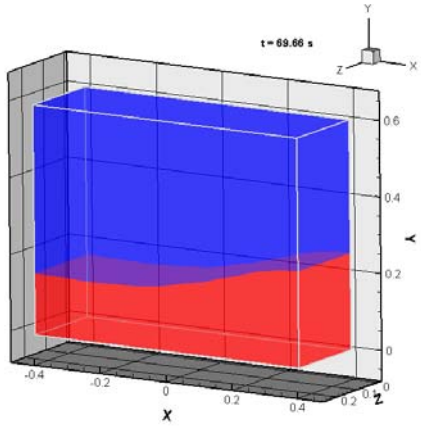

t=69.65s

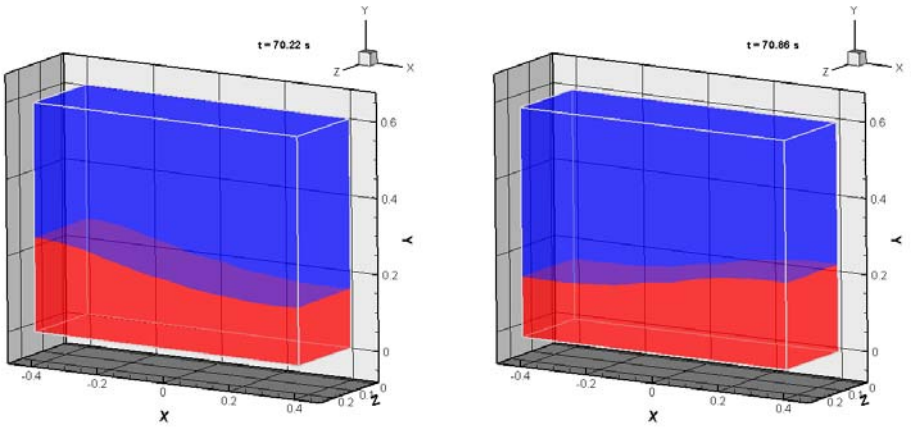

t=70.22s *t=70.86s*

Fig 7.36: sloshing in the tank 2 - H=19cm

The first wave impacts the barge when t = 40s. Subsequently, both the numerical models have produced satisfactory results with respect to the measurements and they have captured the correct period and irregular evolution of the free surface. The comparison of wave amplitude at wave height sensor is given below (fig 7.37-7.44)

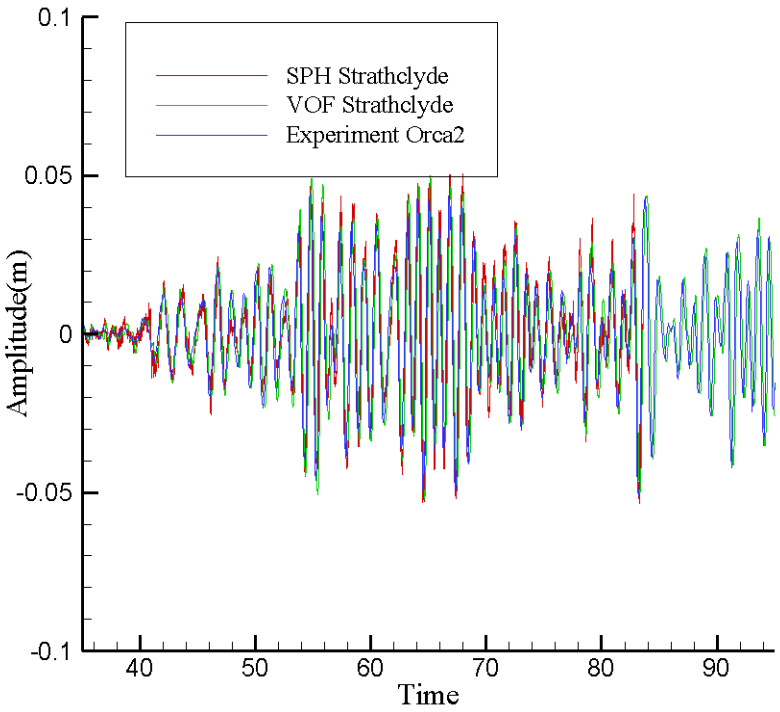

Fig 7.37: Comparison VOF – SPH – experiments at the probe Orca 2

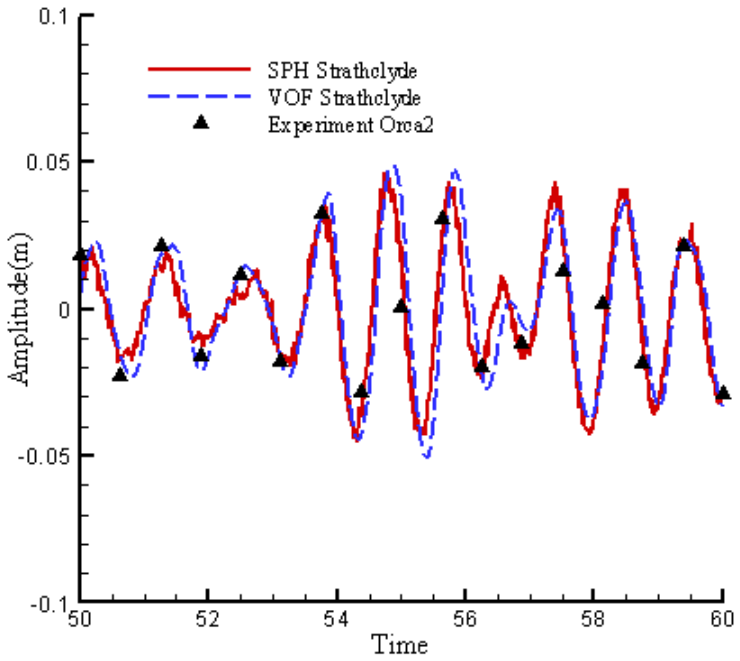

Fig 7.38: Zoom of comparison VOF – SPH – experiments at the probe Orca 2

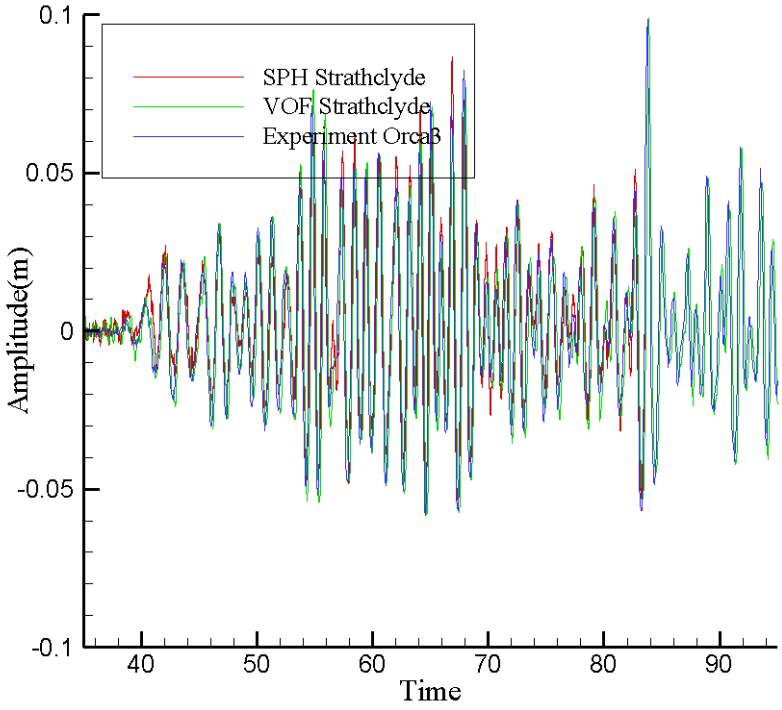

Fig 7.39: Comparison VOF – SPH – experiments at the probe Orca 3

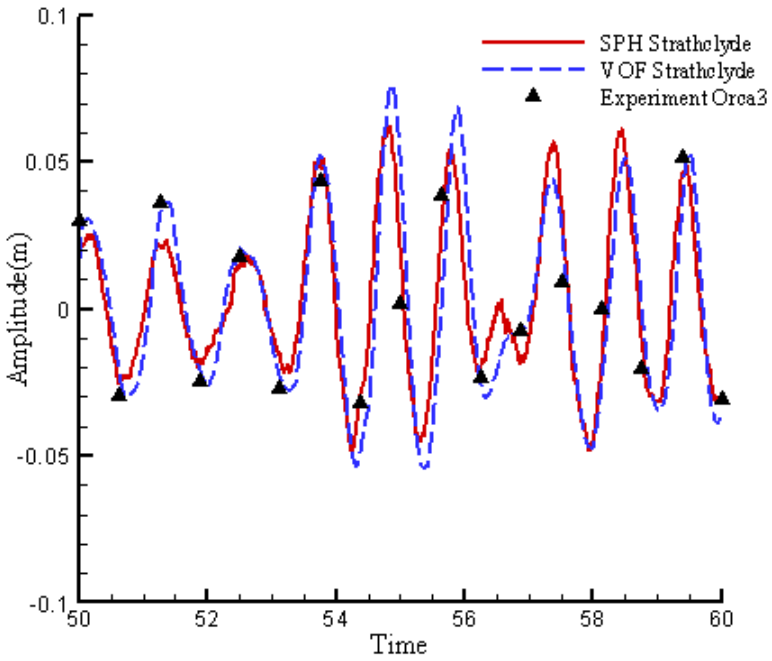

Fig 7.40: Zoom of comparison VOF – SPH – experiments at the probe Orca 3

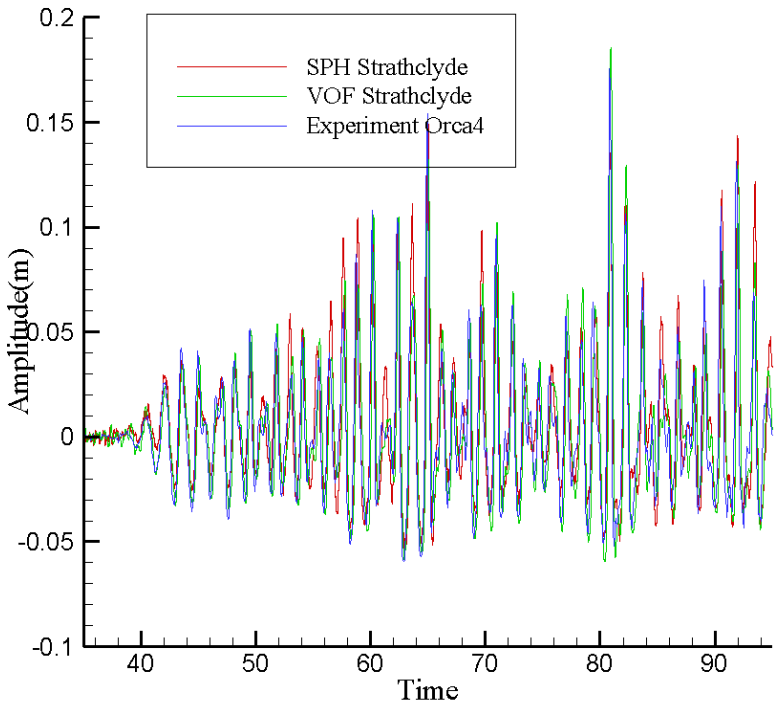

Fig 7.41: Comparison VOF – SPH – experiments at the probe Orca 4

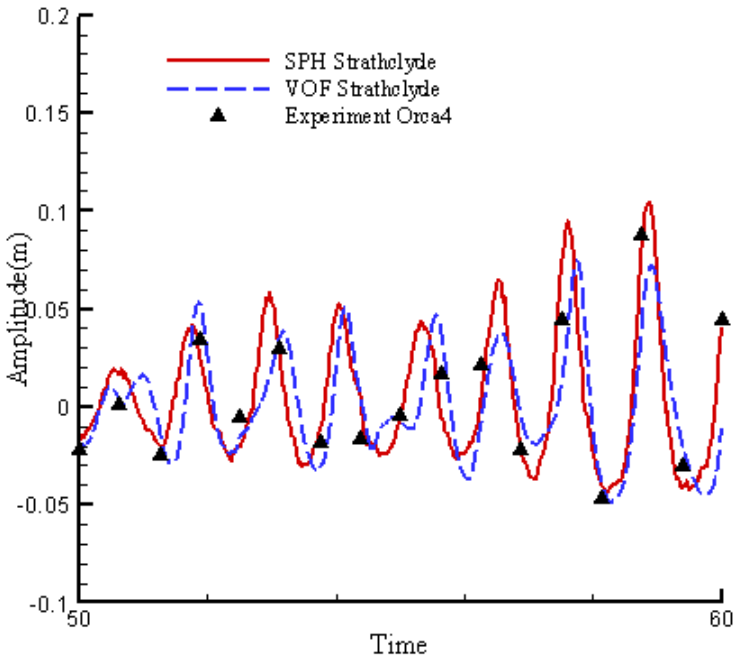

Fig 7.42: Zoom of comparison VOF – SPH – experiments at the probe Orca 4

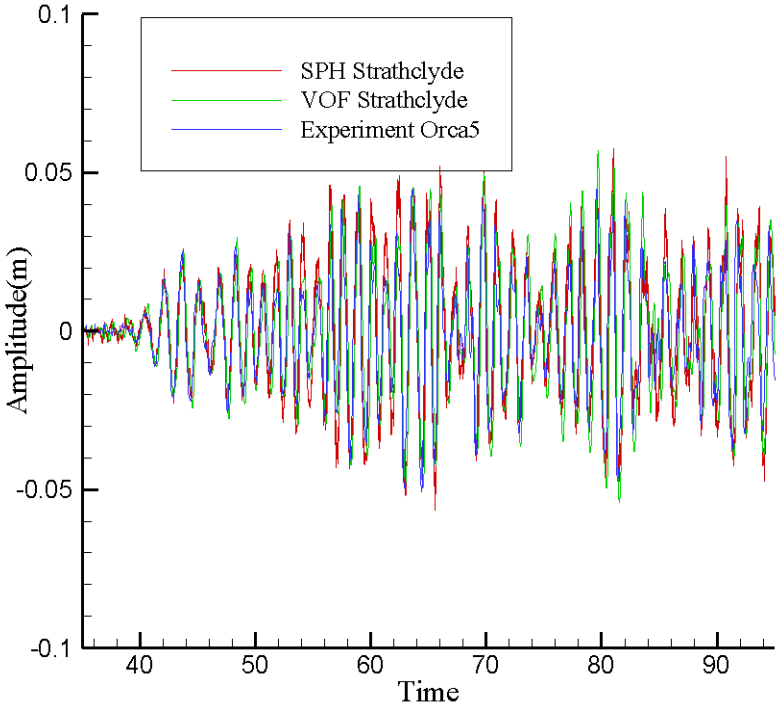

Fig 7.43: Comparison VOF – SPH – experiments at the probe Orca 5

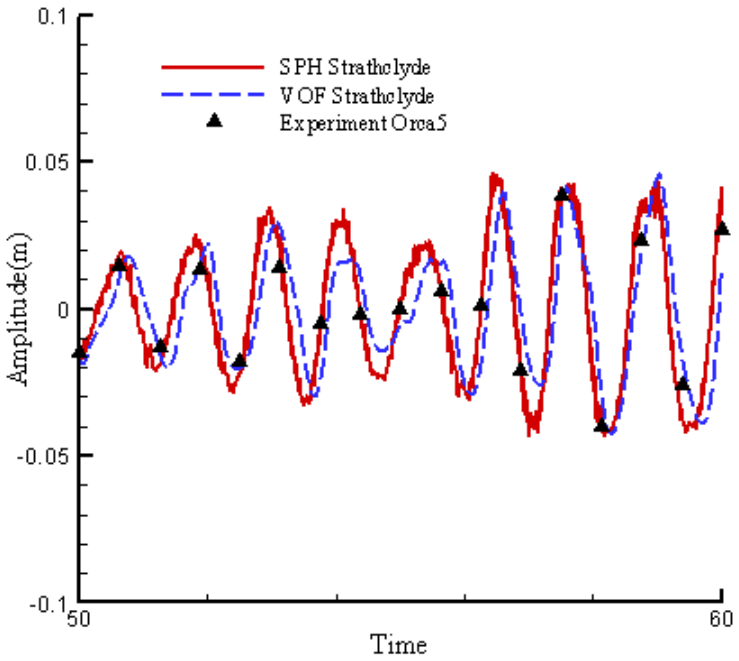

Fig 7.44: Zoom of comparison VOF – SPH – experiments at the probe Orca 5

The amplitudes of free surface elevation between SPH and experiments were satisfactory. Some selections of free surface elevation were slightly underestimated for VOF method which was probably due to the high coarse local mesh for this case of small filling rate. In addition, the SPH simulation has shown high frequency oscillations which was due to the weekly compressible water used in the method. However, it was negligible in the evaluation of wave height.

The simulation time was 100 seconds for both numerical methods. The total calculation cost of SPH is still very expensive (about 10 days), even when 16 processors are used. Under the same scale of mesh (the mesh size for VOF is equal to the size of particles) the comparison for efficiency of both numerical methods is discussed as below

- The number of particles will be much less than the number of cells in VOF method if one-phase model is adopted for SPH method as VOF uses two-phase

model to catch the interface.

- Additional calculation cost to search neighbor particles in SPH method

- The efficiency of calculation is quite similar. VOF allows larger time step because implicit algorithm is adopted but additional iterations is required in each time step.

Moreover, SPH method could produce sharper free surface than using VOF method. In conclusion, SPH is an excellent CFD tool to predict sloshing problems.

8 Flooding due to collision damage

A ship may be damaged due to a collision when it is sailing. As a result, water will flood into the damaged compartment immediately. The internal openings and non-watertight subdivision in the watertight (WT) compartment can have a significant effect on the motions of the ship during the flooding process. When flooding occurs, proper lifesaving measures and evacuation procedures are vital for the safety of human life. In order to establish relevant guidelines, clear understanding of the dynamic behavior of a damaged vessel and the process of water flooding into the damaged area is essential. In this process, vessel motion affects the water flooding and water sloshing in the compartment and conversely, the violent motion of liquid due to water sloshing in the compartment influence the vessel motion.

The non-linearity and strong coupling between flooding loads and ship motion are the main problems during the calculations. Therefore, the development of feasible calculation methods to accurately predict the hydrodynamics of ship with liquid onboard should be based on CFD methods. In this chapter, two dimensional and three dimensional flooding in damaged compartments are simulated with SPH method. The features of flooding are studied with comparison with experiments and other numerical methods.

8.1 Review of flooding

Several sophisticated methods have been developed over the last decade for the simulation of transient flooding of damaged Ro-ro vessels with a flooded vehicle deck. The classical hydraulic model is widely used to calculate the floodwater dynamics in previous studies (Santos et al., 2002; Palazzi and De Kat, 2004; Ruponen, 2007). The inflow and outflow of water through the damage opening is determined by the

modified empirical Bernoulli's equation. The motion of floodwater inside the compartment is ignored and its free surface is assumed to be horizontal. An improved model for the internal water motion was proposed by Papanikolaou et al. (2000), in which the internal water is considered as a lump mass moving freely over a specific path surface, yet the water surface is assumed to remain flat. A more sophisticated model for calculating the internal water dynamics is to use shallow water equation (Santos and Guedes Soares, 2002; Valanto, 2006; Santos and Guedes Soares, 2006). Although all the approaches mentioned above are practical and efficient to predict the floodwater motion and its impact on the vessel, there are some limitations. Firstly, a simple hydraulic model drives the water ingress/egress through the opening, and hence the transient dynamics of the flow are ignored. Secondly, the surface of floodwater in the compartment is assumed to be either horizontal or flat. In the case when the vessel undergoes large amplitudes of motion, these approaches lack the ability to model the violent flows with non-linear free surface, even though the shallow water theory is employed. Thirdly, the above models cannot fully consider the influences of the geometry of damage opening and the internal layout of complex compartment on the motion of floodwater. Therefore, it is required to discover other effective and accurate method to predict the floodwater dynamics.

Some CFD works have been presented for the simulation of flooding in the past few years. Volume of Fluid (VOF) method, proposed by Hirt and Nichols (1981), has become the most popular method for calculating free surface flows. Many studies have shown that the VOF method is capable of capturing sharp interface even with large scale overturning and deforming (Van't Veer and De Kat, 2000; Gao, 2001; Woodburn et al., 2002; Gao et al., 2004; Cho et al., 2005).

SPH (Smoothed Particle Hydrodynamics) method is a mesh free CFD solver which has the natural advantage to capture free surface. In addition, SPH has no grid problem which is particularly attractive for nonlinear wave-body interaction problems, including water flooding and capsizing of a floating body.

The objective of this chapter is to investigate the features of flooding in numerical ways. Parallel SPH code is developed and the results are compared with VOF method and experimental data. Three cases are studied: 1) Water flooding into two dimensional damaged boxes: numerical model is defined with different position of the damaged areas. 2) Three dimensional flooding into the fixed compartment: experiments were carried out by Cho (2005). 3) Simplified ship flooding: Mid-section of an actual ship is tested and wave height in the compartment and outside of the ship is recorded for comparison. The simulations are still performed with one-phase algorithm to avoid high calculation cost.

8.2 Benchmarking results – Flooded compartment

Case 1 – 2D rectangular box

In order to validate the flooding case with SPH concerning the coupling with free motion tank, numerical models and 2d transient flooding under free motion are proposed in fig 8.1-8.3

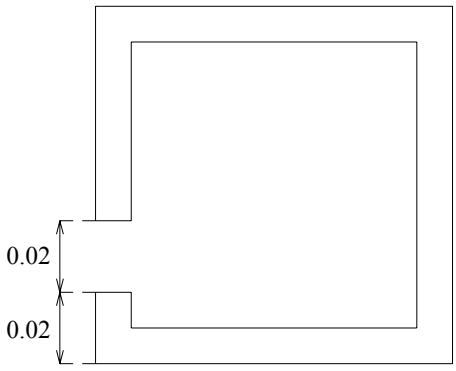

Fig 8.1 Case A with damage open 0.02m above the bottom

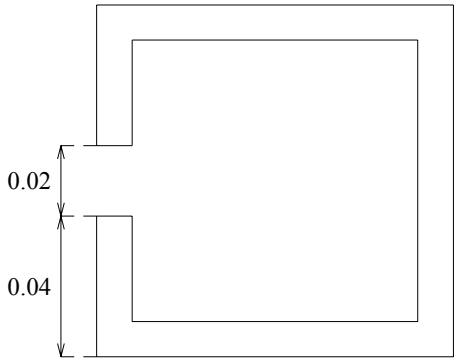

Fig 8.2 Case B with damage open 0.04m above the bottom

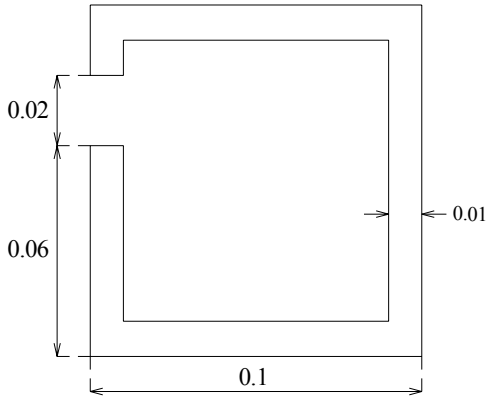

Fig 8.3 Case C with damage open 0.06m above the bottom

All the boxes have the same opening length but with different height on the left frame. Other characters are shown in Table 8 as below.

Weight	7.5kg
Moment of inertia	0.075kg.m2
Length	0.1m
Height	0.1m
Gravity centre above bottom	0.025m
Horizontal gravity center	0.05m
Thickness	0.01m
Draught	0.075m

Table 8: reference of numerical box

The drought of the box is 0.075m before it is open at initial time as it keeps equilibrium in still water shown in fig 8.4

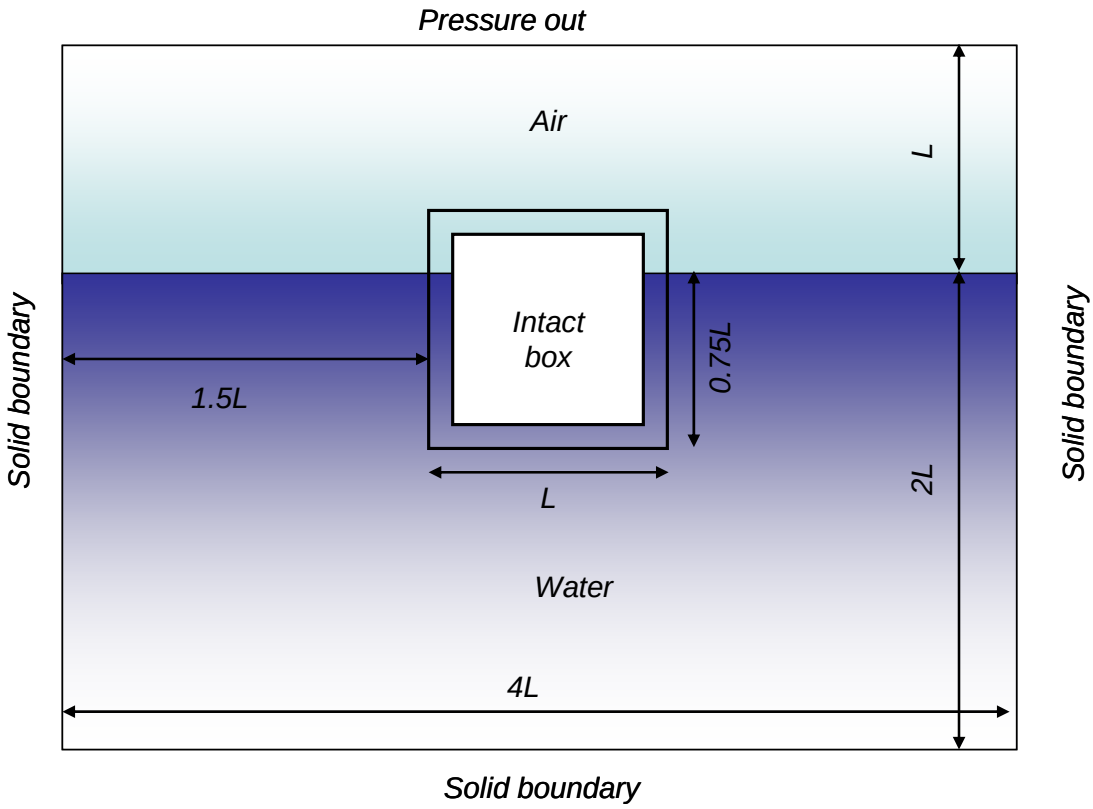

Fig 8.4 numerical calculation domain

Concerning the boundary condition for calculation domain, the bottom boundary can be defined as solid boundary condition which has little effect on the flooding evolution. The depth was set up 2.67 times of the initial drought. The width was set 4 times the length of the box in order to reduce the influence of far field. Regardless of the quality of simulation, the numerical models were aiming at the validation of SPH method for flooding and VOF method was also used to simulate these cases for comparison.

One-phase model was used for SPH method while 1L height of air domain was

defined in VOF method. Uniform particles were initialized in the domain. Dummy particle boundary condition was adopted on the box which was discretized as several layers of boundary particles. The box takes the free motion due to the fluid evolution and its surge. Heave force and roll momentum were calculated with summation of boundary forces (section 4.4). The total number of particles was about 100,000. The damage was opened instantly when the simulation starts.

The snapshots of flooding evolution of Case A, Case B and Case C in time series are shown in Fig 8.5, 8.6 and 8.7 respectively.

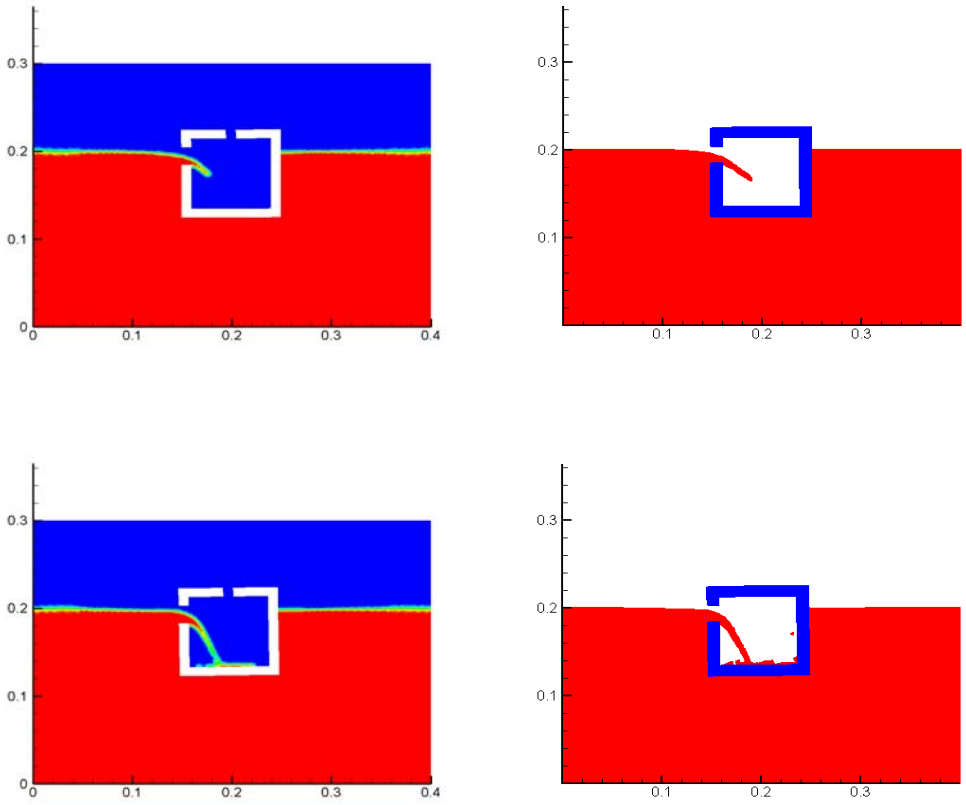

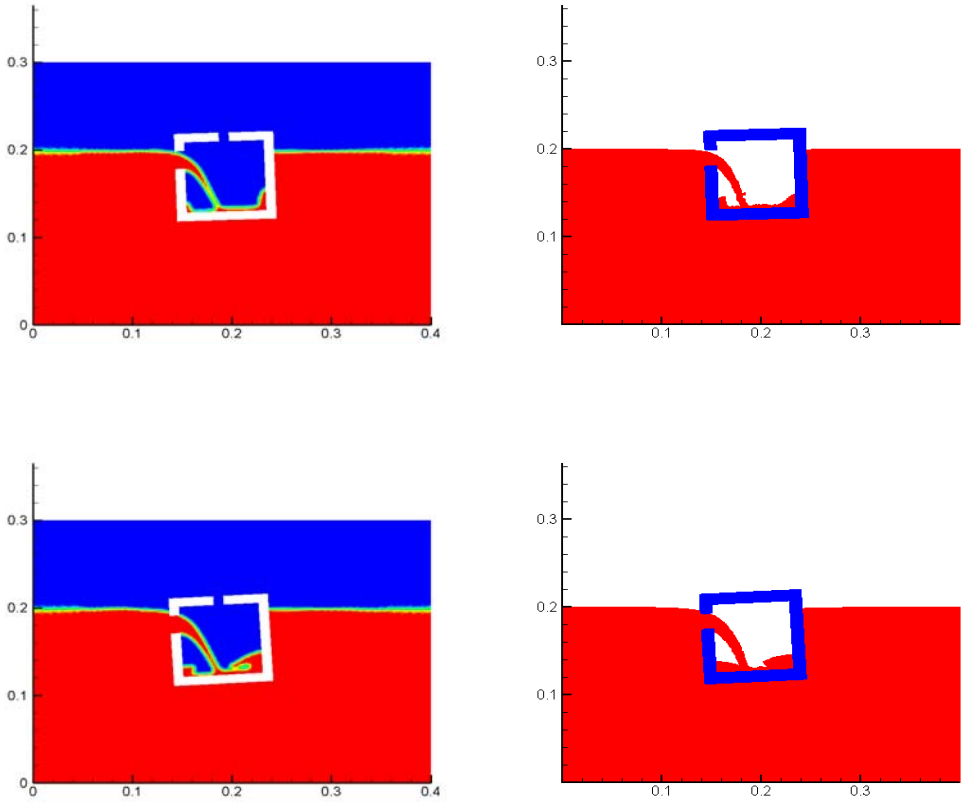

Fig 8.5: Case A - From top to bottom 0.1s, 0.2s, 0.3s, and 0.4s From left to right: VOF, SPH

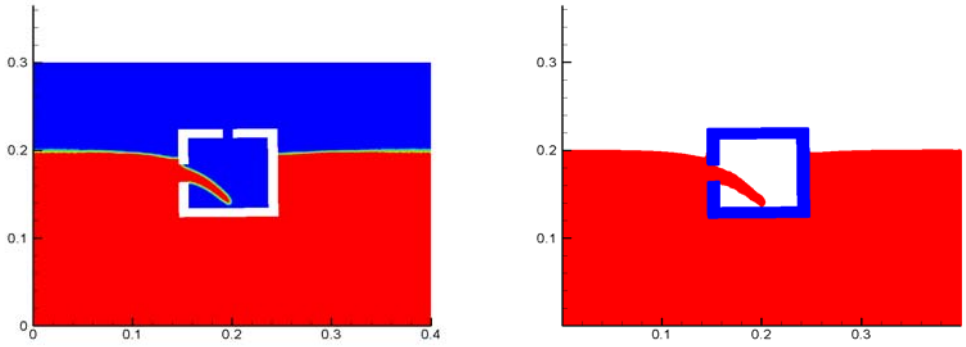

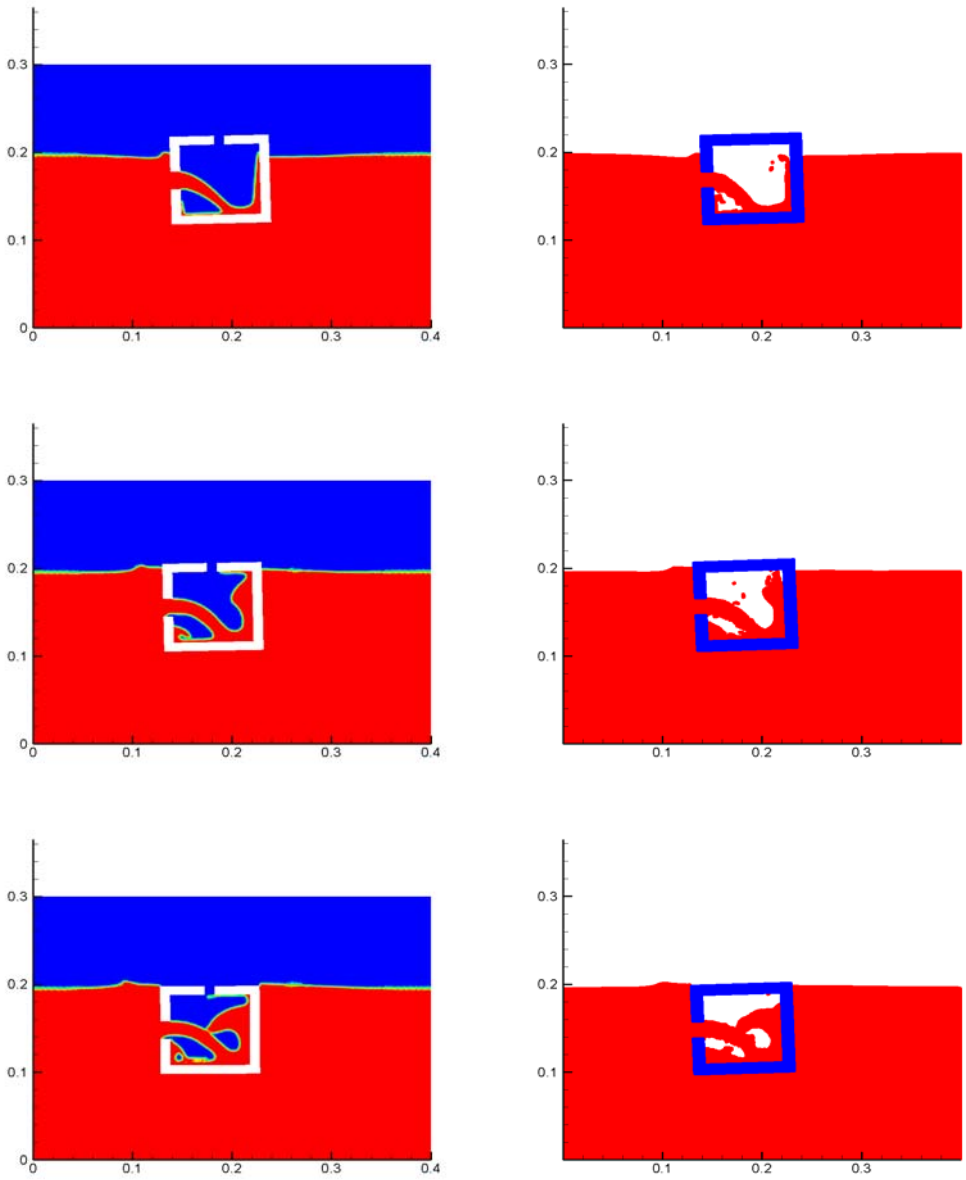

Fig 8.6: Case B - From top to bottom: 0.1s, 0.2s, 0.3s, and 0.35s.From left to right: VOF, SPH

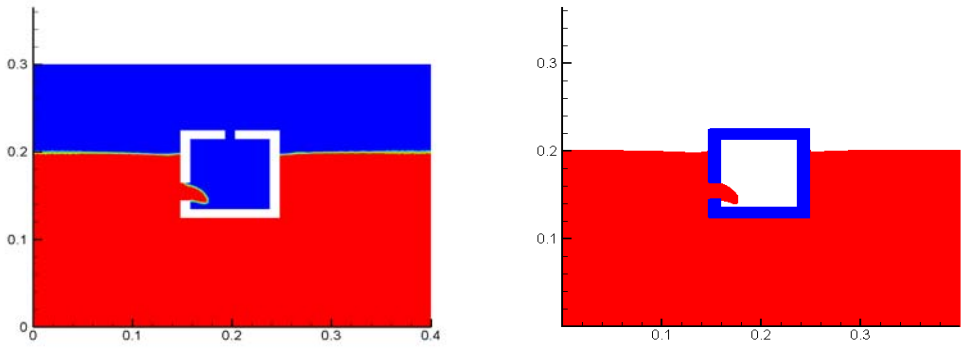

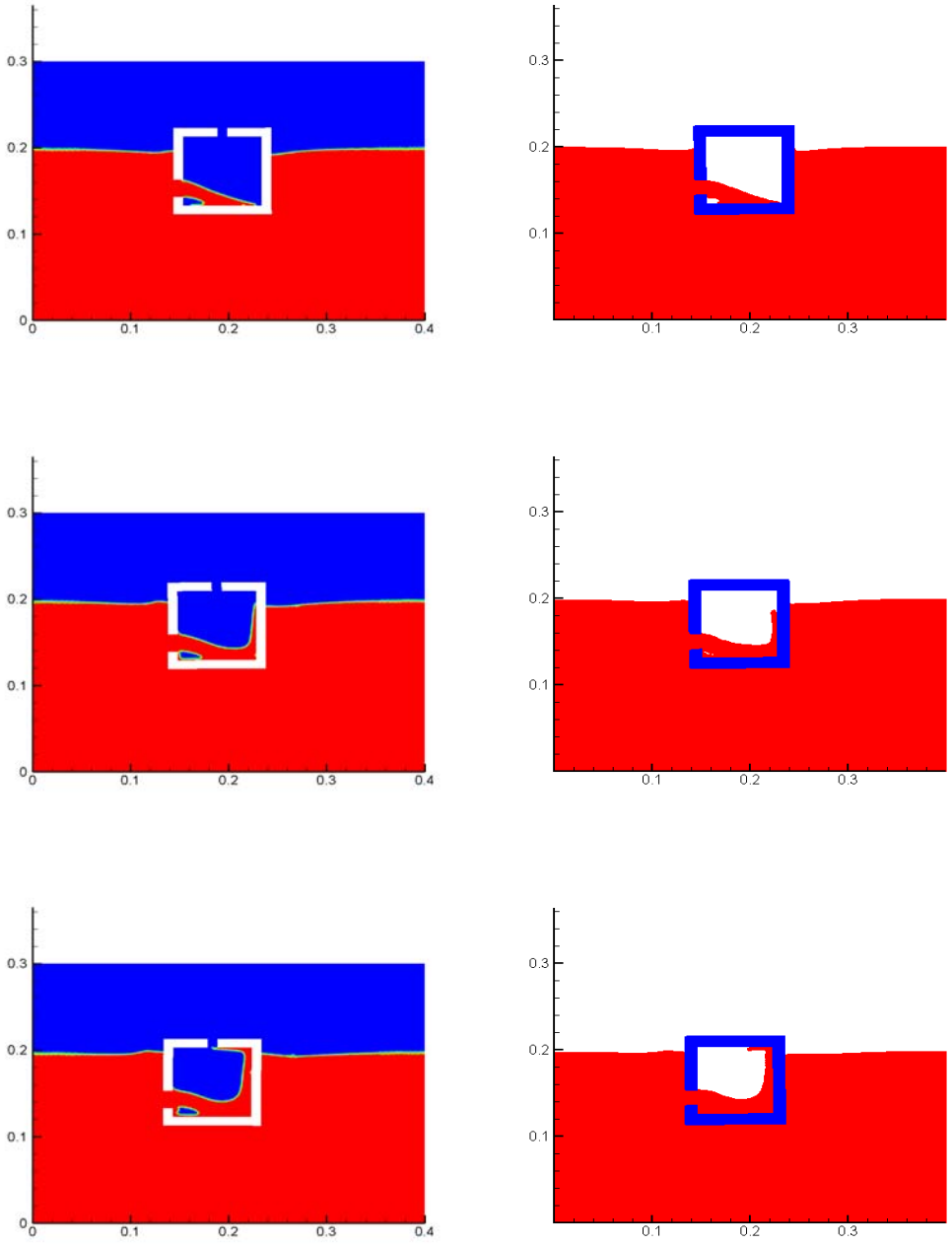

Fig 8.7: Case C -From top to bottom: 0.1s, 0.2s, 0.3s and 0.4s.From left to right: VOF, SPH

The free surface of SPH agreed with VOF method very well. Both methods were able to record the flooding process in time series. When the flooding started, the flooding water evolutions were highly nonlinear and they depend on the damaged open and the impacting and sloshing phenomena in the damaged compartment. The coupling between ship motion and fluid evolution was also very important to predict the final

damaged condition. Therefore, it is necessary to use CFD method such as SPH and VOF to accurately simulate flooding process and the motion of the damaged ship in time-domain. Moreover, the simulation will give an estimation of the available time for orderly evacuation and abandonment, where there is a risk that the ship will capsize or sink.

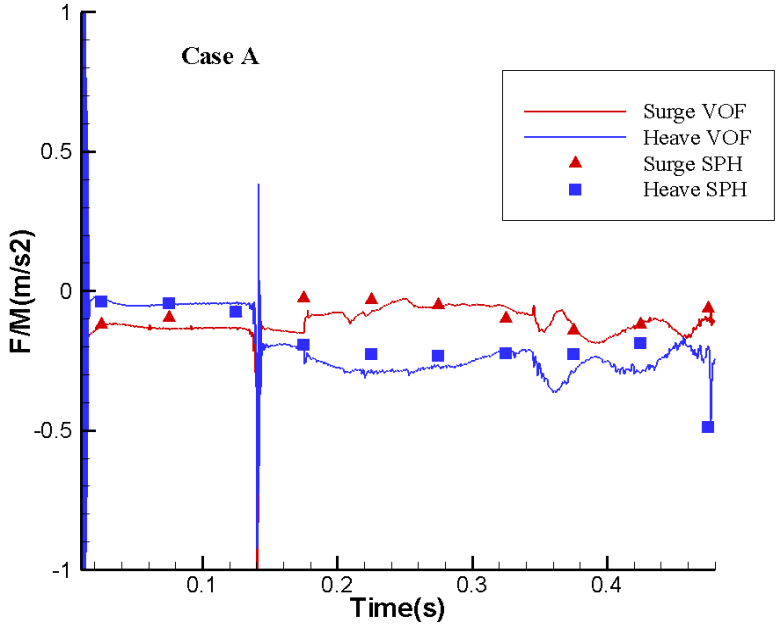

Fig 8.8 SPH vs. VOF of Surge and heave motion in time series (Case A)

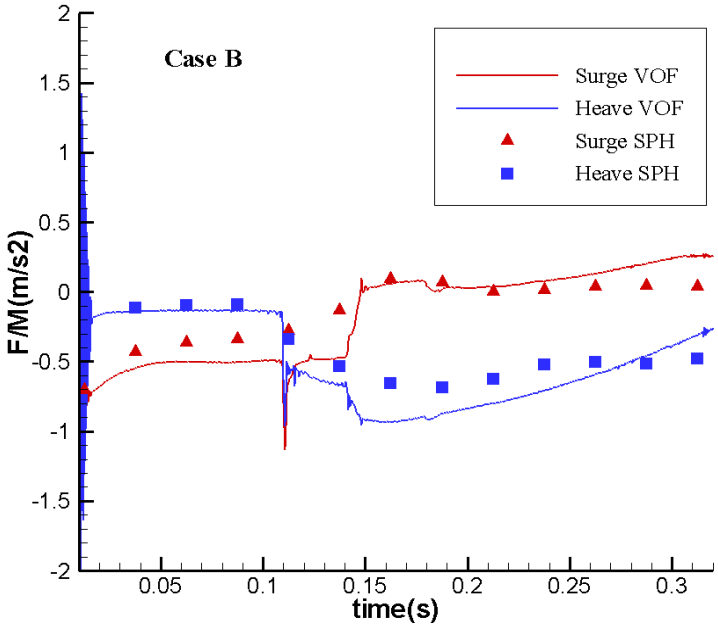

Fig 8.9 SPH vs. VOF of Surge and heave motion in time series (Case B)

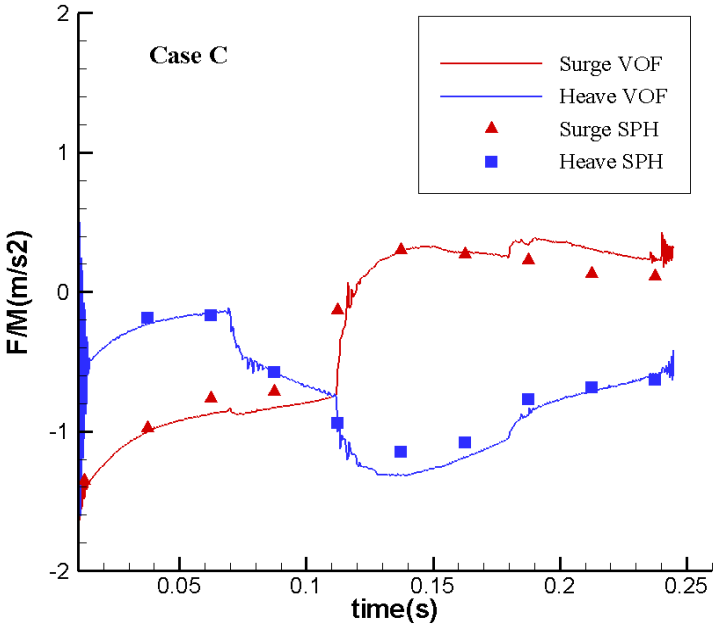

Fig 8.10 SPH vs. VOF of Surge and heave motion in time series (Case C)

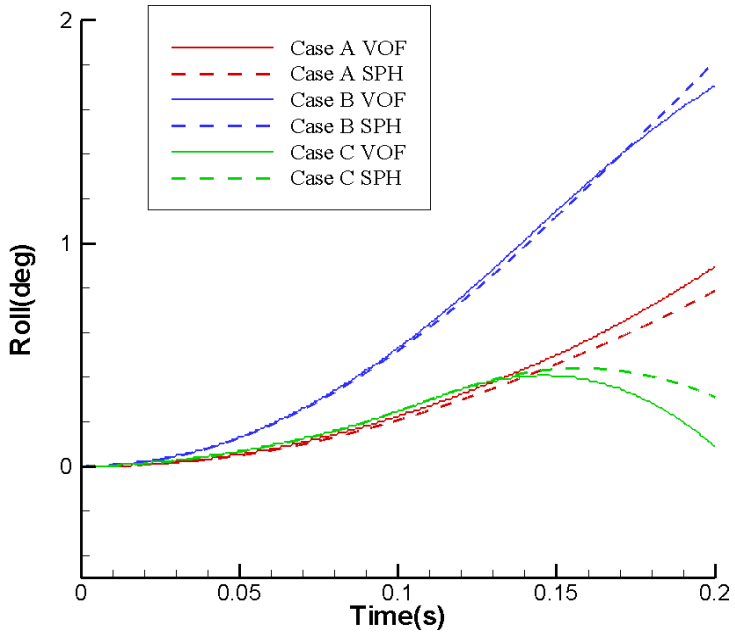

Fig 8.11 SPH vs. VOF of roll motion in time series

Figs 8.09-8.11 show the results of box motion in time series including surge, heave and roll. As expected in linear theory, the flooding will be more violent when the damage opening is deeper. At initial time, the larger pressure difference among two sides of the box cause larger amplitude of surge motion. When the flooding water impacts on the right wall in the box after 0.1s, the box takes positive surge acceleration due to the impacting force. The obvious sinking of box begins when the flooding water reaches the bottom wall in the box. In addition, the capsizing of the box depends on the gravity center of the box and the sloshing phenomena.

SPH results generally are in accordance with FLUENT results. SPH has a simple way to achieve fluid-solid interaction whereas mesh-based method has to solve the problem of mesh distortion due to the large motion response of structures.

Case 2 – 3D rectangular box

Flooding test of Ro-ro ship is proposed in 24th ITTC to investigate the stability under

the scenario of damaged compartment being flooded. Simplified model (Fig 8.12) was tested by Cho (2005, Maritime and Ocean Engineering Research Institute, KORDI, Korea).

This study concentrates on simulation of progressive flooding where the floodwater can proceed to undamaged compartments of the ship through the internal openings. SPH simulation was carried out and the results were compared with VOF method.

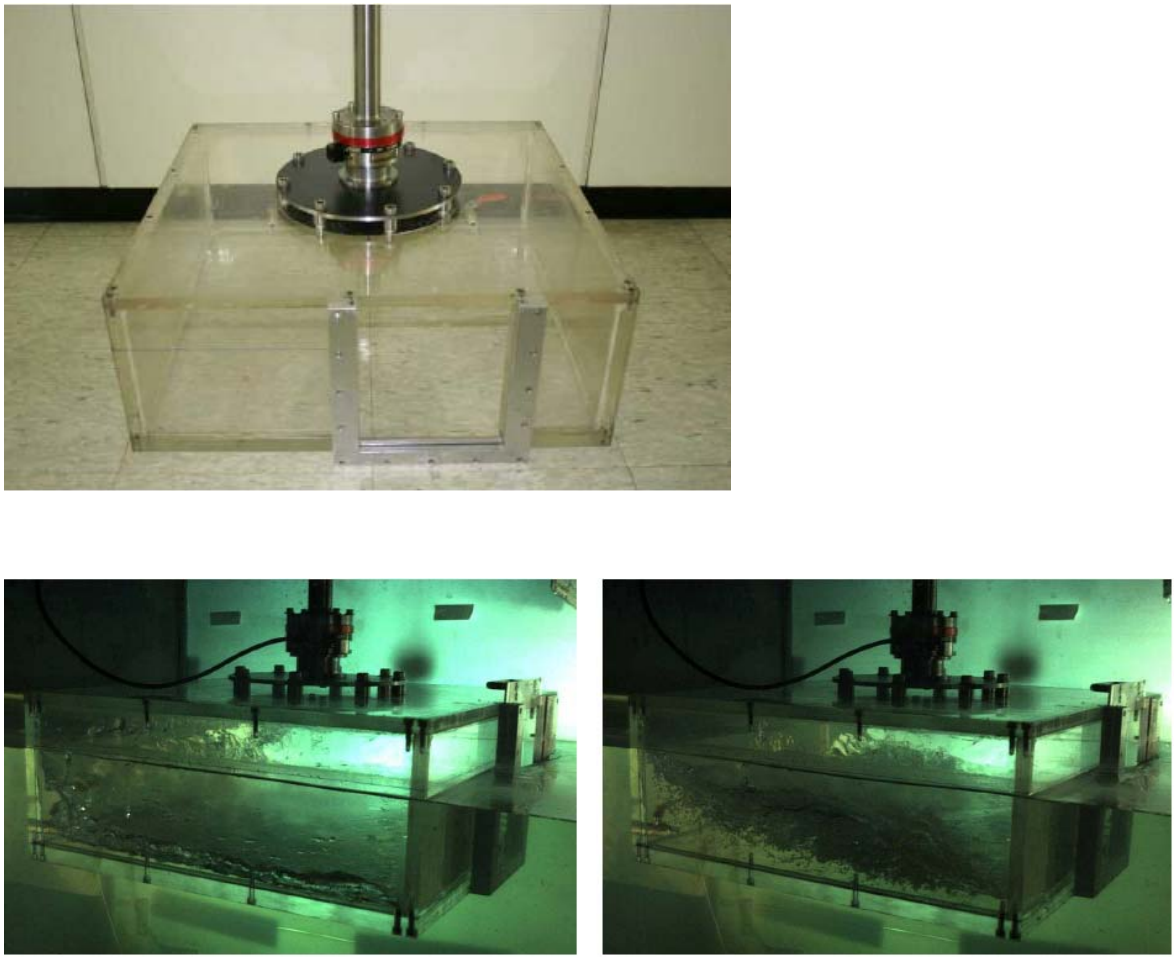

Fig 8.12 Flooding test of Ro-ro ship compartment

The compartment was fixed in the tank with a damage opening along the length of the tank. The main characteristics of the compartments are listed in following Table 9

Model scale	48.57

Damage side	Starboard
Length	26.714m
Breadth	25.000m
Height	9.025m
Draft	6.400m

Table 9: Main characteristics of Damaged Compartment of ITTC Ro-Ro Passenger Ship

For the simple model, the geometry of damage opening was designed as shown in Fig 8.13

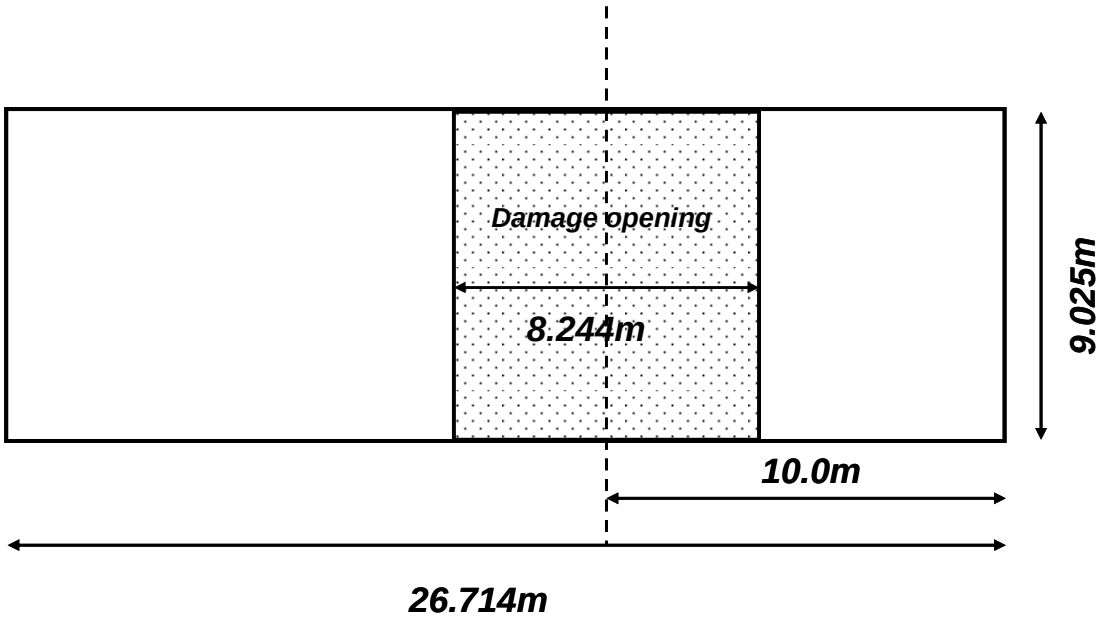

Fig 8.13 Geometry of damage opening

The compartment was flooded from the damage opening on the starboard side. The model was fixed without any motion being considered. The drought of the compartment was 6.4m and the water level outside the compartment was below the upper edge of the damage opening at any time. The air was allowed to escape through the damage opening. In this case, one-phase model for SPH was adopted for efficiency of calculations.

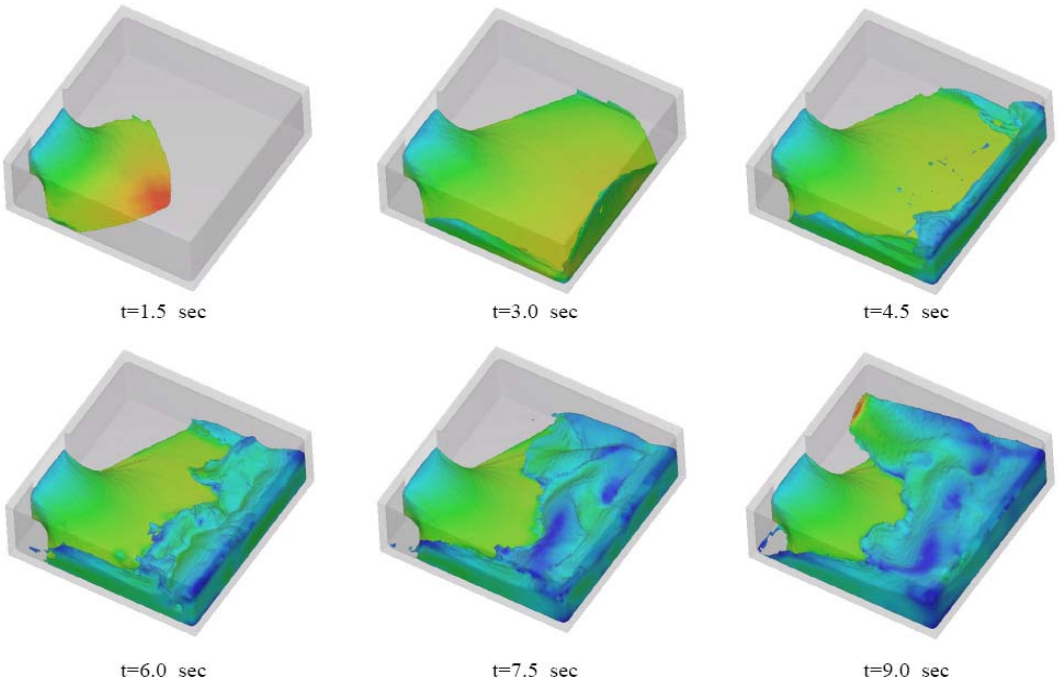

Fig 8.14 Results of VOF (Flow 3D)

Three dimensional images were created in order to visualize the flooding process. Fig 8.14 is the results of VOF method from software Flow 3D (Cho 2005). The case was simulated by both SPH and VOF (Fluent) for comparison. The results are provided in fig 8.15.

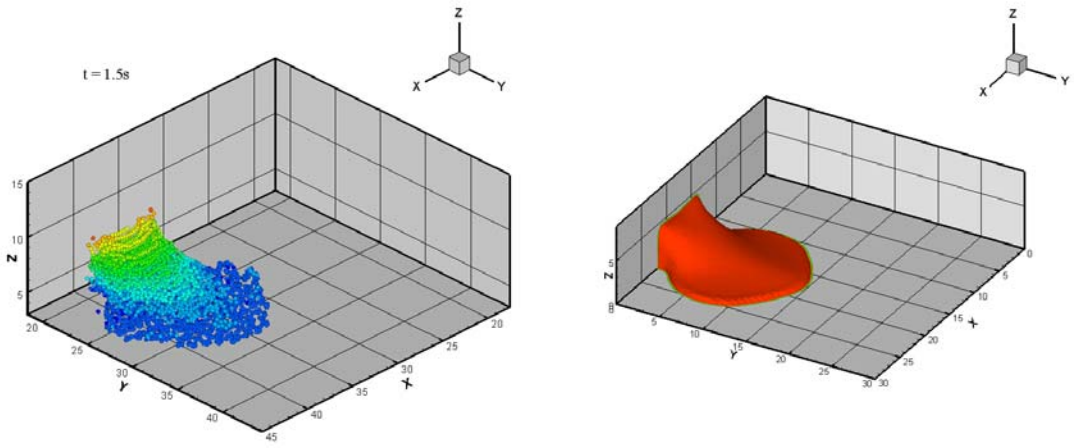

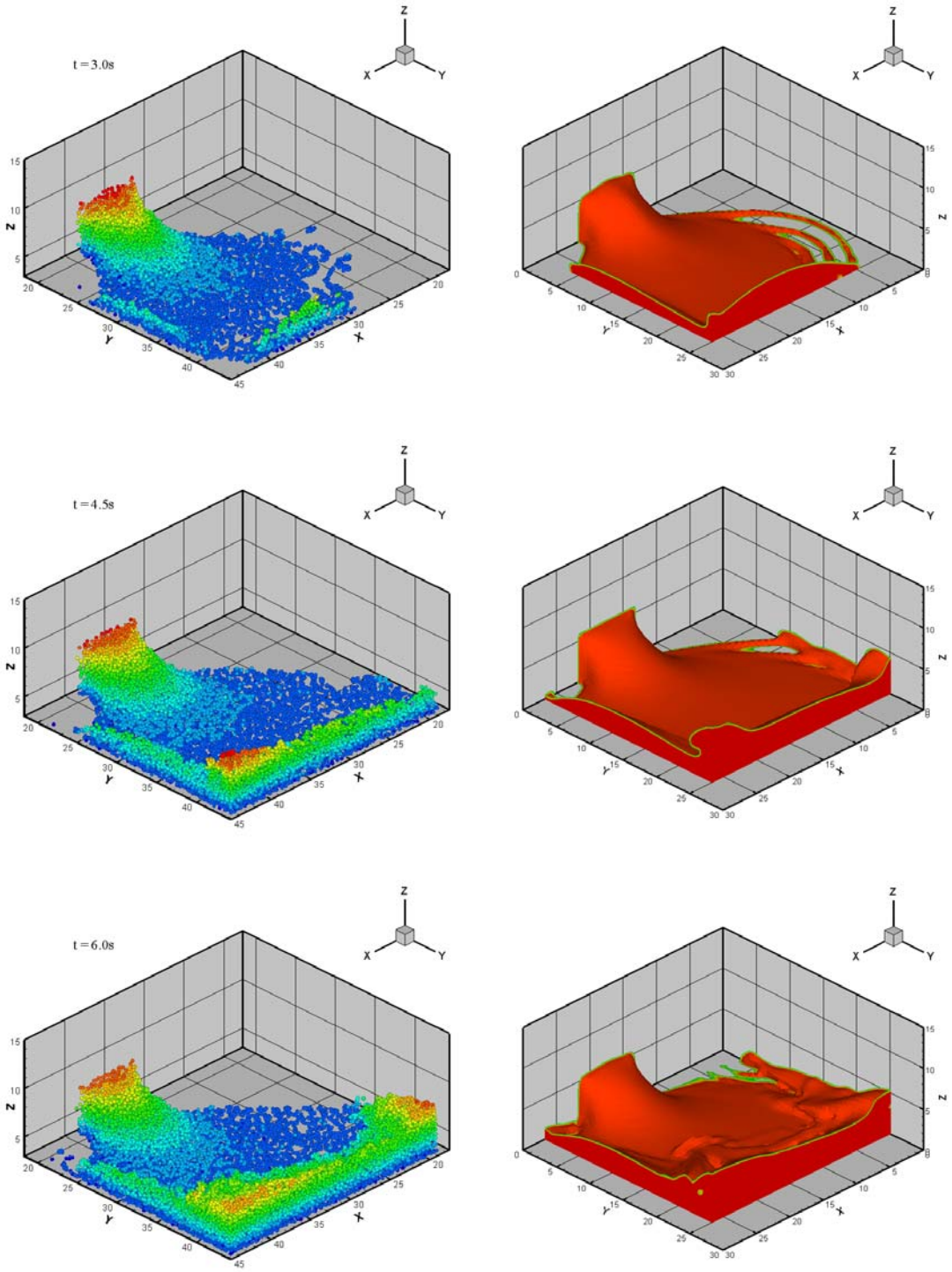
t = 3.0s
t = 4.5s
t = 6.0s
Z
X
Y

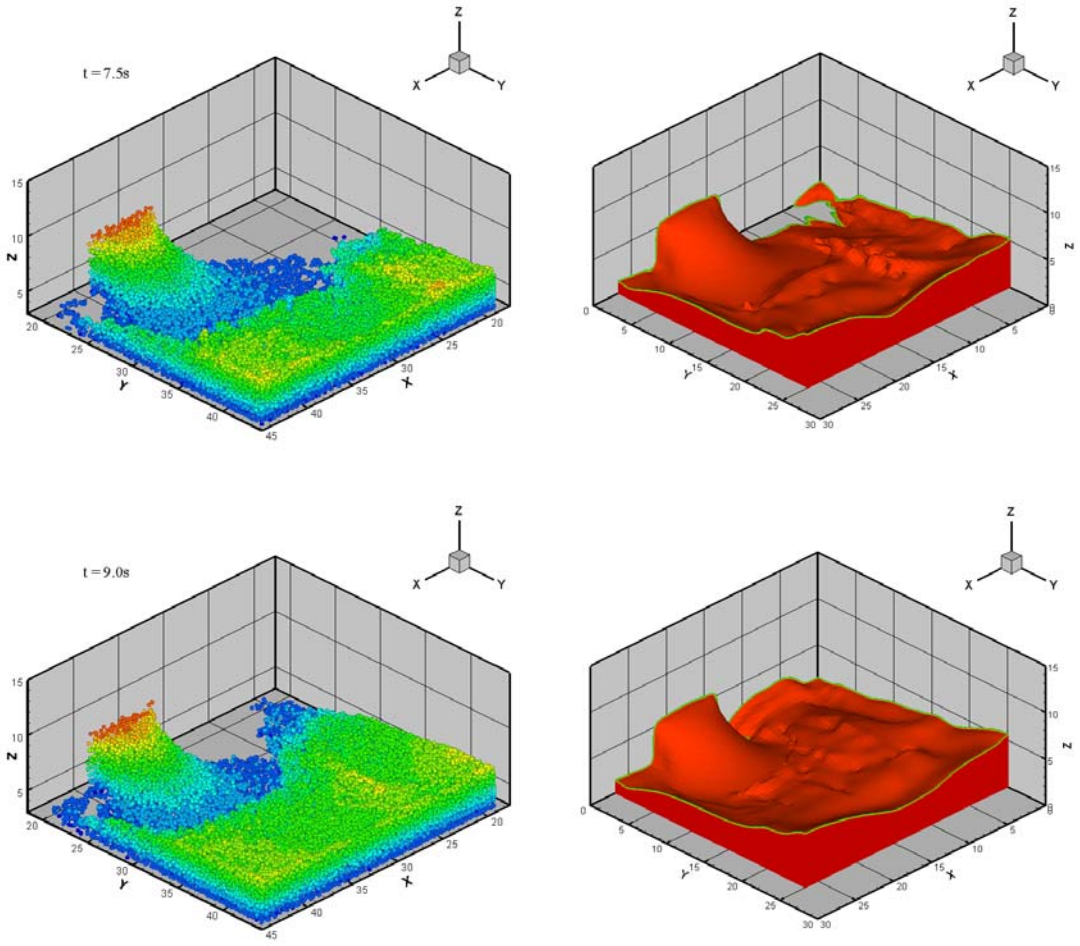

Fig 8.15: Snapshots of Flooding in 3D damaged compartment in time series (From left to right: SPH, Fluent; From Top to Bottom: 1.5s, 3s, 4.5s, 6s, 7.5s, 9s.

Flooded water evolutions in the damaged tank were given at 1.5s, 3s, 4.5s, 6s, 7.5s, 9s. More than one million of uniform particles were used in SPH calculation. The outside tank boundary domain was limited to 5 times the damaged compartment's length (125m x 125m in full scale). 16 processors were used for code parallelization.

The general agreement of the results between three different CFD methods was satisfactory. In the latter time series, SPH method underestimates the volume and velocity of flooded water which was due to the limited tank size which was 7 times the damaged compartment's length for Fluent. The final equilibrium water level in the damaged compartment will be equal to drought if the tank is infinite but in the limited tank, the water level will be 4% (SPH) and 2% (VOF) of initial drought less than

infinite case.

Case 3 – Midship section

Flooding simulation was also performed for the actual damage onboard the damaged ship, on the basis of the measurements by water level sensors.

The model is a 2D midship section of an actual ship (WP4, Model 4, carried out by Project NEREUS), built to the scale of 1:28. All the values were given at model scale in millimetres. The main dimensions of tank were:
Length: 93 m, Width: 6.80 m, Water depth: 2.75 m,

The model mass was adjusted to obtain a 6m full scale draught and a COG height near the reference water plane. The model's natural roll frequency was 0.848 Hz, as measured by free roll decay tests. The following table summarises the main model particulars:

Dimension	Full Scale Intact	Intact Model @ 1:28 (Theory)	Intact Model @ 1:28 (Actual)
Length (m/mm)	60.000	2142.9	2143
Breadth (m/mm)	27.800	992.9	995
Depth (m/mm)	16.000	571.4	628
Draught (m/mm)	6.000	214.3	214
KMT (m/mm)	13.967	498.8	Not measured
GMT (m/mm)	7.967	284.5	Not measured
Desired KGT (m/mm)	6.000	214.3	187
Length of Damage Compartment (m/mm)	19.200	685.7	Not Applicable

Keel to top of car deck (m/mm)	9.000	321.4	307
FW Displacement (Tons/kg)	9385.1	427.5	427.3

Table 10: summarises the main model particulars

Geometry of ship model is below:

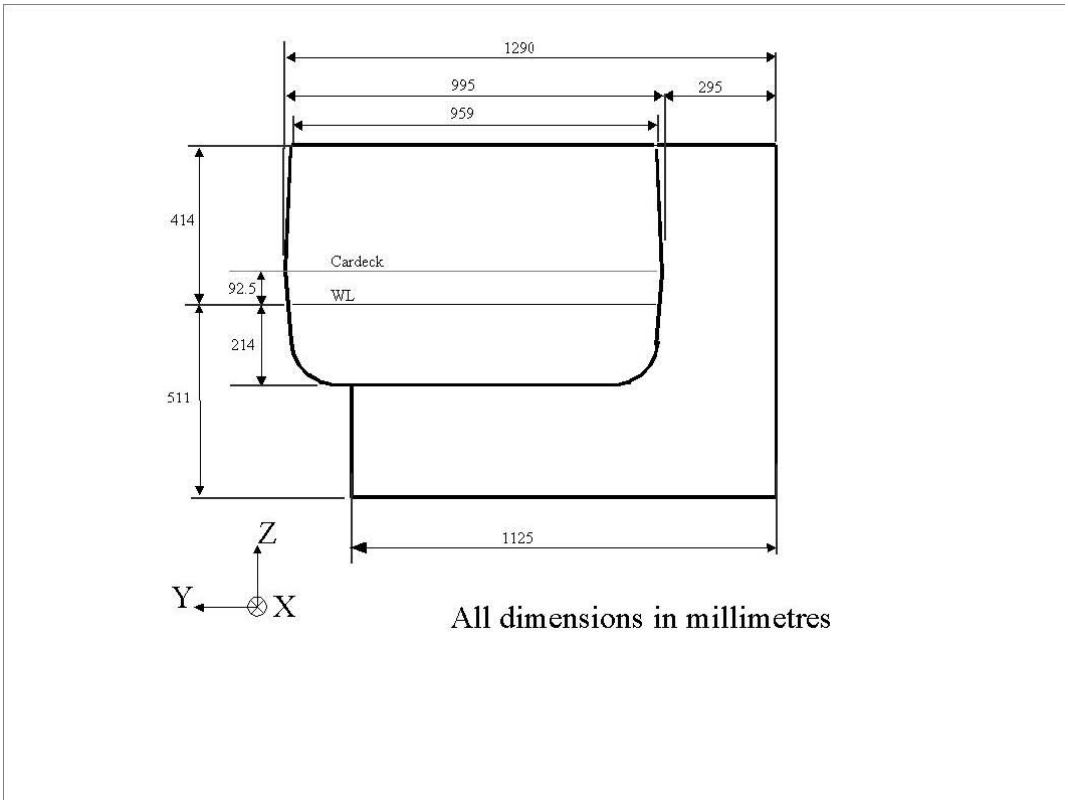

Fig 8.16: Model Characteristics (side view)

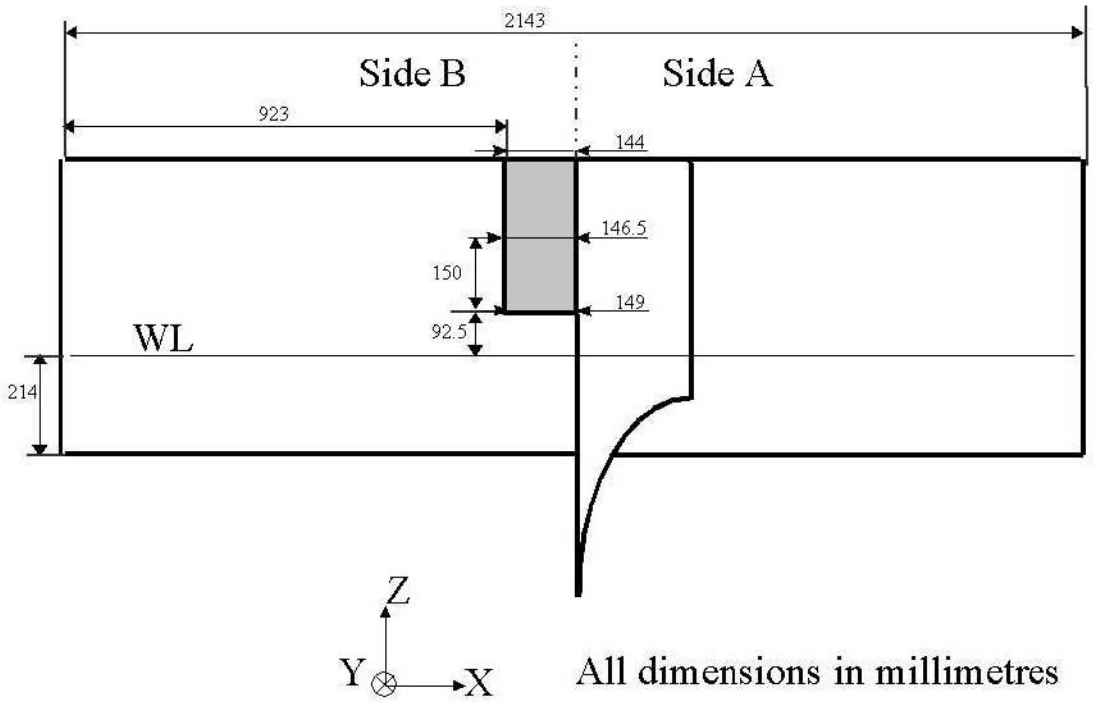

Fig 8.17: Model Characteristics (front view)

Wave height was measured in different positions (Fig 8.18).

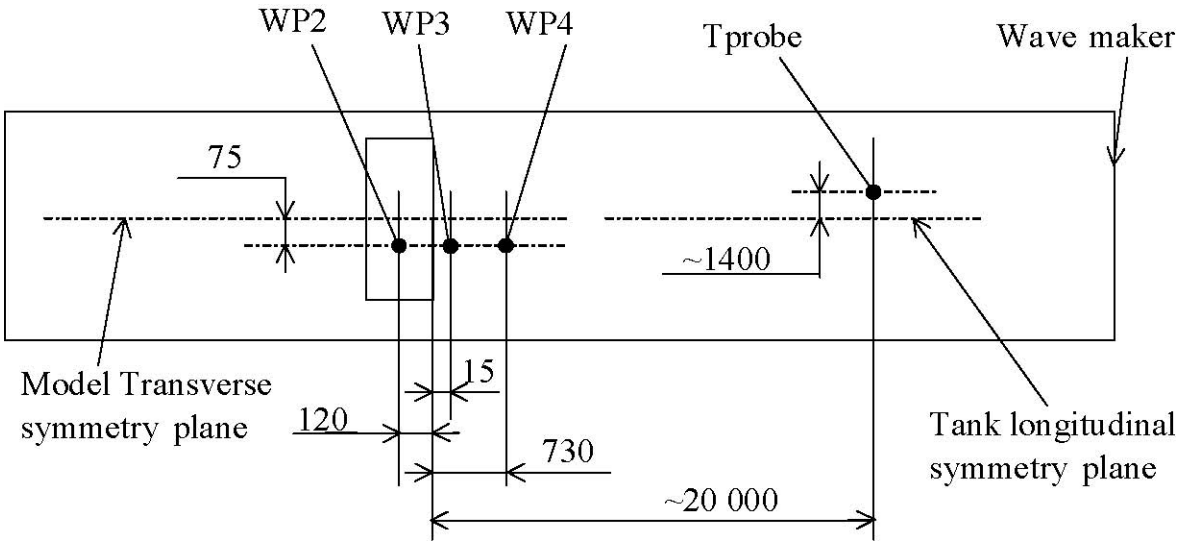

Fig 8.18: Wave probes positions (all dimensions in mm)

In this benchmark case, we have chosen one of the tests as our CFD validation case. The ship model took the captive heave motion with initial heel angle 8.5 degree, the

heave motion amplitude was 53.6mm and frequency was 0.661 Hz.

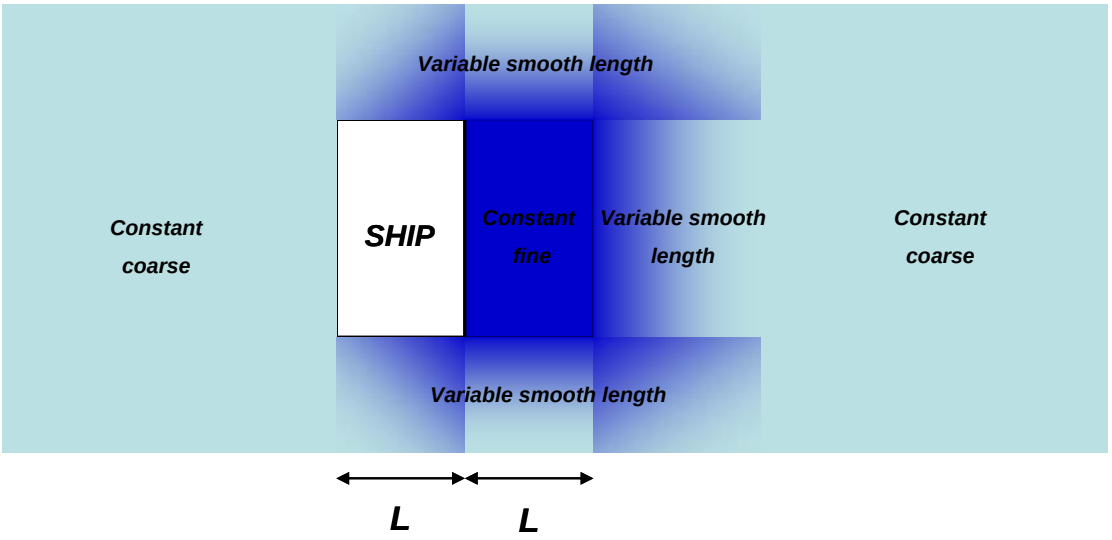

Fig 8.19 Variable smooth length of particles

In the SPH simulation, over 2 millions particles with variable smooth length were initialized in the tank (Fig 8.19). From top view of the tank, constant tiny particles were used in the position of ship and the area close to the damage opening to evaluate the correct wave height in the compartment. Constant large particles were setup in the domain far from the ship and the domain behind the ship. Particles with variable smooth length were used for connection.

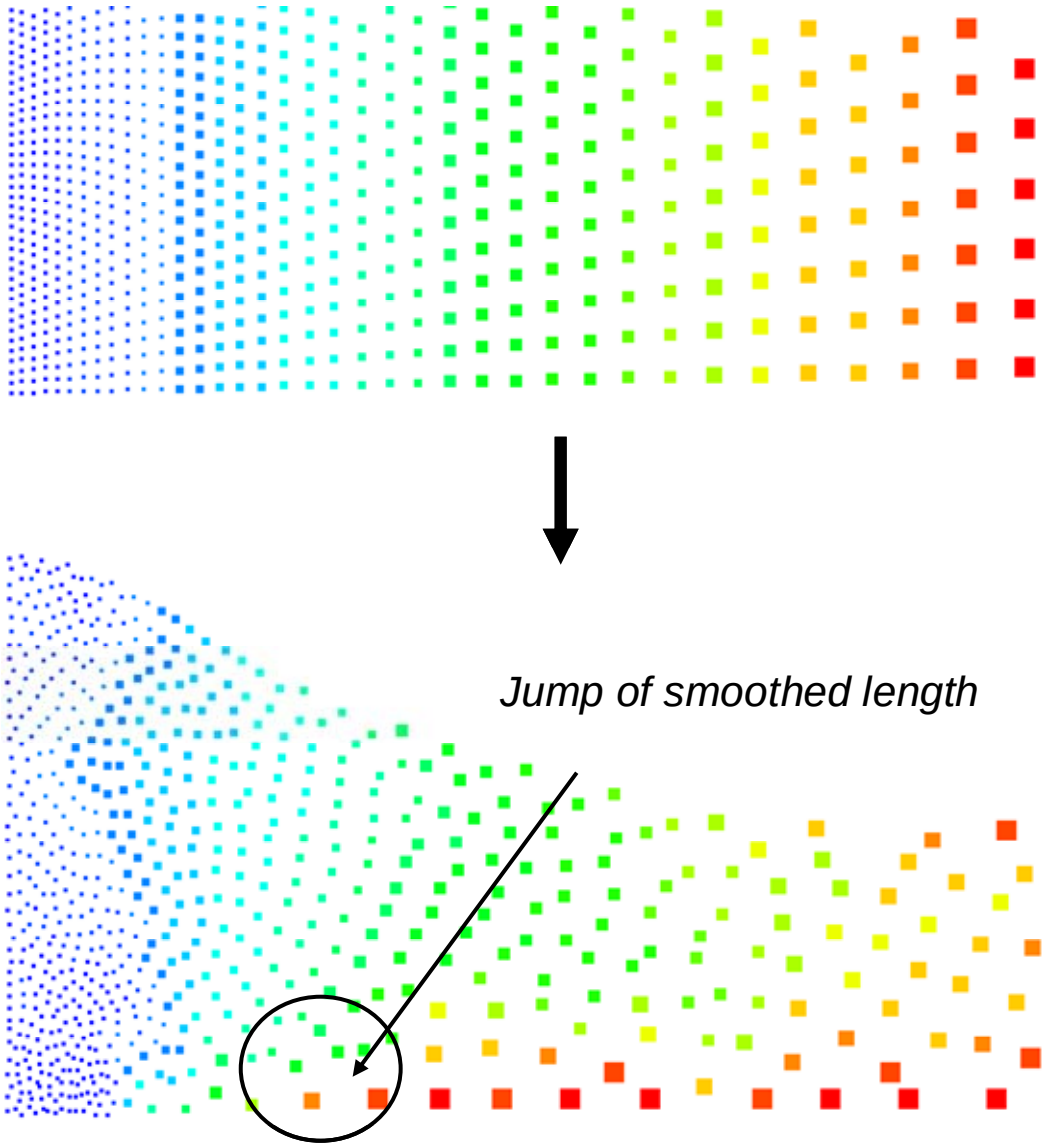

Fig 8.20Jump of smoothed length

About 5 periods were simulated in numerical ways. Contrary to slamming case, after a long time simulation, some particles will move to new position which cannot be predicted in advance. Jump of smoothed length will occur during the simulation. 2D example is shown in Fig 8.20. The interaction of two particles with large difference of mass will cause reflective force from large particle to the small particle. However, in our simulation, the jump of smoothed length has little effect on the results of wave height.

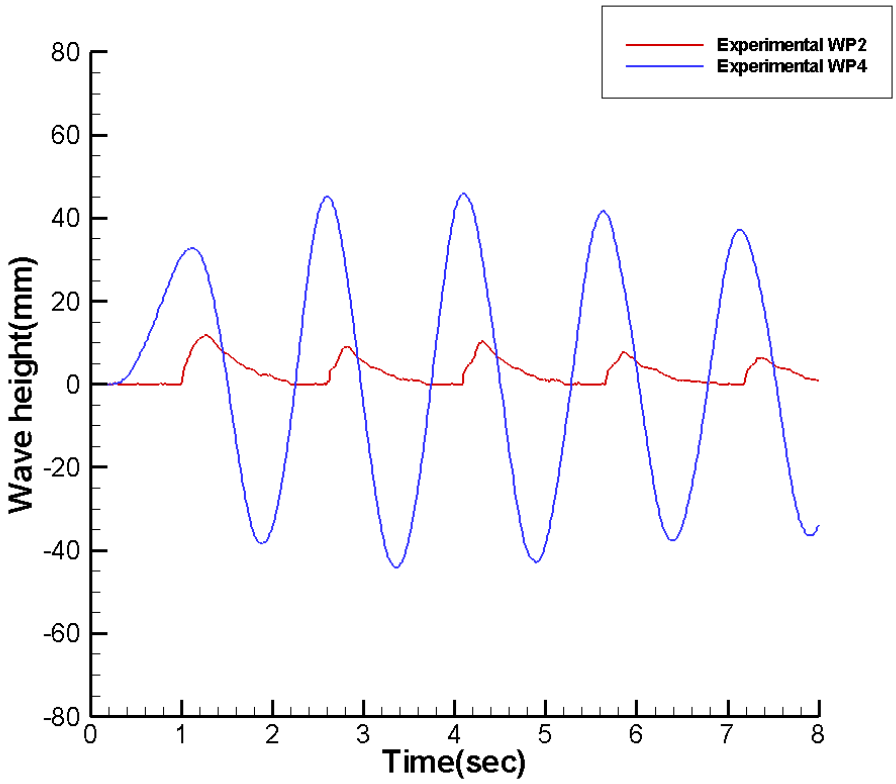

Fig 8.21: wave height - Experiment results at WP2 and WP4

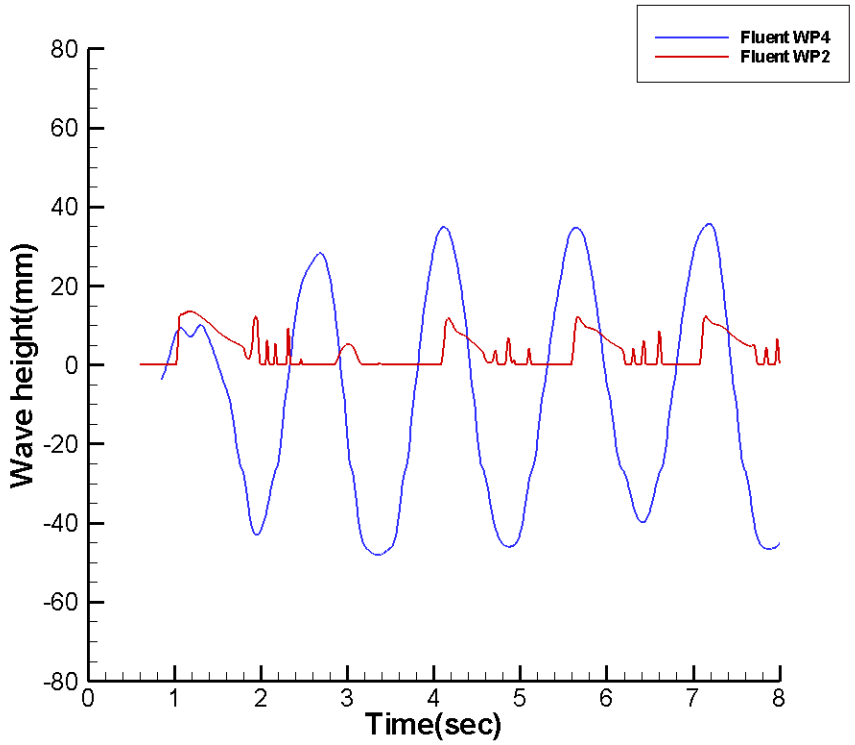

Fig 8.22: wave height -Fluent results at WP2 and WP4

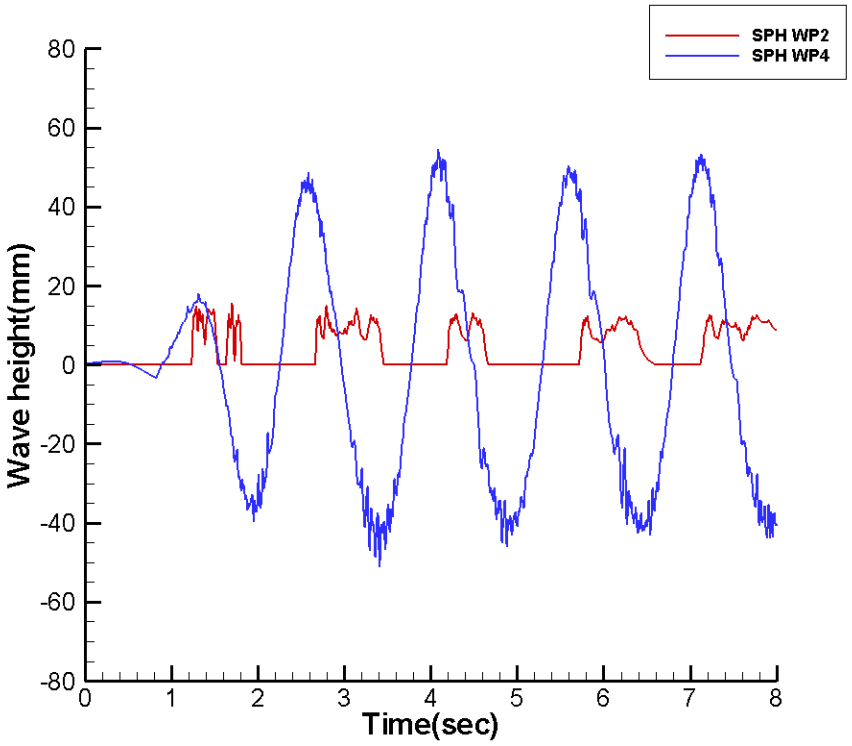

Fig 8.23: wave height -SPH results at WP2 and WP4

The results of wave height at WP2 and WP4 are shown in fig 8.21-8.23. Compared with experimental data, the error at start time is mainly due to the initial situation. Contrary to the experiment, CFD simulation sets the compartment in still water with heel angle and the compartment takes exact proposed heave motion. Since this case is not the about the transient problem, we care more about the flooding water and wave generated after the simulation of cycle becomes steady.

There is a good agreement on the radiation wave height at WP4 caused by heave motion of ship between SPH and experimental results. VOF method underestimated the amplitude slightly, which is due to too coarse meshes that may carry large numerical dissipations. Fig 8.24 shows the SPH results of free surface shapes in the first period. Due to the fact that very shallow flooding water can be detected inside of the compartment, the wave height at WP2 shows oscillations in each period. The same phenomenon is observed in Fluent's results. It requires much finer mesh to solve this

problem but we are concern about the time it will consume. However, the maximum amplitude of wave height in the compartment agrees with the experiments.

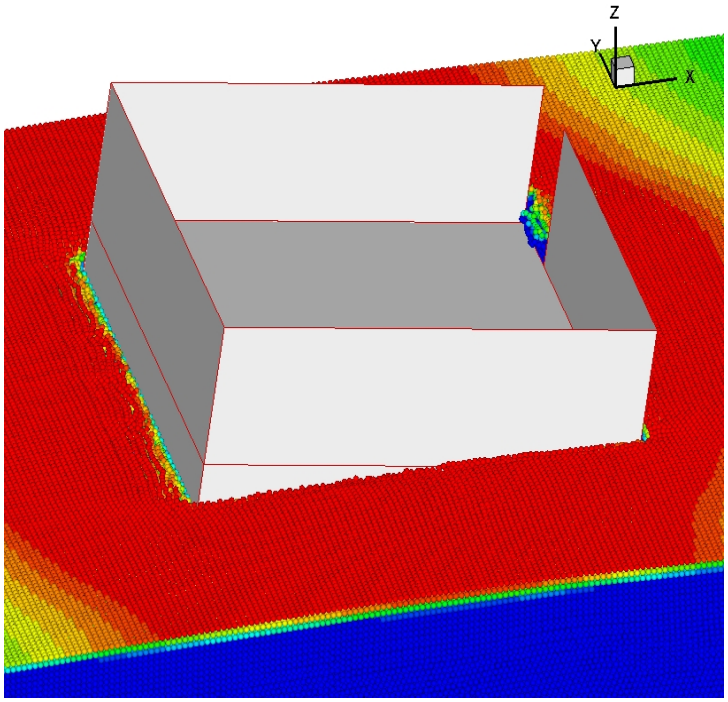

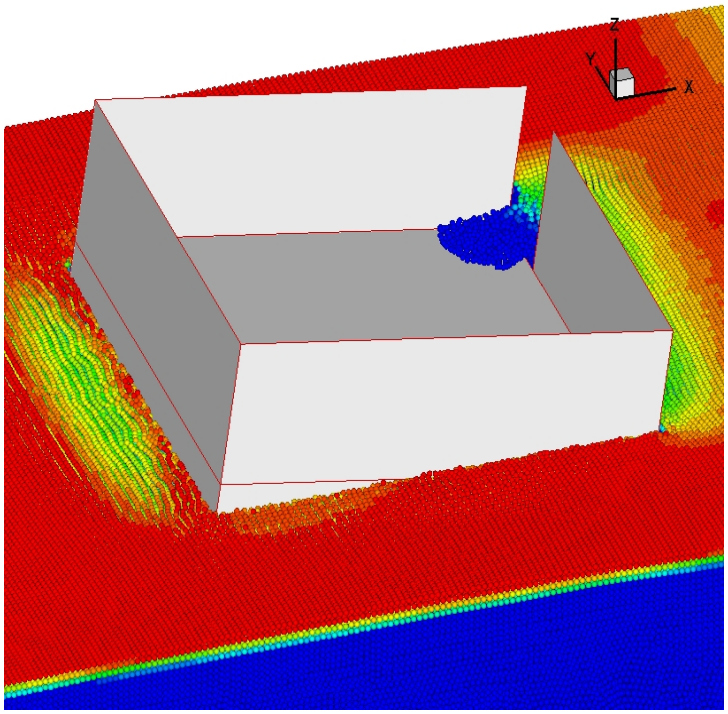

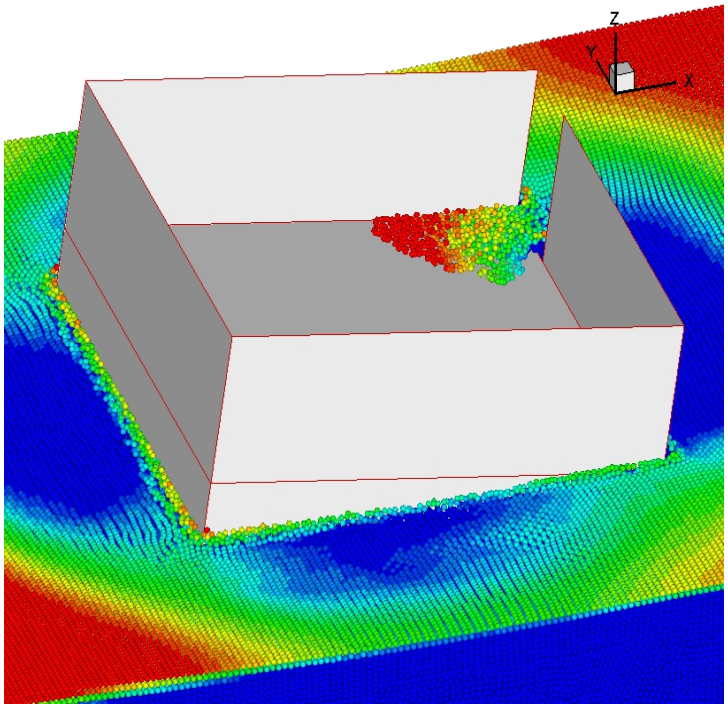

Fig 8.24 Free surface shape - From left to right: 1.2s, 1.4s, 1.6s

8.3 Summary of Results

Three different damaged cases have been analyzed with SPH calculations: two dimensional damaged boxes, a damaged compartment of ITTC Ro-Ro passenger ship and mid-section of an actual ship. The main differences were: in 2D numerical model the motion of damaged box is fully coupled with hydrodynamics, the damaged compartment was fixed, disregarding any ship motion and the mid-section of an actual ship takes captive heave motion in calm water.

Regarding case study 1, two dimensional numerical models were defined to validate the SPH code on flooding process and to fully handle the coupling with compartment motion in time domain. The results of case study 1 were compared with commercial software Fluent. Compared with other CFD method, SPH has great advantage when it comes to dealing with the complicated FSI problem with quite simple initialization of particles and solid boundaries.

Regarding case study 2 and 3, due to the efficient parallel scheme, SPH could predict three dimensional progressive flooding correctly and efficiently. Moreover, further accurate free surface shape can be provided by SPH.

One-phase solver of SPH was adopted in the simulations of flooding since in all cases the air in the compartment was able to escape at any time. In some cases, the effects of air pipes can also be significant due to the compression of air that delays the equalizing flooding to the undamaged side. Two-phase solver of SPH could be used to deal with airflow. However, the time it takes to calculate the additional factors will increase significantly.

9 Discussion

A meshless technique based on the Smoothed Particle Hydrodynamics algorithm has been developed for the simulations of three dimensional nonlinear free surface flows. The Lagrangian character of SPH allows present method to handle accurately large deformation and fragmentation of the interface.

Some techniques were developed and adopted in our code in order to allow the simulation to be more accurate and stable. The fluid was modeled as weakly compressible by introducing an equation of state. This results in a more efficient code since it did not necessitate the solution of a Poisson equation for the pressure. In order to avoid particle clumping, tensile stability was introduced in the code. Variable smoothed length technique was implemented by initializing the particles through Gambit. The efficiency of calculation has improved significantly. SPH strategy has been combined with fourth-order Runge-Kutta scheme for the time integration of the solution.

Furthermore, dam break and wedge entry were tested for verification and validation of SPH code. Different solid boundary conditions were compared in these cases and the proposed approximate boundary technique was proven to be robust and accurate. In addition, this allows a correct evaluation of pressure along the boundary. Two-phase SPH solver was tested for 2D dam break to investigate the air influence. Variable smoothed length technique was used in the simulation of wedge entry and the efficiency was 5~10 times higher than the case using uniform particles. Simulations of breaking and reconnection of the interface in slamming problem can be easily handled by SPH. The impacting force and local pressure were also predicted to be more accurate compared with experiments.

Finally, the method has been applied to sloshing and flooding with simulation of five cases: 1) two dimensional sloshing in rectangular tanks 2) three dimensional sloshing in rectangular tanks 3) two dimensional flooding in damaged box 4) three dimensional flooding in fixed rectangular compartment 5) three dimensional flooding in mid-section of a ship.

SPH method has been used to simulate sloshing with high nonlinear behavior. Comparisons with model tests were presented in the case of 2D sloshing within the rectangular tank. Besides good agreement of height wave at particular position, impacting pressure and free surface visualization were also provided. Subsequently, SPH was extended to simulate 3D sloshing in irregular waves. There have been similar agreements with the demonstrated experiments. Comparisons were also made with other CFD tools.

Time domain simulation is a very efficient tool to accurately predict progressive flooding. SPH method has the natural advantages to handle complicated free surface flow and even more complicated and practical applications were implemented in the present thesis. Two dimensional damaged boxes with free motion were firstly simulated. The coupled motion of the box due to flooding water was predicted and comparisons were made between different heights of damage opening. It is very meaningful to investigate the influence of instant flooding process on the final condition of flooding.

Furthermore, three dimensional compartment flooding cases were tested. Transient progressive flooding into the fixed compartment was successfully predicated. Finally, a mid-section of ship with damage opening was studied. The ship took a forced heave motion. Wave height of flooded water and radiation wave in time series were compared with experiments and other numerical results. There was generally a satisfactory agreement that occurred during the comparison.

10 Conclusion

The main objective of this thesis is to develop a fast and accurate simulation method for 3D Nonlinear Free Surface Flow. Main contributions of present thesis are outlined below:

1. Robust and comprehensive SPH parallel codes were developed. Computation ability is always the bottleneck of CFD method. Parallelization is the optimal option to solve this problem. In our code, MPI technique was adopted for parallelization. Since SPH method adopts explicit algorithm in interactions, the efficiency of parallel is higher than traditional CFD tool (VOF).

2. Efficient and robust solid boundary condition was proposed which was suitable for the complex geometry. Approximated boundary for ghost particles technique was introduced in the present thesis. Most of the complex geometries can be discretized into simple flat faces, and the algorithm is efficient and stable. The benchmark cases have proved the accuracy in the simulation of the solid boundary.

3. Variable smooth length technique was developed to improve the calculation efficiency. Wedge slamming case was used to demonstrate the stability and accuracy of this technique.

4. Multi-phase SPH model was developed. Dambreak case was used to demonstrate its advantage to predict the free surface flow with cavity and breaking wave.

5. There were acceptable evaluations of local pressure, tank motion model coupling with hydrodynamics. Plenty of general fluid problems which require the knowledge of local pressure on solid boundaries. However, the standard SPH method suffers from the lack of stability which leads to irregular pressure in

specific points. In order to extract the accurate local pressure, some new techniques were proposed which were called 'Pressure Integration and Summation of Boundary force'. Furthermore, the solid response loads and momentums were derived from this technique. Fully coupling cases between fluid and solid were studied in this thesis successfully.

6. Sloshing case with violent resonance was studied and SPH method could predict the free surface shape with large deformation and local impacting pressure correctly.

7. Flooding cases coupling with free motion tank were studied. The transient flooding process and the motion response of damaged tank could be predicted by SPH method correctly.

8. The applications of SPH were extended to 3D free surface flows. Three dimensional sloshing and flooding cases were studied in the present thesis. SPH could simulate 3D free surface flows correctly and efficiently.

Recommendations for Future work

The present SPH method can be further improved in several aspects

- Variable smoothed length technique

  This technique could reduce the computation time significantly, but currently it is the only suitable technique in slamming case. Improved model should be developed to extend the application of variable smoothed length on additional general cases.

- Incompressible SPH for two-phase model

  Conventional SPH (weekly compressible assumption) suffers the problem of

calculation cost to simulate multi-phase model. Incompressible SPH could avoid this problem and it will not have the problem to capture free surface particles in multi-phase model.

- Coupling SPH with BEM

More investigation could be done on inflow and outflow boundaries of SPH which leads to couple meshless method with Boundary Element Method or VOF method.

References

Antuono, M. et al. 2011. "*Propagation of gravity waves though an SPH scheme with numerical diffusive terms*". In: Comp. Phys. Comm. 182, pp. 866-877.

Balsara, D.S. 1995. "*Von Neumann stability analysis of smoothed particle hydrodynamics — Suggestions for optimal algorithms*", J. Comput. Phys. 121, 357–372.

Bass, R., Bowles, E., Trudell, R., Navickas, J., Peck, J., Endo, N., Pots, B., 1985, "*Modeling criteria for scaled LNG sloshing experiments*". Trans. ASME 107. 272-280

Batchelor, G.K. 1973, "*An introduction to Fluid Dynamics*" Cambridge University Press

Belytschko, T., Gu, L., and Lu, Y.Y. 1994 "*Element Free Galerkin Methods*", International Journal for Numerical Methods in Engineering, 37, pp. 229-256

Benz, W. 1988, "*Applications of Smooth Particle Hydrodynamics (SPH) to Astrophysical Problems*". Comp. Phys. Comm. 48(1), 97-105

Berg, A. 1987, "*Scaling laws and statistical distributions of impact pressures in liquid sloshing*". Tech. Rep. no. 87-2008, Det Norske Veritas (DNV).

Buechmann, B.A. 1996, "*2D numerical wave based on a third order boundary*

element model". In 9th Conf. European Consortium for Mathematics in Industry, Lyngby/Copenhagen, Denmark, June 25-27, 1996, pp. 417-420.

Chen, Sh., Johnson, D.B., Raad, P.E. & Fadda, D. 1997, "*The Surface marker and micro cell method*". Intl J. Numer. Meth. Fluids 25, 749-778.

Cho, S.K., Hong, S.Y., Kim, Y.H., Lee, K.J., 2005, "*Investigation of dynamic characteristics of the flooding water of the damaged compartment of an ITTC RORO passenger ship*", Proceedings of the 8th International Ship Stability Workshop, Istanbul, Turkey.

Colagrossi, A. 2004 Dottorato di Ricerca in Meccanica Teorica ed Applicata XVI CICLO "*A meshless Lagrangian method for free-surface and interface flows with fragmentation*". PHD Thesis Universita di Roma, La Sapienza

Colagrossi, A. and Landrini, M. 2004, "*Numerical simulation of interfacial flows by smoothed particle hydrodynamics*" J. Comput. Phys. 191 448-75

Colagrossi, A., Lugni, C., Douset, V., Bertram, V. and Faltinsen, O. 2003, "*Numerical and experimental study of sloshing in partially filled rectangular tanks*", 6th Numerical Towing Tank Symp. (Rome, Italy)

Colagrossi, A. et al. 2010. "*Theoretical analysis of SPH in simulating free-surface viscous flows*". In: 5th ERCOFTAC SPHERIC Workshop. Manchester, UK

Cummins, SJ. and Rudman, M. 1999, "*An SPH Projection Method*" J. Comp. Phys. 152, 584-607

Dalrymple, R.A., Rogers, B. 2006. "*Numerical modeling of water waves with the SPH method*". In: Coastal Engineering 53 (2-3), pp.141-147.

Di Monaco, A. et al. 2009. "*A semi-analytic approach for SPH modeling of solid boundaries*". In: 4th ERCOFTAC SPHERIC Workshop. Nantes, France.

Dilts, G.A. 1999 "*Moving Least Squares Particle Hydrodynamics – I. Consistency and Stability*". International Journal for Numerical Methods in Engineering 44, 1115-1155

Faltinsen, O. 1974, "*A nonlinear theory of sloshing in rectangular tanks*" J. Ship Res. 18(4), 224-241

Faltinsen, O. M., Rognebakke, O. F. 1999, "*Sloshing and slamming in tanks*". In Hydronav'99 Manoeuvering'99 Gdansk, Ostroda, 1999, Poland. Technical University of Gdansk

Feldman, J., Bonet, J. 2007. "*Dynamic refinement and boundary contact forces in SPH with applications in fluid flow problems*". In: Int. J. Numer. Meth. Engng 72, pp. 295-324.

Ferrari, A. et al. 2010. "*Three-dimensional flow evolution after a dam break*". In: J. Fluid Mech. 663, pp.456-477.

Gao, Q., 2001, "*CFD simulation of water ingress into damaged ships*", Journal of Ship Mechanics, 5 (3), 8-17.

Gao, Q., Kara, F., Shigunov, V., Vassalos. D., 2004, "*Numerical simulation of damage ship flooding*", Proceeding of the 7th Numerical Towing Tank Symposium, Hamburg, Germany.

Gingold, R.A., Monaghan, J.J. 1977, "*Smoothed particle hydrodynamics: theory and*

application to non-spherical stars" Mon. Not. R. Astron. Soc. 181 375-89

González, V., Talens, M., Riola, J.M., Valle, J., Queseda, T., and Espin, M., 2003 "*Numerical Prediction of the Behaviors of a Ro-Ro Ship after a Hull Side Damage*", Proceedings of the 8th International Conference on Stability of Ships and Ocean Vehicles, Madrid, Spain, pp.215-227

Gray, J.P., Monaghan, J.J., Swift, R.P. 2001, "*SPH elastic dynamics*", Comput. Methods Appl. Mech. Engrg. 190(2001) 6641-6662

Hernquist, L., Katz, N. 1989, "*TREESPH: a unification of SPH with the hierarchical tree method*" The Astrophysical J. Supp. Ser. 70, 419-446

Hirt, C.W., Nichols, B.D. 1981, "*Volume of fluid (VOF) method for the dynamics of free boundaries*" Journal of Computational Physics, Vol.39,1: 1981.pp.201-225

Koshizuka, S., Oka, Y. 1996, "*Moving-Particle Semi-implicit Method for Fragmentation of incompressible Fluid*". Nuclear Science and Engng. 123, 421-434

Kulasegaram, S. et al. 2004. "*A variational formulation based contact algorithm for rigid boundaries in two-dimensional SPH applications*". In: Comp. Mech. 33, pp.315-325.

Landrini, M, et al. 2007. "*Gridless simulations of splashing process and nearshore bore propagation*". In: J. Fluid Mech. 591, pp.183-213.

Landrini, M., Colagrossi, A., Faltinsen, O., Sept. 2003, "*Sloshing in 2d flows by the SPH method*". In: 8th Int. Conf. no Num. Ship Hydrodynamics. Busan. Korea. pp. 1 – 15.

Lee, D., Kim, M., Kwon, S., Lee, Y., 2007, "*A parametric sensitivity study on LNG tank sloshing loads by numerical simulations*". Ocean Engineering 34, 3 – 9.

Lancaster, P., Salkauskas, K., 1981 "*Surface Generated by Moving Least Squares Methods*" Mathematics of Computation, 37, pp. 141-158

Libersky, L.D., A.G. Petschek, T.C.Carney, J.R. Hipp, and F.A.Allahdadi 1993, "*High Strain Lagrangian Hydrodynamics. A Three-Dimensional SPH code for Dynamic Material Response*". Journal of Computational Physics 109, 67-75

Liu, M.B., Liu, G.R., Lam, K.Y. 2003 "*Constructing smoothing functions in smoothed particle hydrodynamics with applications*", Journal of Computational and Applied Mathematics 155, 263 – 284

Lucy, L.B. 1977 "*A numerical approach to the testing of the fission hypothesis*" Astron. J. 82 1013-24

Marrone, S. et al. 2011. "*δ-SPH model for simulating violent impact flows*". In: Comput. Methods Appl. Mech. Engng. 200, pp.1526-1542.

Marsh, A.P. et al. 2010. "*A shallow-depth sloshing absorber for structural control*". In: J. Fluid. Struct. 26, pp.780-792

Monaghan, J.J., Gingold, R. 1983, "*Shock Simulation by the Particle Method SPH*". J. Comput. Phys. 52, 374-389.

Monaghan, J.J. 1989, "*On the problem of penetration in particle methods*". Journal of Computational Physics 82, 1–15

Monaghan, J.J. 1992, "*Smoothed particle Hydrodynamics*" Ann. Rev. Astron.

Astrophys 30, 543-574

Monaghan, J.J. 1994, "*Simulating free surface flows with SPH*" J.Comput.Phys. 110 399-406

Monaghan, J.J., Kocharyan, A. 1995 "*SPH simulation of multi-phase flow*". Comp. Phys. Comm. 87, 225-235

Monaghan, J.J. 1995, "*Simulating Gravity Currents with SPH III: Boundary Forces, Technical report*", Monash University. Applied Mathematics Reports and Preprints, 95/11

Monaghan, J.J., Cas, R.F., Kos, A., and Hallworth, M. 1999, "*Gravity currents descending a ramp in a stratified tank*" J, Fluid Mech. 379 36-9

Monaghan, J.J. 2000, "*SPH without a Tensile Instability*", Journal of Computational Physics 159, 290-311

Monaghan, J.J., Kos, A. and Issa, N. 2004 "*Fluid motion generated by impact*" J. Waterway Port Coastal Ocean Eng. 129 250–9

Morris, J.P. 1996, "*Analysis of smoothed particle hydrodynamics with applications*" Ph.D thesis, Dept. Math. Monash University

Morris, JP. 1996, "*A study of the stability properties of smooth particle hydrodynamics*". Publ. Astron. Soc. Aust. 13.

Morris, JP., Fox, P., Zhu, Y. 1997, "*Modeling Low Reynolds number incompressible flows using SPH*" J. Comp, Phys. 136, 214-226

Morris, JP. 2000, "*Simulating surface tension with smoothed particle hydrodynamics*". Int. J. Number. Meth. Fluids 2000; 33: 333-353

Moussa, B., Villa, J.P. 2000 "*Convergence of SPH method for scalar nonlinear conservation law*". SIAM J. NUMER. NAL Vol.37, No.3, pp. 863-887

Nayroles, B., Touzot, G., Villon, P. 1992 "*Improved Free Surface Boundary Conditions for Numerical Incompressible Flow Calculations*", J.Comp. Phy., 8.

Nelson, R., Papaloizou, J. 1994, "*Variable smoothing lengths and energy conservation in SPH*" Mon. Not. R. Astronom. Soc. 270, 1-20

Nugent, S., Posch, H.A. 2000, "*Liquid drops and surface tension with smoothed particle applied mechanics*" Physical Review E, Volume 62,Number 4, 4968-4975.

Oger, G. 2005, "*Two-dimensional SPH simulations of wedge water entries*" J.Comput. Phys. 213 803-822

Oger, G. 2007, "*SPH simulations of 3-D slamming problems 9th International Conference on Numerical Ship Hydrodynamics*" Ann Arbor, Michigan, August 5-8, 2007

Olsen, H., Johnsen, K. 1975, "*Nonlinear sloshing in rectangular tanks. A pilot study on the applicability of analytical models*". Technical Report II, Det Norske Veritsa Report 74-72-S

Palazzi, L., de Kat, J. 2004, "*Model Experiments and Simulations of a Damaged Ship with Air-Flow Taken into Account*", Marine Technology, Vol41, 1:2004.pp.38-44

Papanikolaou, A., Zaraphonitis, G., Spanos, D., Boulougouris, E., Eliopoulou, E.

2000, "*Investigation into the Capsizing of Damaged Ro-Ro Passenger Ships in Waves*", Proceedings of the 7th International Conference on Stability of Ships and Ocean Vehicles, Launceston, Tasmania, Australia, 7.-11. February 2000, pp. 351-362.

Pawell, A. 1997, "*Free Surface Waves in A Wave Tank*". Intl Series Numer. Maths 124, 311-320. Birkhäuser.

Potapov A, Hunt, M., Campbell, M. 2001, "*Liquid solid flows using SPH and the discrete element method*". Powder Technology 116, 204-213

Quinlan, N.J. et al. 2006. "Truncation error in meth-free particle methods". In: Int. J. Numer. Meth. Engn 66, pp. 2064-2085.

Reza, ISSA 2005, "*Numerical assessment of the Smoothed Particle Hydrodynamics gridless method for incompressible flows and its extension to turbulent flows*" Ph.D thesis

Ritchie, B. Thomas, P. 2002, "*Multiphase smoothed-particle hydrodynamics*". Monthly Notices of the Royal Astronomical Society, Volume 323 Issue3, Pages 743-756

Ruponen, P. 2007, "*Progressive Flooding of a Damaged Passenger Ship"*, PhD Thesis, Department of Mechanical Engineering, Helsinki University of Technology, Helsinki, Finland

Santos, T. A., Winkle, I. E., Guedes Soares, C. 2002, "*Time Domain Modeling of the Transient Asymmetric Flooding of Ro-Ro Ships*", Ocean Engineering, Vol. 29, pp. 667-688.

Santos, T.A., Guedes Soares, C. 2006, "*Study of the Dynamics of a Damaged Ro-Ro*

Passenger Ship", Proceedings of the 9th International Conference on Stability of Ships and Ocean Vehicles, Rio de Janeiro, Brazil, 25-29 September

Shepard, D. 1968, "*A two-dimensional interpolation function for irregularly spaced points*", In: Proc of ACM National Conf, 517-524

Skaar, D., Vassalos, D., Jasionowski, A. 2006, "*The Use of a Meshless CFD Method in Modeling Progressive Flooding and Damaged Stability of Ships*", Proceedings of the 9th International Conference on Stability of Ships and Ocean Vehicles, Rio de Janeiro, Brazil, 25-29.9.2006, Vol. 2, pp. 625-632.

Souto-Iglesias, A., P´erez-Rojas, L., Zamora Rodríguez, R., 2004, "*Simulation of anti-roll tanks and sloshing type problems with smoothed particle hydrodynamics*". Ocean Engineering 31, 1169 – 1192.

Souto-Iglesias. A. 2006, "*Liquid moment amplitude assessment in sloshing type problems with smooth particle hydrodynamics*" Ocean Engineering 33 (2006) 1462-1484

Springel, V. 2010. "*Smoothed Particle Hydrodynamics in Astrophysics*". In: Ann. Rev. Astron. Astrophys. 48, pp. 391-430.

Su Tsung-Chow 1992, "*Nonlinear sloshing and the coupled dynamics of liquid propellants and Spacecraft*". NASA Tech. Rep. AD-A250023.

Swegle, J.W., Hicks, D.L., Attaway, S.W. 1995 "*Smoothed particle hydrodynamics stability analysis*", J. Comput. Phys. 116:123-234

Tanizawa, K. 1996, "*A nonlinear simulation method of 3D body motions in waves extended formulation for multiple fluid domains*". In 11th Intl Workshop on Water Waves and Floating Bodies, March 1996, Hamburg, Germany.

Valanto, P. 2006 "*Time Dependent Survival Probability of a Damaged Passenger Ship II – Evacuation in Seaway and Capsizing*", HSVA Report No. 1661, Hamburg May 31, 101 p

Van't Veer, R., and de Kat, J.O., 2000, "*Experimental and Numerical Investigation on Progressive Flooding in Complex Compartment Geometries*", Proceedings of the 7th International Conference on Stability of Ships and Ocean Vehicles, Launceston, Tasmania, Australia, pp. 305-321

Von Neumann, J., Richtmyer, R.D. 1950, "*A method for the Numerical Calculation of Hydrodynamic Shocks*". Journal of Applied Physics 21. 232-237

Wagner, G.J. and Liu, WK. 2000, "*Hierarchical enrichment for bridging scales and meshfree boundary conditions*", Int. J . Numer. Methods Eng. 50, 507-524

Welton, WC. 1998, "*Two-dimensional PDF/SPH simulations of compressible turbulent flows*", J. Comput. Phys. 139, 410-443

Woodburn, P., Gallagher, P., Letizia, L., 2002, "*Fundamentals of damage ship survivability*", Transactions of the Royal Institution on Naval Architects, 144 (2002), pp. 143 – 163

Yildiz, M, et al. 2009. "*SPH with the multiple boundary tangent method*". In: Int. J. Numer. Meth. Engng 77, pp. 221-254.

Zhao, Faltinsen, O., Aarsnes, J. 1997, "*Water entry of arbitrary two-dimensional sections with and without flow separation*", in: 21st Symposium on Naval Hydrodynamics, pp. 408-423

Zhou, Z.Q., De Kat, J.O., Buchner, B. 1999, "*A nonlinear 3D approach to simulate green water dynamics on deck*", in: J. Piquet (Ed.), Proc. 7Th Int. Conf. Num. Ship Hydrod., Nantes, pp. 5.1-1, 15.

Publications

Shen, L., Vassalos, D. 2009, "*Applications of 3D Parallel SPH for Sloshing and Flooding*". P. 723-733, 10th International Conference on Stability of Ships and Ocean Vehicles